

NCR 75-15-1
NASB-31109

Final Technical Report

May 1975

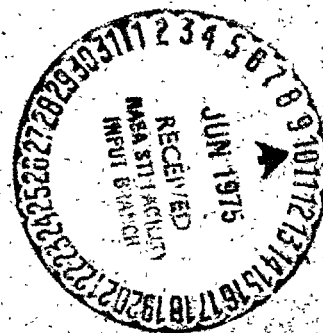
Analysis of Skylab Fluid Mechanics Science Demonstrations

(NASA-CF-120765) ANALYSIS OF SKYLAB FLUID
MECHANICS SCIENCE DEMONSTRATIONS Final
Technical Report, Sep. 1974 - May 1975
(Martin Marietta Corp.) 159 p HC \$6.25

N75-238881

Unclas

CSCL 20D G3/34 21908



MARTIN MARIETTA

MCR-75-151-1
NAS8-31109

FINAL
REPORT

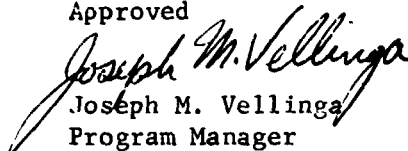
MAY 1975

ANALYSIS OF SKYLAB FLUID
MECHANICS SCIENCE DEMONSTRATIONS

Authors

James R. Tegart
James R. Butz

Approved


Joseph M. Vellinga
Program Manager

Prepared for

National Aeronautics and Space
Administration
George C. Marshall Space Flight Center
Huntsville, Alabama 35812

Prepared by

MARTIN MARIETTA CORPORATION
DENVER DIVISION
DENVER, COLORADO 80201

FOREWORD

This report, prepared by the Martin Marietta Corporation, Denver Division, under Contract NAS8-31109, presents the results of an analysis of the fluid mechanics science demonstrations performed during the Skylab missions. The effort was performed from September 1974 to May 1975 and was administered by the National Aeronautics and Space Administration, George C. Marshall Space Flight Center, Huntsville, Alabama, under the direction of Mr. Tommy C. Bannister.

ABSTRACT

This report presents the results of the data reduction and analysis of the Skylab fluid mechanics demonstrations. All the fluid mechanics data available from the Skylab missions was identified and surveyed. The significant fluid mechanics phenomena were identified and reduced to measurable quantities wherever possible. Using existing theories, obtained from a literature search, data correlations were performed. Among the phenomena analyzed were: static low-g interface shapes, oscillation frequency and damping of a liquid drop, coalescence, rotating drop, liquid films and low-g ice melting. A survey of the possible applications of the results was made and future experiments are recommended.

**ORIGINAL PAGE IS
OF POOR QUALITY**

ACKNOWLEDGEMENT

The authors would like to express their appreciation to the following individuals who contributed to the data reduction and analysis: Messrs. K. C. Lunden, A. Mahrer, J. C. Carpenter and J. Anderson.

ORIGINAL PAGE IS
OF POOR QUALITY

CONTENTS

	<u>PAGE</u>
FOREWORD	ii
ABSTRACT	iii
ACKNOWLEDGEMENT.	iv
CONTENTS	v
LIST OF SYMBOLS.	ix
I. INTRODUCTION.	1
II. DESCRIPTION OF SKYLAB FLUID MECHANICS DATA.	3
A. Specification of Data	3
B. Data Reduction.	7
C. Properties of Water	12
D. Skylab Environment.	14
III. INVESTIGATIONS.	16
A. Static Interface Shape.	16
B. Oscillating Drop.	37
C. Coalescence	71
D. Rotating Drop	85
E. Immiscible Liquids.	98
F. Liquid Films.	100
G. Ice Melting	106
H. Foams	110
I. Low-G Transfer of Liquids	112
J. Diffusion	115
K. Liquid Floating Zone.	118
L. Cavitation.	125
IV. APPLICATIONS SURVEY	130
V. FUTURE EXPERIMENTS.	134
VI. CONCLUSIONS	138
VII. REFERENCES.	140
APPENDICES	
A. Film Data Identification.	146
B. Analytic Derivations.	148

Figure

1	Data Format	9
2	Free Floating Water Drop	20
3	Water Drop Colored with Ink and Tethered with Thread	20
4	Interface of Drop at Thread	21
5	Calculated Shape of Drop on Thread, 50 cc Volume, 30° Contact Angle, 1 mm diameter Thread	23
6	Calculated Shape of Drop on Thread, 100 cc Volume, 30° Contact Angle, 1 mm diameter Thread	24
7	Smaller drops will assume an interface shape that is tangent to the thread	26
8	Capillary Area vs. Thread Diameter	28
9	Drop on a tube	30
10	Sessile drop (the tube is freely resting on the drop surface)	32
11	Adhesiveness of liquid drop to a needle (top) and a tube (bottom)	33
12	Low-g Drinking Cup as designed by William R. Pogue	35
13	Low-g Drinking Cup as designed by MMC	35
14	The four lowest modes of an oscillating drop	38
15	First mode oscillation of a drop. Top photo is just before pulling away plungers, next is just after. Others are spaced every one-half cycle	40
16	Drop oscillating at second mode frequency, pictures spaced every one-half cycle	44
17	First mode oscillation of drop, perturbed perpen- dicular to the plane of view. First photo - plungers against drop, others are spaced one-half cycle apart	45
18	An air bubble is added to a drop before it is oscillated	48
19	Oscillation of drop with internal air bubble. Top photo is immediately following pull away of the plungers, others follow every one-half cycle	49
20	Oscillating soap drop. Top photo is immediately following pull away of plungers. Pictures are spaced one cycle apart in time	51
21	Oscillating drop. Plungers pulled away and lower photos are one-half cycle apart	52
22	Effect of Oscillation Amplitude on Period	55
23	Tube as pulled out of sessile drop inducing oscillation. Photos are every one-half cycle	64

Figure

24	Spurt formed by high frequency oscillation.	67
25	A tube is rotated on top of the drop.	67
26	Rapid lateral motion of surface causes drop to lag movement.	69
27	Two sessile drops for Liquid Floating Zone demonstration	69
28	Drop configuration for coalescence demonstration.	73
29	Coalescence - Test 1.	75
30	Coalescence - Test 2.	76
31	Coalescence - Test 3.	77
32	Coalescence - Test 4.	79
33	Coalescence - Test 5.	80
34	Coalescence - Test 6.	81
35	Regimes of Interaction (from Ref. 36)	82
36	Interface shape for a drop of the toroidal form	86
37	Variation of ω^* with drop distortion	86
38	Methods of Rotating Drops	90
39	The drop tends to center on the threads, even though disturbed as it is in right photos	91
40	Peanut shape assumed by rotating drop	91
41	Rotating Drop Configuration	92
42	Fission of a Rotating Drop.	96
43	Comparison of demonstration data and toroidal theory.	97
44	The module with three vials for the Immiscible Liquids demonstration is shown following centrifugal separation (above) and after mixing (below)	99
45	Wire Frames Used in Liquid Film Demonstration	101
46	Film formed with "plain" water.	102
47	Film formed with soap solution.	102
48	Cube Wire Frame with Soap Film and Bulk Liquid Soap Solution in Center	102
49	Ice Melting Demonstration	107
50	Adding air to a soap and water solution increases the volume until it reaches a static size	111
51	Transfer of blood from syringe to evacuated bottle.	113
52	Diffusion Front Progress, SL-3 Liquid Diffusion Demonstration	116
53	Unstable modes of rotating zone, axisymmetric above and unsymmetric below	119
54	Coalescence of sessile drops from Liquid Floating Zone demonstration	121
55	Drop dynamics in Liquid Floating Zone demonstration: shooting drop, lateral oscillation and oscillating sessile drop.	122

Figure

56	Bubbles within the Liquid Floating Zone	123
57	Rope Fibers in Zone	124
58	Melting Ice in Zone	124
59	Drop with internal air bubble immediately before rupture.	126
60	Jet of Liquid shoots out of view as bubble collapses	126
61	Air is being added with a syringe to a drop	127
62	Collapse of the internal air bubble	127
63	A jet of liquid is formed by injecting water into a drop	129

Table

1	Skylab Fluid Mechanics Data	3
2	Oscillating Drop Tests (Drop on thread)	43
3	Correlation of Oscillation Frequencies.	47
4	Oscillating Drop Tests (Free Floating Drop)	54
5	Calculated Damping Coefficient.	59
6	Measured Damping Coefficient.	59
7	Oscillating Sessile Drop Data	63
8	Coalescence Data.	74
9	Coalescence Parameters.	83
10	Rotating Drop Data.	93

**ORIGINAL PAGE IS
OF POOR QUALITY**

List of Symbols

a	amplitude
A	area
b	amplitude
f	frequency, Hz
K	curvature
l	integer
n	number of cycles
P	pressure
r	radius
R	radius of curvature
t	time
u	velocity
V	volume
σ	surface tension
ρ	density
ν	kinematic viscosity
θ	contact angle
β	damping coefficient
ω	angular rate, rpm

I. INTRODUCTION

During the Skylab SL-3 mission (the second manned mission) the crew requested additional scientific activities. Planned experiments were being successfully completed at a faster rate than expected, due to the diligent work of the crew, so they had time for additional investigations. The NASA George C. Marshall Space Flight Center defined the objectives and equipment for two simple fill-in-experiments. These and other fill-in activities defined by MSFC were categorized as science demonstrations since rigorous experiment protocols could not be followed. However, the objective of most of the MSFC demonstrations was acquisition of data on basic phenomena that would contribute to the definition of future experiments. Diffusion and ice melting demonstrations were successfully performed during the SL-3 mission.

Anticipating that there would be available time during the SL-4 mission, a number of science demonstrations were prepared before the mission. The astronauts performed a large portion of the planned demonstrations, whenever their normal schedule of activities permitted. These demonstrations covered a wide range of scientific disciplines, but only those concerned with fluid mechanics are discussed here.

This was a unique opportunity to demonstrate known scientific principles in a low-g environment. The demonstrations allowed a comparison between a typical phenomena, as it occurs in one-g, and the observed low-g behavior. Low-g theory, based on the influence of the force of surface tension, has in many instances received very little experimental verification. On earth, low-g test periods can be, at best, only one minute, while in the Skylab a test period of hours was not unreasonable. Since basic principles were involved, the film data from the demonstrations makes very good science education material.

By adding the demonstrations to the Skylab missions an appreciable increase in the scientific benefits of the program was achieved at very little additional cost. Hardware did not have to be developed or qualified since equipment available in Skylab was used to perform the demonstrations and only a few small items were taken up to Skylab by the crew. The videotape television system was the prime method of documenting the demonstrations.

The objectives of the demonstrations were specifically defined. However, the astronauts were allowed to use their innovative abilities in determining the methods and procedures for performing the demonstrations. This approach permitted the astronaut to try various approaches if one was not successful, and to expand the demonstration based upon what he learned. It provided a change of pace from the usual, carefully detailed scientific work of the crew. Only through the effort of the Skylab crews were these demonstrations possible.

The initial task of this program was to identify and collect all the Skylab fluid mechanics data. This data was surveyed and reduced to a usable form wherever possible. The observations were then correlated with available theory. The applicability of these results to various sciences that make use of low-g fluid mechanics phenomena (e.g. space processing of materials, cloud physics, cryogenics and space physics) was considered. Finally, future low-g fluid mechanics experiments were recommended.

An important part of the effort was a literature search that identified the available theory related to the observed fluid mechanics phenomena. From this information, explanations of the observed phenomena were derived. Reports of the investigators on their demonstrations were also collected and are included in the reference list.

Some of the fluid mechanics data provided by the fluid mechanics demonstrations had not been analyzed prior to this program. Preliminary evaluations of other portions had been accomplished. In a few cases the data reduction and analysis was complete. One objective of this program was to review all the prior work and to complete the data analysis wherever it was deemed necessary. In Chapter II, the specific Skylab fluid mechanics data items are identified along with the prior work that was accomplished.

The primary purpose of visually showing a phenomena was achieved for each of the demonstrations performed. In some instances the astronauts, through their own initiative, documented and controlled the test parameters to make the demonstration more of an experiment. However, due to the apparatus being used, accurate measurement, control and documentation of all test parameters was not always possible.

II. DESCRIPTION OF SKYLAB FLUID MECHANICS DATA

The purpose of this chapter is first to specifically identify the Skylab fluid mechanics data, and then to discuss the quality and format of this data. For most of the demonstrations the test liquid was water, so its properties are defined. The environment of the Skylab, in which the demonstrations were performed, is also described.

A. SPECIFICATION OF DATA

A complete survey of all the data, in the form of video tape and 16 mm film, was accomplished to identify all data that is related to the science of fluid mechanics. Those data items that were selected to be part of this study are listed in Table 1. Most of the items are identified by their television operations number and the assigned science demonstration title. A brief description of the subject matter of the data is included in the table.

Table 1 Skylab Fluid Mechanics Data

Title	Description
SL-4 Fluid Mechanics Series (TV-107)	Free floating drops - oscillation, coalescence, rotation; sessile drops - oscillation, wetting; air bubbles inside drops.
SL-3 Fluid Mechanics Data	Miscellaneous demonstrations with drops.
SL-4 Liquid Floating Zone (TV-101)	Oscillation and rotation of liquid zone.
SL-4 Immiscible Liquids (TV-102)	Separation of immiscible liquid mixtures.
SL-4 Liquid Films (TV-103)	Planar and 3-dimensional liquid films.
SL-3 Demonstration (Film 3589)	Diffusion, ice melting, and addition of soap, colored liquid and air to drop.

All of this data, except for Film 3589, was initially acquired with a TV camera and was recorded on magnetic tape. This information was later transferred to 16 mm film (usually called a kinescope copy). Film 3589 is the only exception, it was originally acquired on 16 mm film. Most of the film data has a sound track, so the observations and comments of the astronaut performing the demonstration are included.

Two of these data items, the Fluid Mechanics Series and the Liquid Floating Zone, consists of a number of reels of 16 mm film. This list of data amounts to approximately 3,600 meters of film. All data reduction for this effort was accomplished using the 16 mm film.

A complete listing of the data, with the identification number of each film reel and information regarding how copies of this film data can be obtained, has been compiled in Appendix A.

Each of the data items is briefly described in the paragraphs that follow:

1. Fluid Mechanics Series (TV-107)

The Fluid Mechanics Series is the most significant collection of data, both in size and the number of low-g fluid mechanics phenomena that were demonstrated. The series consists of approximately 1200 meters of film and it was performed during SL-4 by astronauts E. Gibson and W. Pogue.

Drops were oscillated at a number of different times during the series. Wires or syringe plungers were used to induce the oscillations. In some cases the drop was free floating when oscillated. In one sequence the drop was restrained by a thread so a close-up view could be obtained. The effects on the oscillation of an internal air bubble and soap in the liquid were demonstrated. In another sequence a single drop on a flat plastic surface (sessile drop) was perturbed in a number of different ways with a tube, with a syringe, by striking the surface with a wrench and by moving the surface. Drops were placed on various materials to demonstrate wetting. Using various means of inducing the motion, drops were set into rotation. Some of the sequences show how the astronauts formed, maneuvered and manipulated the drops.

The investigators for this demonstration were B. Facemire and O. Vaughan of NASA Marshall Space Flight Center (MSFC), Dr. S. Bourgeois of Lockheed Missiles and Space Co. (LMSC) and Dr. T. Frost of General Electric Co. O. Vaughan, in conjunction

with others, has written papers on specific demonstrations within the Fluid Mechanics series (Refs 1, 2, 3 and 4). There are some differences between the data presented in those papers and the results presented in this report, apparently due to some basic differences in the way the data was reduced and interpreted.

A preliminary analysis of most of the data in the Fluid Mechanics Series was performed by M. Klett and S. Bourgeois of LMSC (Ref 5).

2. Skylab SL-3 Fluid Mechanics Data

This data is identified in a number of ways since it includes all the fluid mechanics demonstrations performed on SL-3 by astronaut O. Garriott. The total amount of film is 450 meters in length. Included in this collection is one of the student experiments (ED-78, Liquid Motion) that was not successful. Some miscellaneous demonstrations in which the astronaut formed and maneuvered drops (TV-71) are also included. In one sequence a drop on a tube was oscillated, filled with air and maneuvered. Air was injected into drops and liquid was added to and squirted at drops. However, in most cases the image of the drop is small and the background is poor, making it difficult to observe the phenomena and make any measurements.

3. Liquid Floating Zone (TV-101)

This was a rather specialized demonstration aimed at determining the static and dynamic behavior of a liquid zone. It was performed by astronaut E. Gibson on SL-4. The liquid floating zone is one means by which metals can be melted and refined in low-g without a container. The zone was simulated by a cylindrical column of liquid suspended at its ends between two parallel disks.

By rotating the disks independently or simultaneously, the dynamic stability of the zone was demonstrated. It was also oscillated longitudinally. The zone was formed by joining drops placed on each disk. Before the zone was formed these sessile drops were oscillated. The coalescence of the two drops to form the zone is also part of the data. By using two differently colored drops, mixing can be observed following coalescence, during rotation and oscillation. Rope fibers were also added to the zone to detect the internal circulation.

Air bubbles were added to the zone. In one sequence the zone was initially ice, and its behavior as it melted was demonstrated.

This demonstration consists of 1200 meters of film. In all the tests the image is large and there is a good background. The sound track provides the pertinent parameters for each sequence and valuable comments from the astronaut.

The investigator for this demonstration is Dr. J. Carruthers of Bell Research Labs. He has written two papers presenting preliminary results of his analysis of the data (Refs 6 and 7) and plans to present another (Ref. 8). Dr. M. Klett of LMSC accomplished the data reduction and compilation for Dr. Carruthers (Ref. 9).

4. Immiscible Liquids (TV-102)

This demonstration, performed by astronaut W. Poque on SL-4 is on about 100 meters of film. Three vials, prefilled with immiscible oil and water, were assembled in a frame and the method of centrifugally separating the liquids was demonstrated. The two liquids were then mixed and viewed for a short period to observe any separation. Longer term experiments were accomplished, but were documented with a still camera.

The investigators for this demonstration are Dr. L. Lacy of NASA MSFC and Dr. G. Otto of the University of Alabama. They have written two papers on the demonstration (Refs 10 and 11), with the latter adding to the analysis presented in the first.

5. Liquid Films (TV-103)

Thin liquid films were formed on wire frames in this demonstration by astronaut G. Carr. Films were formed on a wire hoop using both plain and soapy water. The hoop was expanded until the film ruptured. Similar films were formed on a rectangular frame with one sliding side. Three-dimensional films were formed on wire frames in the form of a tetrahedron and cube.

The principal investigator is W. Darbro of NASA MSFC, who has published a report on the demonstration (Ref. 12).

6. SL-3 Demonstration (Film 3589)

On SL-3 astronaut J. Lousma performed a diffusion and ice melting experiment. It was photographed with a 16 mm camera

operating at 2 frames per second, starting and stopping as required. A tape measure, thermometer and stop watch were all in the field of view, but unfortunately slightly out of focus. The film is about 60 meters in length.

A diffusion experiment, in which a concentrated solution of tea and water was placed on water, was performed three times with the last one being the most successful. During this same period an ice cube on a stick was placed in the field of view of the camera so the melting of the ice could be observed. After the ice had melted, soap and a red colorant were added to the water drop. The drop was perturbed and oscillated as it sat on the stick. Air was injected onto the drop, producing a foam.

The investigator for the diffusion experiment is B. Facemire of NASA MSFC and the results are presented in Reference 13. The investigators for the Ice Melting experiment are Dr. G. Otto of the University of Alabama and Dr. L. Lacy of NASA, MSFC who have written a paper on the experiment (Reference 14).

In addition to the above data, that was intended as low-g fluid mechanics demonstrations, the vast collection of video tapes from the Skylab missions was reviewed to see if any interesting fluid mechanics phenomena might be found. A few pertinent sequences were found.

One was Blood Sampling (TV-4) that has a short sequence in which there is a closeup view of the transfer of blood from a syringe to an evacuated tube. Another was the film of the bag of water, that included a number of air bubbles, for the Fish Otolith demonstration (TV-53).

A general description of the purpose, apparatus and some preliminary results of all the SL-3 and SL-4 science demonstrations can be found in Reference 13.

B. DATA REDUCTION

One of the first steps in the evaluation of the fluid mechanics data was its reduction to measurable quantities wherever this was possible. The format of the data acquired using the television camera is discussed and the accuracy and techniques used in measuring parameters from the film are presented in the following paragraphs.

1. Television Data Format

Some description of the process used to transfer the data from magnetic tape to film is required since the process has a significant effect on the quality and content of the data. Figure 1 is a simplified diagram of the three formats in which the data is available. It illustrates the two conversion processes required to transfer the data to film. The Skylab television cameras used a field sequential format in order to make the camera simple and compact. The color television camera is only a black and white camera with a color wheel that successively places red, green and blue filters in front of the video tube. The intensity of the black and white image is varied by the filter. A new image, with each successive filter, is formed every one-sixtieth of a second. The data was acquired in this format and stored on magnetic tape in Skylab. It was transmitted from Skylab to a ground station and relayed to the NASA Lyndon B. Johnson Space Center where the information was again placed on magnetic tape.

This tape can be played back on a video tape player that operates using the field sequential format, and a color image is formed by the successive overlaying of the three color fields. If the optical image that was recorded was static or moving slowly, the successive images exactly overlay one another and an accurate reproduction of the color is possible. However, only a single color will be recorded at any position of a rapidly moving object, so the colors will not overlay one another during playback. This does not happen with the format used for standard commercial color television (NTSC format) because the three colors are simultaneous whenever they are recorded or played back.

The first conversion the data underwent was a conversion from field sequential format to the NTSC (standard color TV) format. This is a purely electronic process making use of delay lines. In the NTSC format a new image is formed every one-thirtieth of a second. A single NTSC frame is formed from three consecutive frames (a red, blue and green) from the field sequential data. As shown by Figure 1, this is done by merging the two current frames with the one previous field sequential frame and creating one NTSC frame. Due to this process each field

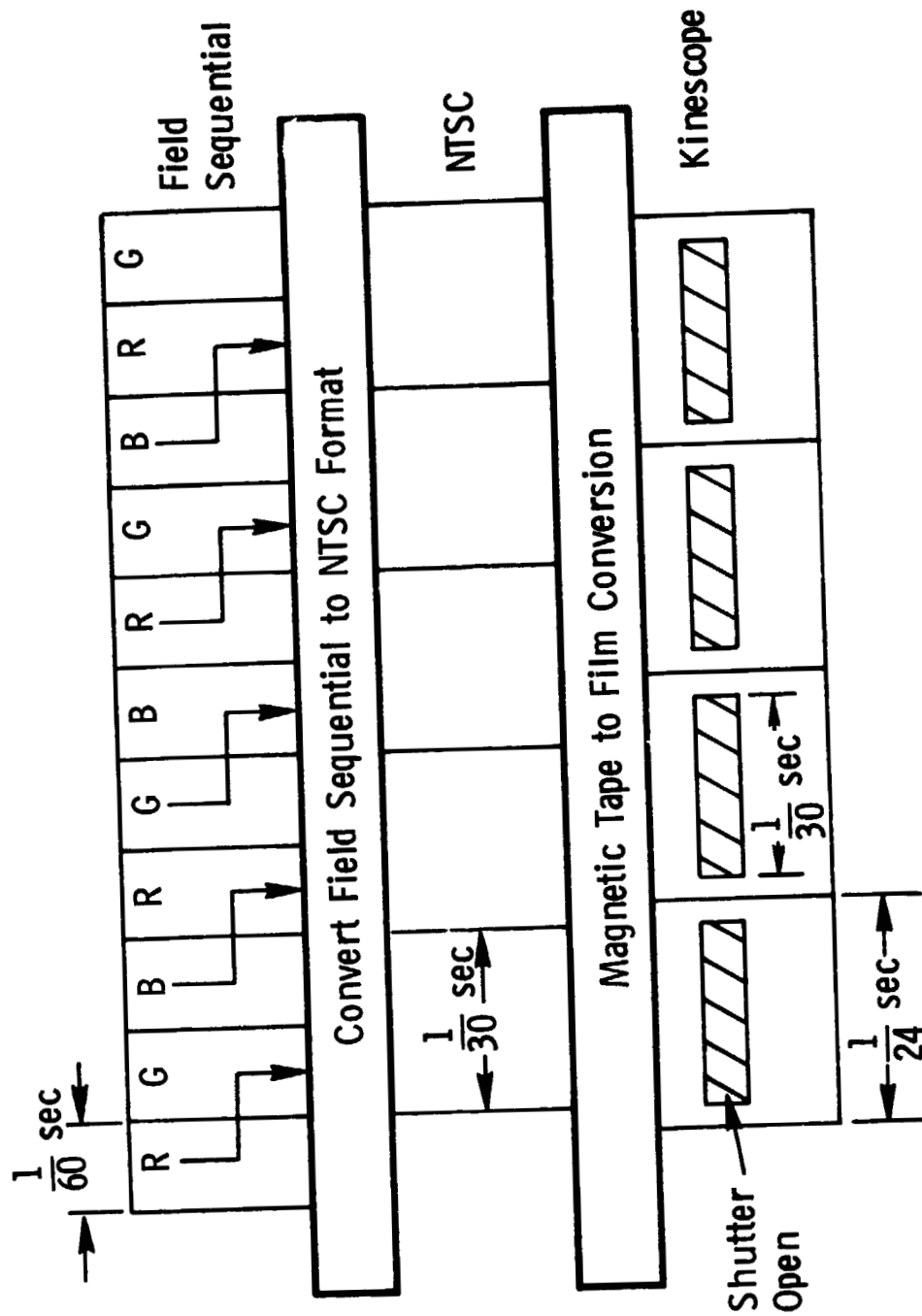


Figure 1. Data Format

ORIGINAL PAGE IS
OF POOR QUALITY

sequential frame is held for a period of three - sixtieths of a second so the three colors can be merged. If the object is static or moving slowly, the effect of this process is not evident when the images from the NTSC tape are displayed. For a fast moving object, the colors will be smeared to a greater extent than they are with the field sequential tape. The additional smearing is due to the added period that each frame of the field sequential tape is retained.

The next step in the process was the transfer of the data from the NTSC tape to 16 mm film, the kinescope. This was accomplished at the NASA George C. Marshall Space Flight Center. Sound movie projectors operate at 24 frames per second so a conversion from a one-thirtieth of a second frame of the NTSC tape to a one-twenty-fourth of a second frame is part of the process. A film camera views a cathode ray tube on which the image from the NTSC tape is formed. The camera shutter is electronically synchronized with the tape. Figure 1 shows that the camera shutter is open for a one-thirtieth of a second period during each one-twenty-fourth of a second frame (Ref. 15). While the shutter is closed the film is pulled down so the next frame can be exposed. Additional smearing of the image is introduced here because a film frame can overlap two frames of the NTSC tape. The manner in which the NTSC frame is formed on the cathode ray tube by sweeping an electron beam and the persistence of the phosphor of the cathode ray tube are other factors that influence the smearing.

The implication of these conversion processes on the data reduction using the kinescope film is that the color smearing can produce a distorted image of any moving object. Depending upon the parameter being measured, the data reduction process must consider the effects of the image smearing. The obvious conclusion from this evaluation of the various forms of the data is that the data reduction would be best accomplished using the field sequential tape. This would require a field sequential type tape player that is capable of displaying a single frame at a time. Since such equipment was not available at Martin Marietta, the kinescope film had to be used. Only in certain cases, where it was necessary to view a rapidly moving object, did the use of the kinescope film impose any limitation on the data reduction process.

2. Measurable Parameters

A film analyzer was used to accomplish the data reduction. This projector is capable of projecting a single film frame or projecting at various rates up to 24 frames per second. The image size projected was varied as required to obtain the necessary resolution. Using this analyzer the phenomena could be observed first in real time (24 frames/sec), observed at a slower rate, to take a more detailed look at the phenomena, and then viewed frame-by-frame to make the measurements.

One of the most basic measurements made was the relative size of objects within a single film frame. This is a dimensionless measurement, not requiring any scaling. The image size within the frame is one factor influencing the accuracy of this type of measurement. This can be improved by increasing the size of the projected image. However, a television image consists of 525 discrete lines, so the resolution of the projected image from the film is limited.

If the object was moving, the smearing of the image due to the data conversion processes will also affect this type of measurement. Measurements along the direction of motion can not be very accurate. When measuring oscillation amplitudes, there was a momentary pause as the velocity reached zero and amplitude reached a maximum. There was a noticeable improvement in the resolution of the image at this point because there was no smearing, making it possible to make a more accurate measurement.

Another significant factor influencing any measurements of size is the fact that a two-dimensional image of a three-dimensional scene is being used. Two separate measurements can only be compared when their relative separation in the direction perpendicular to the plane of the image is known. Usually the location of the object in the third dimension was difficult to discern.

Dimensions can be applied to the measurement only if the size of some object in the field of view is known. The object of known size must be in the same plane, parallel to the image plane, or the distance between the objects in the third dimension must be known. A scaling factor was established from the object of known length and was applied to the measured lengths. Objects such as syringes and food cans, that appear in the field of view, were used to determine the scaling

factor. The most common dimensional measurement, involving length, in the data reduction was the determination of the volume of a drop of liquid. Since this measurement involves the length cubed, accuracy becomes very critical.

The frame rate of the film provides the time base for any time dependent measurements. Each frame represents a period of one-twenty-fourth of a second. By counting the number of elapsed frames, and dividing by 24, the number of elapsed seconds is established. Oscillation frequencies and rotation rates were determined in that manner. Oscillation frequencies were on the order of 1 Hz, so fairly good resolution of the time was possible. If the oscillation rate remains fairly constant, the number of frames can be counted over a number of cycles, improving the resolution of the frequency.

Measurements of velocity involve both length and time. Care must be taken to account for the image smearing of the moving object so the length measured corresponds to the time period represented by the frame.

C. PROPERTIES OF WATER

The test liquid used in most of the demonstrations was water. One exception is the Immiscible Liquids demonstration in which oil was one of the liquids. Water was a readily available liquid in Skylab and does not present any hazards. Ink, grape drink and strawberry drink were added to color the water. The colorants reduced the transmission and reflection of light, improving the image. Soap was added to the water to change its properties. Four properties of water were used in the correlation of the data: density, viscosity, surface tension and contact angle.

The density of water is insensitive to the additives and the fluctuations in temperature that occurred in Skylab. A density of 1.0 gm/cc was used in all the correlations.

Viscosity would only be influenced by the addition of soap, and then it would be dependent upon the concentration. A viscosity of 1.0 centipoise was used in the correlations, when soap was not present.

Very few liquids (other than liquid metals) have a higher surface tension than water. Pure water has a surface tension of 72 dynes/cm. Since water has such a high surface energy, it is readily contaminated and a considerable lowering of the surface tension takes place (Reference 16). Contaminants that lower the surface tension of a liquid are referred to as surface active agents. A small amount of a surface active agent will impose its low surface tension on a liquid of much higher surface tension. As the concentration of the impurity is increased the surface tension of the solution decreases until it becomes saturated. Further addition of the impurity does not cause any change in surface tension (Ref. 17).

The surface tension of water with grape and orange Tang (trade mark General Foods Corporation, representative of fruit drinks used on Skylab) was measured. It was found that adding a minute amount of orange to water, barely coloring it, caused a reduction in the surface tension to 61 dynes/cm. One teaspoon of orange in 200 ml of water, giving a coloring as it appeared in the film, reduced the surface tension to 53 dynes/cm. Adding more did not produce any further change in the surface tension. Grape has less of an effect on surface tension, reaching a minimum at 60 dynes/cm.

Marker pens, the same as those used on Skylab, were provided by NASA Johnson Space Center so that the effect of the ink on surface tension could be determined. It was found that the ink is a mild surface active agent. In small concentrations, coloring the water as it appeared on the films, the surface tension was only slightly reduced to 70 dynes/cm. The surface tension continued to decrease as larger amounts of ink were added.

Adding soap of the type used on Skylab to water, in approximately the concentrations used in the demonstrations, reduced the surface tension to 20 dynes/cm (data provided by NASA Marshall Space Flight Center).

The contact angle is the angle formed by a liquid and a surface which it contacts, measured within the liquid. A wetting liquid spreads on a surface and has a contact angle of near zero. Pure water on a clean surface, such as a metal, can have a near zero contact angle. The contact

angle is a function of the relative surface energies of the liquid and the surface. Metals have a higher surface energy than water, so the contact angle will be near zero. Any impurities such as oil or grease on a surface, reduce its surface energy and water can have larger values of contact angle. Plastic has a relatively low surface energy so the contact angle of water on plastic will be large. Therefore, the contact angle for water cannot be specified unless the exact nature of the surface is known.

D. SKYLAB ENVIRONMENT

The acceleration environment of the Skylab was evaluated to determine if it would have any influence on the fluid mechanics demonstrations. An acceleration, due to atmospheric drag on the Skylab on the order of $10^{-5}g$ was always present. "G-Jitter" due to various disturbances such as movement of the astronauts or operation of the attitude control system, produced accelerations as large as $10^{-3}g$. The frequency of the G-Jitter could range from one to several thousand Hertz (Ref. 18).

If a drop of liquid was free-floating it would not sense these accelerations. Only when the liquid was directly in contact with Skylab, such as a drop on a surface or a drop on a thread (where the thread was attached to Skylab), would these accelerations be transmitted to the liquid. For the volumes of liquids used in the demonstrations, the gravity forces due to these accelerations were very small in comparison to the surface tension forces. The Bond number, the ratio of gravity forces to surface tension forces, provides an indication of the relative size of the two forces. Based on the radius of a typical water drop used in the demonstrations, the Bond number is on the order of 10^{-2} showing that surface tension forces do dominate.

Another source of perturbations due to the Skylab environment was the flow of air of the ventilation system. Measurements of the air velocity in the vicinity in which the demonstrations were performed were made. Values on the order of 0.5 cm/sec were obtained using a 0 to 50 cm/sec velocity meter with a 5% accuracy. Considering the accuracy of the meter, velocities as large as 2.5 cm/sec were possible. It should be noted here that Skylab air consisted of approximately 70% oxygen and 30% nitrogen at a total pressure of 3.4 N/cm².

Free-floating drops would be carried along with the air flow. Air flowing around a restrained drop, such as a drop on a thread, can cause distortion of the drop from its spherical shape. It will distort from a sphere to an oblate spheroid and some flattening of the leading surface of the drop will also occur (Ref. 19 and 20). The distortion of a drop, falling at its terminal velocity in one-g has been correlated, but such results can not be readily applied to this case. The Reynolds number gives some indication of the amount of distortion that would be present (Reference 21). Reynolds numbers based on the largest value of air velocity (2.5 cm/sec) are about 100, indicating that the distortion would be slight. The presence of surface active agents tends to reduce the distortion (Reference 20) but the shape is determined primarily by the hydrodynamic forces and the static surface tension, and to a lesser extent by the presence of surface active molecules along the surface (Reference 19).

III. INVESTIGATIONS

In this chapter the specific investigations that were accomplished, using the identified data, are presented. Each investigation considers a phenomenon of fluid mechanics that was demonstrated. In each case the phenomenon is explained and if measurable data could be derived from the film, it is presented. The data is correlated with available theory, obtained from the literature search, wherever possible.

A. Static Interface Shape

One objective of the Fluid Mechanics Series demonstration is to show the static interface shape assumed by a liquid in contact with various solid surfaces in a low-g environment. The analysis of the observed interface shapes shows that surface energy and contact angle are important parameters. Correlation between calculated and observed interface shapes was possible.

The shape of a gas-liquid interface in low-gravity (gravity forces are negligible) is determined solely by capillary forces. Surface tension and contact angle, if the liquid is in contact with a solid surface, are the properties of the liquid that establish the interface shape. The Young-Laplace equation relates these properties to the curvature of the interface and the pressure differential between the gas and liquid as follows:

$$P_L - P_G = \sigma \left(\frac{1}{R_1} + \frac{1}{R_2} \right) \quad (1)$$

where the subscripts L and G refer to the liquid and gas respectively, and R_1 and R_2 are the radii of curvature of the interface. The sign convention for the radii of curvature is that they are positive when their center of curvature is within the liquid. The sum of the reciprocals of the radii, $(1/R_1 + 1/R_2)$, is referred to as the curvature of the interface (Ref. 22).

Under static conditions the pressure of the gas in contact with the liquid is uniform over the entire liquid surface. An equilibrium interface will be established when the pressure in the liquid is also uniform and the pressure differential defined by equation (1) is a constant. If the pressure difference is constant, then the curvature must also be uniform over the entire surface.

Considering a globule of liquid in low-gravity, not in contact with any surface, the requirement of uniform curvature can only be satisfied if both radii of curvature are equal. The globule then has the form of a sphere, with the radii of curvature equal to its radius. Equation (1) simplifies to:

$$P_L - P_G = \frac{2\sigma}{r} \quad (2)$$

where r is the radius of the sphere. The pressure within the drop of liquid is greater than the surrounding gas by an amount that is directly proportional to the surface tension and inversely proportional to the radius of the drop.

When the liquid is in contact with a surface, the determination of the interface becomes more complex. The curvature of the surface will still be a constant, but the two radii of curvature will vary over the surface. The usual approach to calculating the interface shape is to define the curvature in terms of some coordinate system, taking advantage of any symmetry. A differential equation for the interface is obtained that can be either solved directly or solved using numerical methods. The shape of the interface is independent of the value of the surface tension in zero-g, since the equation is of the form: curvature equals a constant. Contact angle is a boundary condition that must be satisfied by the equation.

The surface energy of the interface of a gas, liquid and solid is a useful parameter. Surface energy is defined as the sum of the surface energy of three interfaces: liquid-vapor (LV), solid-vapor (SV), and solid-liquid (SL) (Ref. 23). Therefore

$$\text{Surface Energy} = \sigma_{LV} A_{LV} + \sigma_{SV} A_{SV} + \sigma_{SL} A_{SL} \quad (3)$$

where A is the area of the respective interface. The surface tensions of the solid-vapor and solid-liquid interfaces are not well understood and are difficult to measure. The Young equation eliminates these difficulties by providing a relation between these surface tensions which is valid for a solid that is not easily deformed and is smooth.

$$\sigma_{LV} \cos\theta = \sigma_{SV} - \sigma_{SL} \quad (4)$$

Where θ is the contact angle between the liquid and solid as defined in Chapter II. Substituting the Young equation into equation (3) yields

$$\text{S.E.} = \sigma_{LV} (A_{LV} - A_{SL} \cos \theta) + \sigma_{SV} (A_{SV} + A_{SL}) \quad (5)$$

The term on the right of the equation can be treated as a constant since the area of the solid is a constant. For the purpose of this discussion that term can be neglected, so

$$\text{S.E.} = \sigma_{LV} (A_{LV} - A_{SL} \cos \theta) \quad (6)$$

A capillary area can be defined as follows:

$$A_C = A_{LV} - A_{SL} \cos \theta \quad (7)$$

for any given interface. So the surface energy can be further simplified to

$$\text{S.E.} = \sigma_{LV} A_C \quad (8)$$

While the Young-Laplace equation (equation (1)) can define more than one interface for any given set of conditions, the equation for surface energy defines the preferred configuration. A stable interface shape is achieved when the surface energy is a minimum.

Again consider a free-floating globule of liquid. The surface energy will be a minimum when the capillary area, which is the area of the liquid vapor interface in this case, is a minimum. That area is a minimum when the globule assumes a spherical shape, which again confirms that this is the static shape assumed by a liquid drop.

If liquid is in contact with a solid surface, it can be shown (Ref. 34) that the capillary area is less than it was when the liquid was not in contact with the surface. Therefore, contact

with a surface is a preferred equilibrium configuration for a liquid drop. This decrease in surface energy accounts for the adhesiveness of a liquid on a surface. Energy must be added to remove a drop from a surface.

Free-floating drops of water appear in many different places in the fluid mechanics film data (Figure 2). In none of these sequences was the drop ever static. The drops were of the spherical form, but oscillations were present. Perturbations induced when the drop was formed damp very slowly. Since the drops drift with the circulating air, the drop would contact a surface before a completely static interface could be achieved. These factors made it difficult to perform and photograph some of the demonstrations.

Drop on a Thread

The astronauts found that a liquid drop could be restrained by placing it on a thread (Figure 3). The adhesive capillary force between the drop and the thread was sufficient to overcome small perturbing forces. Damping was increased by the thread, as will be discussed under the oscillating drop, so a static interface shape could be achieved.

In the fluid mechanics series, drops of 30, 50 and 100 cc were placed on a thread so as to perform the oscillating drop and coalescence demonstrations. While the drop did come off the thread due to some severe perturbations, in most of the demonstrations it was strongly retained by the thread. In those sequences the drop centered on the thread, so the thread was an axis of symmetry.

Where the liquid interface contacts the thread, the boundary condition of contact angle must be satisfied. Therefore, rather than being completely spherical, there was some distortion of the drop shape due to the thread. When the drop was centered on the thread, as shown in Figure 4a, the curvature of the interface is uniform around the thread (and over the entire surface) and the pressures are uniform. If some external force caused a displacement of the drop from the centered position, as shown by Figure 4b, the curvatures are no longer constant. On the side of the thread towards the center of the drop the interface will be more sharply curved (larger curvature) than it is on the far side. Therefore the pressure in the liquid is less on the side of the thread near the drop center. A net force acts to return the drop to the centered position.



Figure 2. Free Floating Water Drop

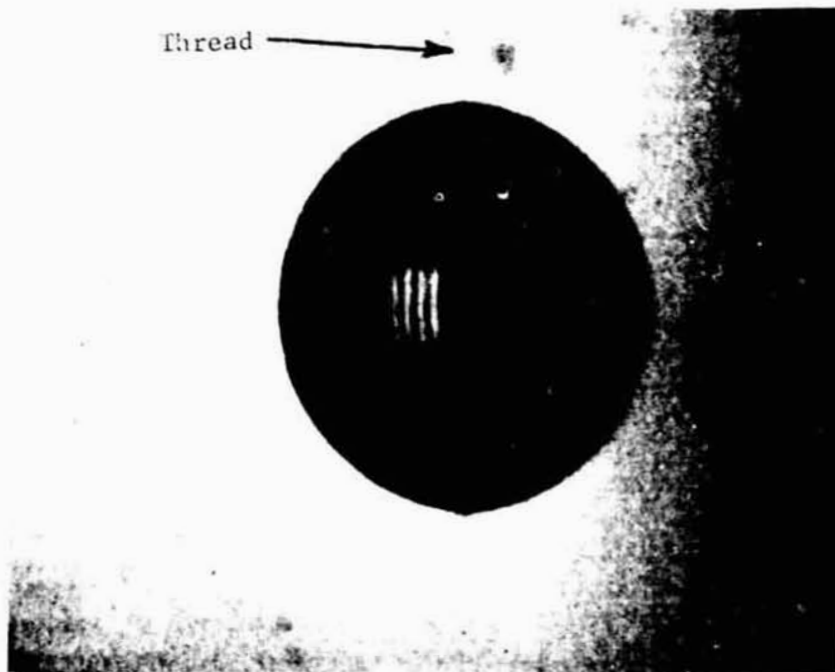
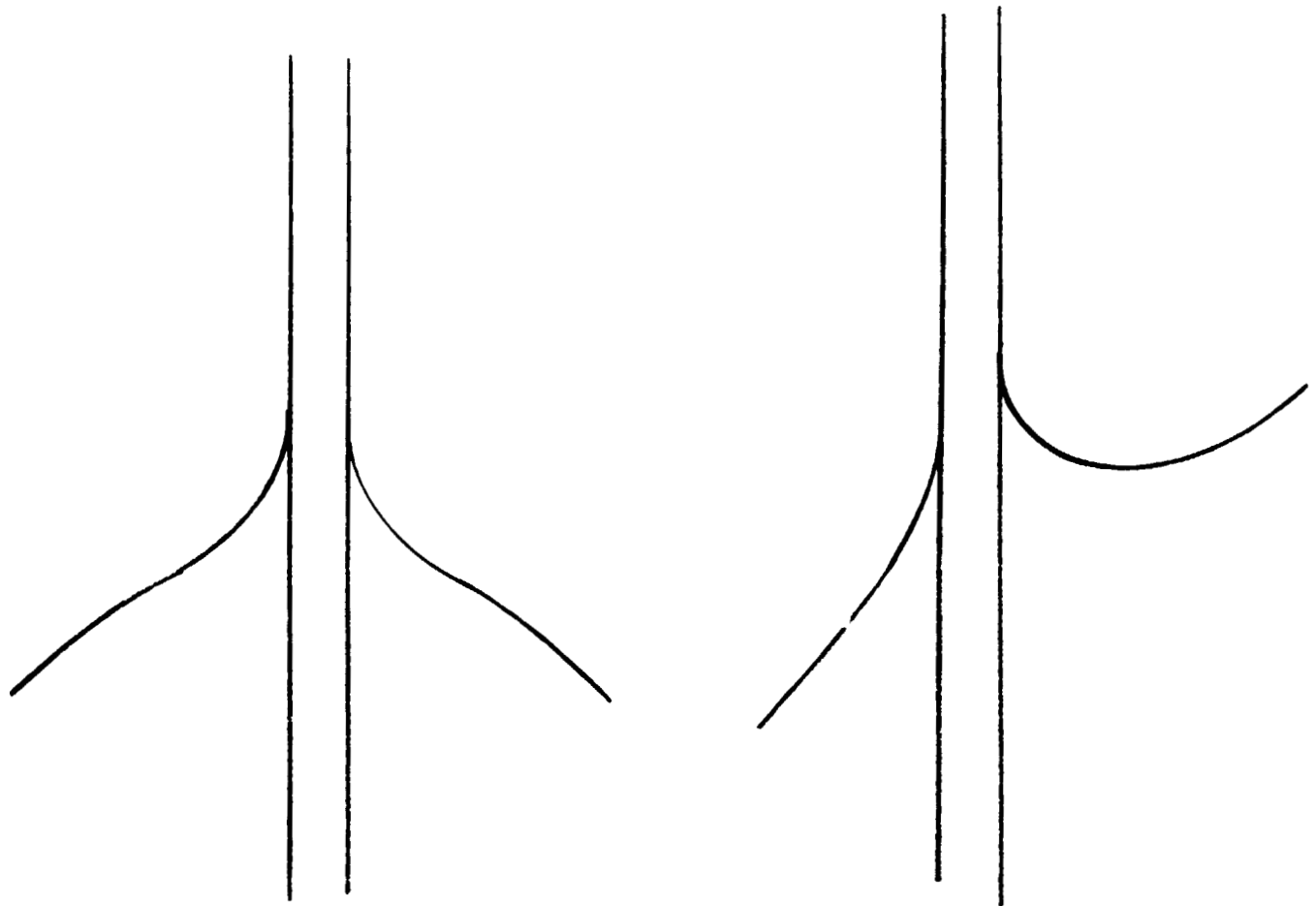


Figure 3. Water Drop Colored with Ink
and Tethered with Thread



a. Centered

b. Displaced

Figure 4. Interface of Drop at Thread

The behavior of an interface, where it meets a surface, provides a force to restrain the drop from moving along the thread. When an interface is displaced along a surface, the contact angle does not remain the same as its static value. There is a hysteresis to the contact angle, so contact angle increases as an interface advances or decreases as the interface recedes. This "sticking" of the interface must be overcome before movement of the drop along the thread can occur. The sticking is most pronounced for an advancing interface if the surface over which the interface must move is completely dry. Once the surface is wetted, a film of liquid will remain on the surface and the sticking is reduced.

Displacement of the drop perpendicular to the thread is opposed by the capillary forces produced by the curvature of the interface of the drop. Axial displacements are opposed by the hysteresis of the contact angle. Together, these two forces keep the drop oriented on the thread.

The effect of the thread on the interface of the drop was more than just a disturbance limited to the vicinity of the thread. The drop was elongated, in the direction of the thread, by 5 to 6% in comparison to its diameter. Instead of a sphere, the drop was more a prolate ellipsoid, with the thread being the axis of symmetry.

A computer program was written to calculate the shape of the interface of a drop centered on a thread. (The derivation of the equations used in the computer program is presented in Appendix B). Drop volume, thread diameter and the contact angle are the parameters that determine the interface shape. The volume of the drop was stated on the sound track and the thread diameter could be scaled from the known drop diameter. As discussed in Chapter II, contact angle is a difficult parameter to specify, especially for water on a fibrous and water saturated thread. Using the known volume and a measured thread diameter of 1mm, interfaces for various values of contact angle were calculated. The calculated elongation was compared with the measured elongation. This comparison was accomplished by ignoring the small protrusion of the interface at the thread, since it was difficult to discern in the film.

The calculated shape of the drop on a thread is shown in Figures 5 and 6 for volumes of 50 and 100 cc respectively. It was found that the proper calculated elongation could be obtained when a contact angle of 30 degrees was used, which is a

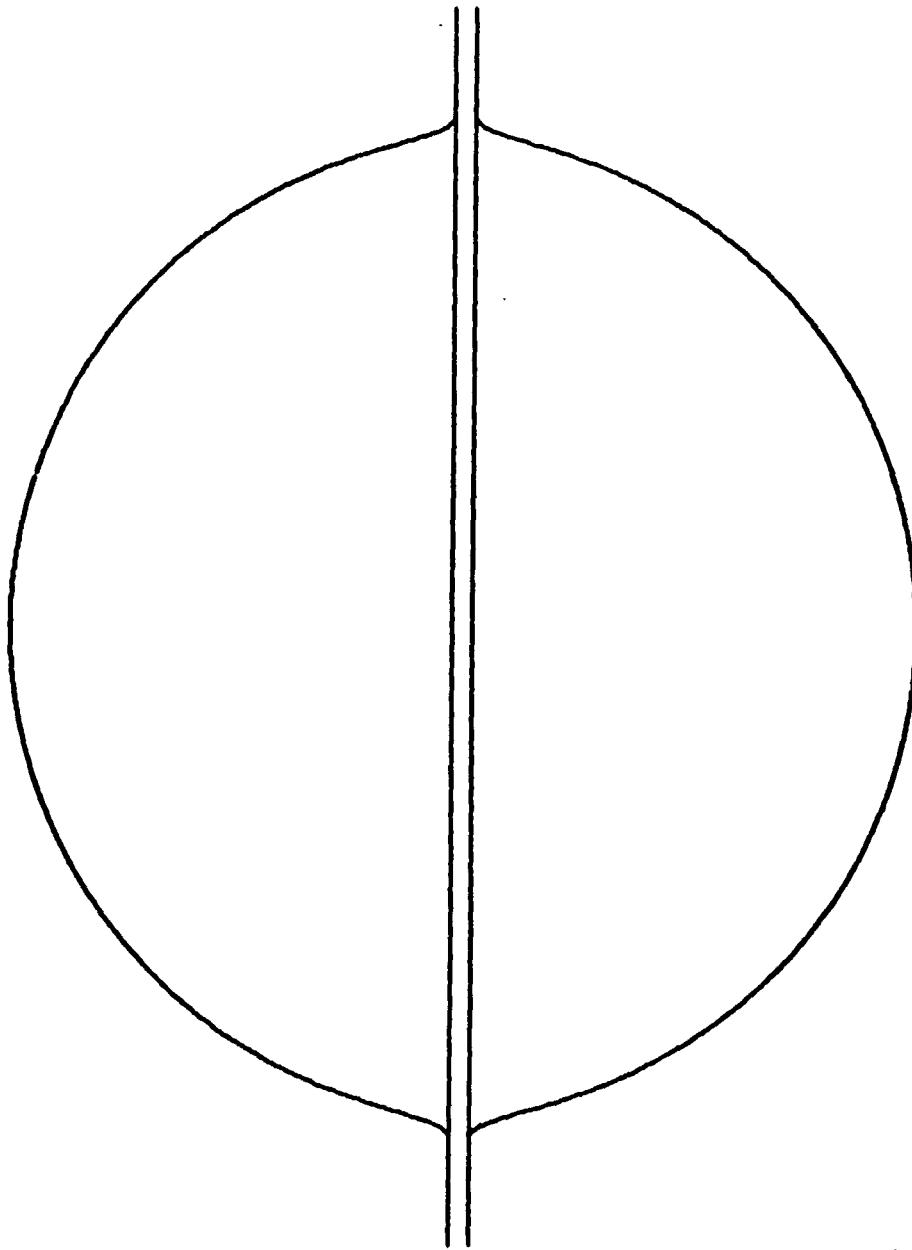
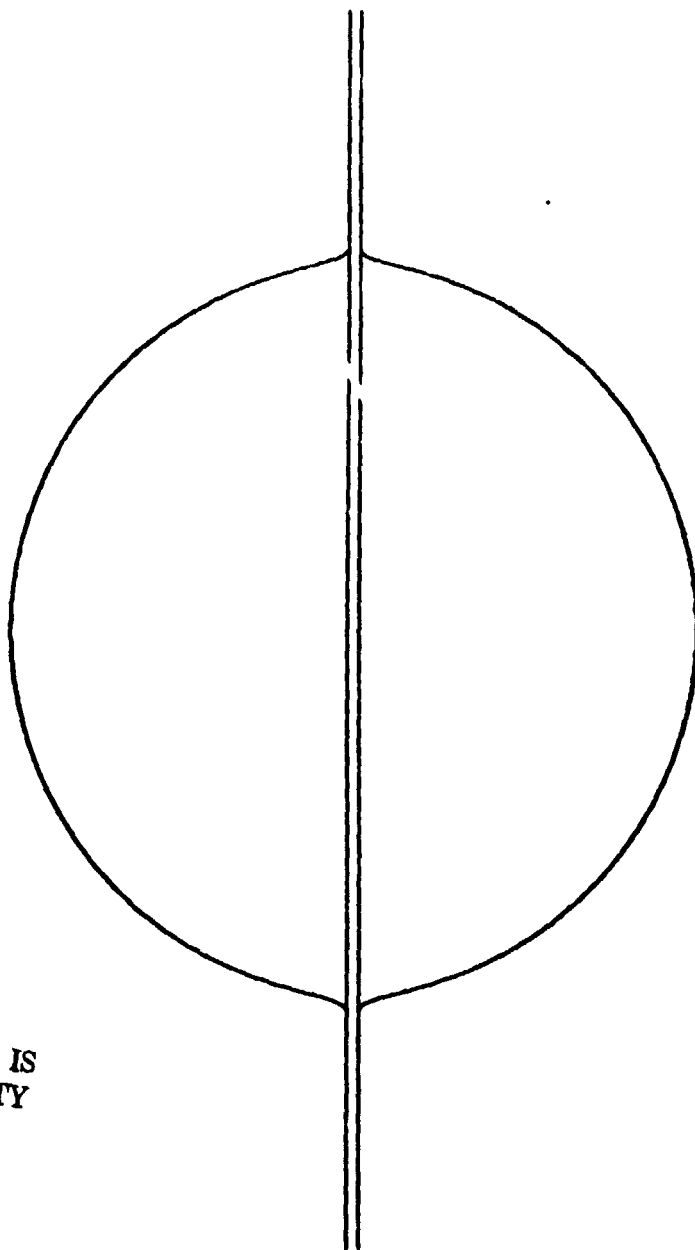


Figure 5. Calculated Shape of Drop on Thread, 50 cc Volume,
30° Contact Angle, 1 mm Thread Diameter



ORIGINAL PAGE IS
OF POOR QUALITY

Figure 6. Calculated Shape of Drop on Thread,
100 cc Volume, 30° Contact Angle,
1 mm diameter Thread

reasonable value for water in contact with a material such as thread. The calculated and measured length to diameter ratio for the 50 cc drop is 1.06. For the 100 cc drop the distortion is slightly less and equal to 1.05.

For a thread diameter of 1 mm, the ratio of the drop to thread diameter ranged from 40 to 60 for drop volumes of 30 to 100cc. All of these drops centered on the thread. Small drops were shown to establish an interface shape that was tangent to the thread. This was demonstrated in the Fluid Mechanics Series data and in some of the SL-3 data (Figure 7). While the drop volume was not known for any of these sequences, the image size was sufficiently large during one of the sequences in the SL-3 data to make a relative measurement of the drop and thread diameter. The ratio was measured as 20.

The reason that this occurred involves the concept of capillary area and minimum surface energy. Surface energy varies as a function of thread diameter for both orientations: drop centered on the thread and drop tangent to the thread. For a given drop volume and thread diameter, the orientation that has the smaller capillary area determines which of the two orientations the drop will assume. Based on the data, if the ratio of drop to thread diameter was around 40 or more, the drop centered on the thread because that orientation had the smaller capillary area. When the ratio was 20 or less, the drop was tangent to the thread and that orientation gave the minimum capillary area. Somewhere between 40 and 20 there is a transition from one orientation to the other. No other data was available to further define when the transition occurs. Since capillary area is a function of contact angle, the above conclusions are valid only for contact angles of approximately 30 degrees.

Near the transition point from one orientation to the other, it would be expected that either orientation could be assumed and a small perturbation would drive the drop from one to the other. For the drops observed on the films, they behaved as if only one equilibrium configuration was possible. As a large drop was brought into contact with the thread, its surface freely passed through the thread. It would overshoot the centered position as the capillary forces acted to center the drop. Small drops could be strongly perturbed but they would continue to set tangent to the thread.

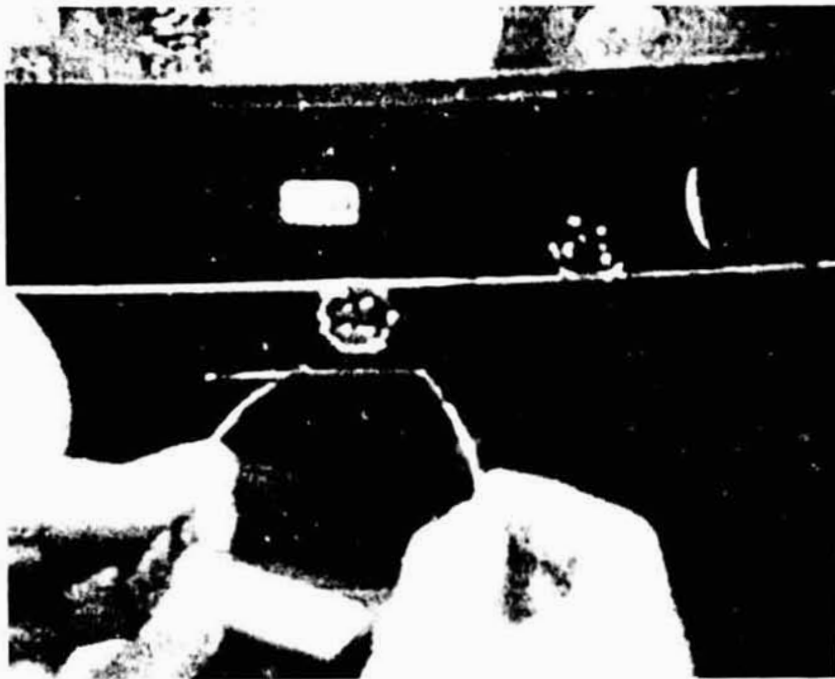
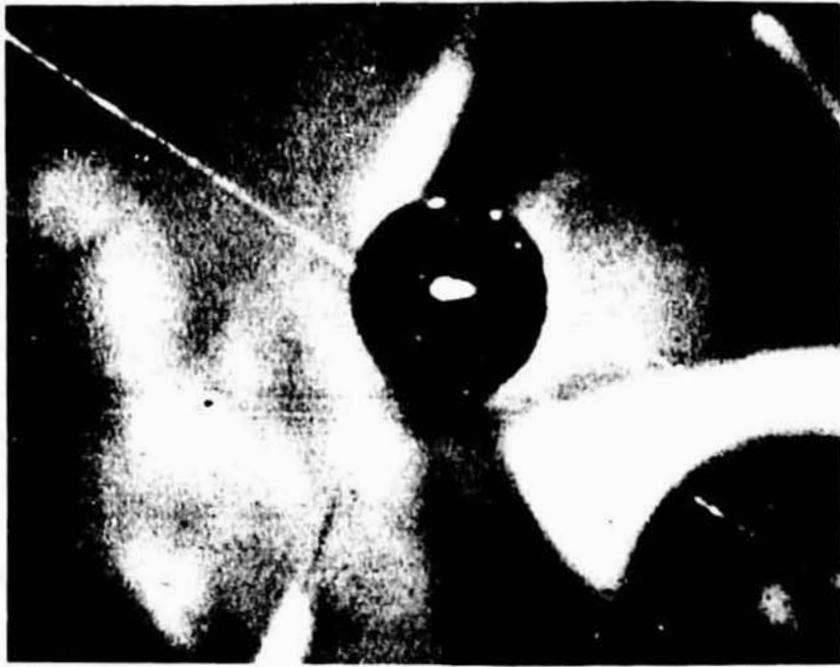


Figure 7. Smaller drops will assume an interface shape that is tangent to the thread.

The computer program used to calculate the shape of the drop on a thread was used to investigate the influence of thread diameter and contact angle on the equilibrium configuration of the drop interface. Only half of the problem can be exactly analyzed since we did not develop a way to calculate the three-dimensional drop shape when it is tangent to the thread. By making some assumptions about the effect of a thread tangent to the drop, the general behavior of the drop can be established.

The interface of a drop centered on the thread was calculated for a given set of conditions and then its capillary area was calculated. Figure 8 shows how the capillary area of the drop is changed by the thread diameter at a contact angle of 30 degrees. The capillary area and the thread diameter are ratioed to the area and diameter respectively, of a free floating spherical drop. Based on data from both 50 and 100 cc drops, it appears that the curve is independent of drop volume.

When the thread diameter is very small, the capillary area approaches the surface area of a free-floating spherical drop. Over a certain range of thread diameters, the capillary area decreases as the thread diameter increases, indicating a lower energy state in comparison to a free drop. Near a drop to thread diameter ratio of 20, the capillary area reaches a minimum and then increases with increasing thread diameter. At large thread diameters, interface shapes can be calculated that have a capillary area greater than that of a sphere. Obviously, these are not equilibrium interface shapes since a free drop would have a lower surface energy.

Similar curves could be produced for the case of the drop tangent to the thread. At small thread diameters these curves would lie above the drop-centered curves, indicating the drop-centered case is the minimum energy configuration. Somewhere after the minimum in the drop-centered curve, the two curves must cross and the drop-tangent configuration becomes the minimum energy configuration. The drop-tangent curve must become asymptotic to the surface area of a sphere at very large thread diameters. Based on the test data and the theory, an assumed drop-tangent curve is shown on Figure 8 for a contact angle of 30 degrees. Crossover occurs somewhere near a drop to thread diameter ratio of 15 to 1.

Contact angle was found to have a very strong influence on the point at which the minimum in the drop-centered curve occurs,

ORIGINAL PAGE IS
OF POOR QUALITY

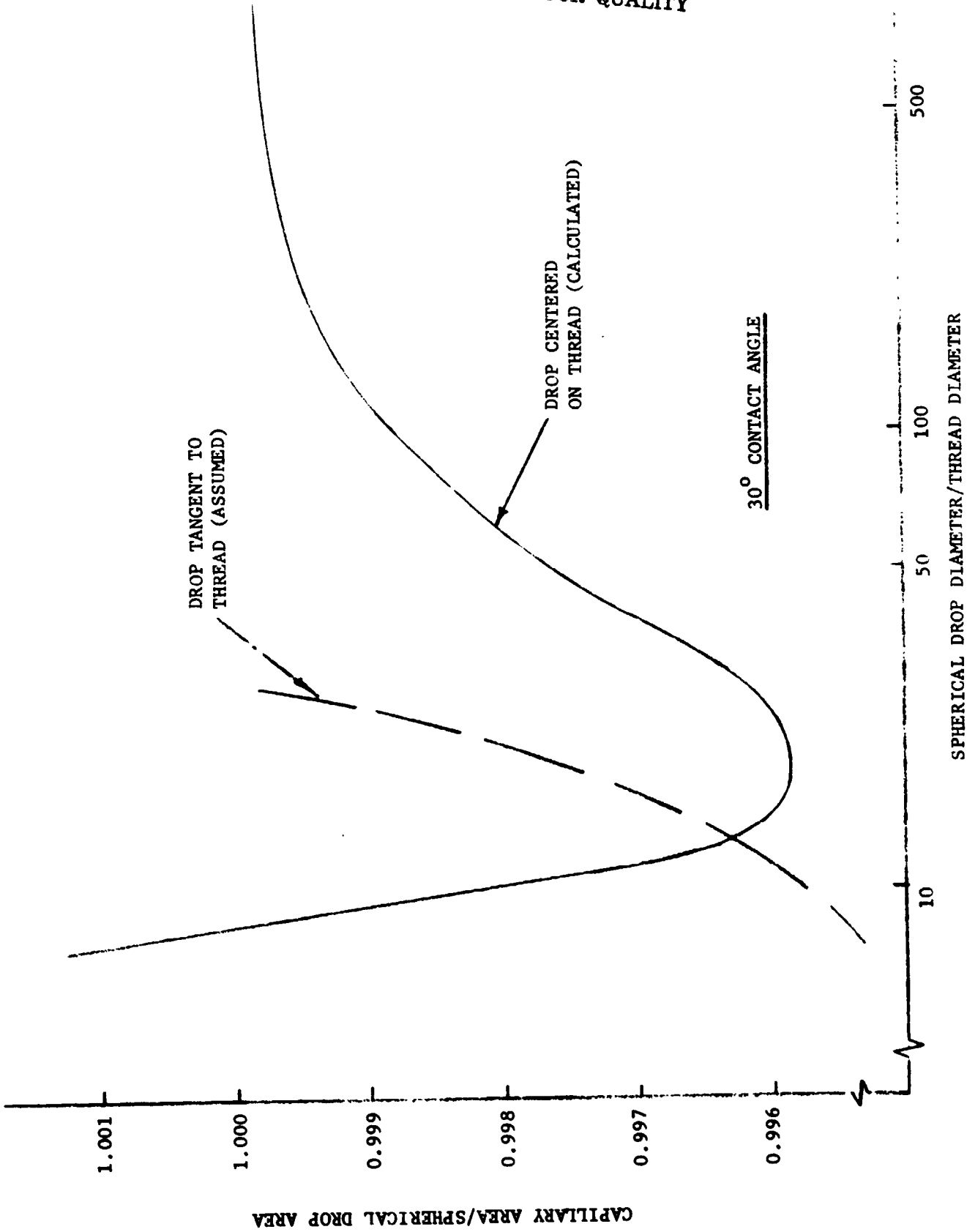


FIGURE 8. CAPILLARY AREA VS. THREAD DIAMETER

which should also influence the cross-over from the drop-centered to drop-tangent configuration. The form of the curve remains the same, but at a contact angle of 28° the minimum occurs at a diameter ratio of about 5000 and at a 32° contact angle it occurs at 0.7. If the contact angle had been much different from 30° only one equilibrium state would have been observed for the drops and threads used in the demonstrations.

The larger drops that centered on the thread were found to be laterally oscillating in a periodic manner about the equilibrium position. The drops would slowly drift first to one side of the thread and then to the other. This oscillation could be observed in a number of film data sequences. The amplitude of the oscillation was about 0.5 cm, measured perpendicular to the thread, and it remained fairly constant. The period of the oscillation was between 20 and 30 seconds per cycle.

Air flow must have been the source of the driving force for these oscillations, with the capillary force opposing the displacement. The air flow in the vicinity of the demonstration was in the direction of the axis of the thread, so periodic oscillations of the type observed could be induced. Capillary forces acting to center the drop are weaker than the resistance of the interface to displacement along the thread, so the disturbance of the air flow causes a lateral displacement. No axial displacement along the thread was observed.

Perturbations to the smaller drops that sit tangent to the thread caused them to rotate about the thread. The penetration of the thread into the drop remained relatively constant.

Drops on Various Surfaces

Other sequences in the Fluid Mechanics Series and the SL-3 data showed drops of liquid attached to other surfaces. In one SL-3 sequence a drop was oscillated and maneuvered on a tube. The tube was large in comparison to the drop so an interface with the drop tangent to the tube was formed.

The larger size of the tube, compared to the thread, permitted the distortion of the interface in the vicinity of the surface to be observed in detail. At every point the interface meets the tube, the contact angle must be the same and the curvature of the interface must be constant over the entire drop (Figure 9).

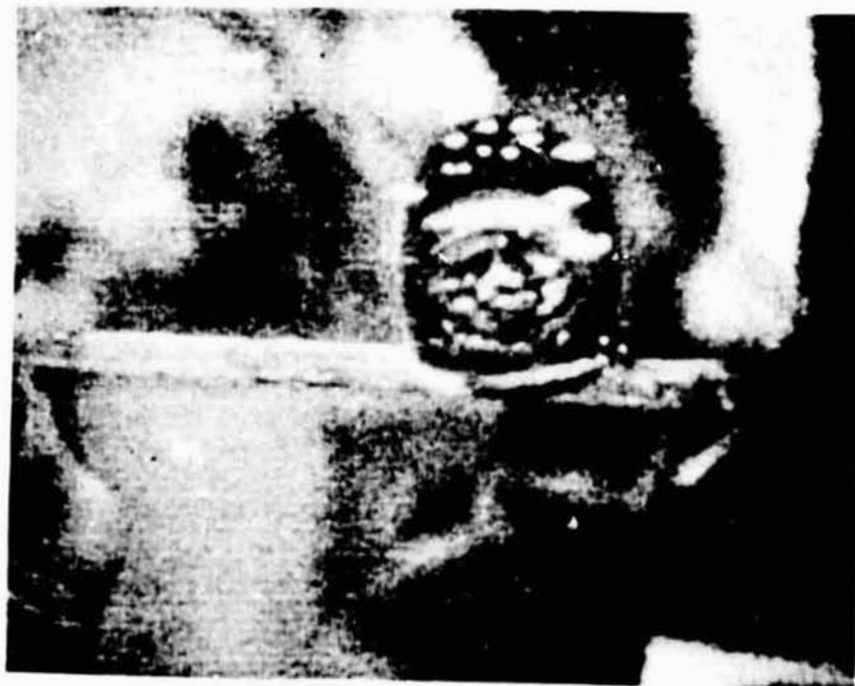


Figure 9. Drop on a tube

ORIGINAL PAGE IS
OF POOR QUALITY

A drop on a flat surface, referred to as a sessile drop, appeared in the Fluid Mechanics Series. The drop was approximately 50 cc in volume and was resting on a plastic surface. The contact angle in this case was near to 90 degrees. A hemispherical shape was assumed by the drop with a large circular area of contact between the drop and the surface (Figure 10). The shape of a drop on a surface can be calculated, knowing its volume and contact angle. Calculated sessile drop shapes presented in Reference 25 correspond to the observed shapes.

The astronauts took advantage of the adhesion between a surface and a drop in maneuvering them and inducing oscillations for the demonstrations. Syringe needles and wires served as a way of applying small forces to maneuver the drops. Many successive passes of a needle through a drop were required to produce a noticeable change in its momentum. By passing a string through a drop it could be pulled into its proper position and then the string could be carefully withdrawn. Only very low amplitude oscillations of a drop could be induced using wires and needles. Plungers from syringes, that have a circular disk on their ends, were brought into contact with the opposite sides of a drop and then pulled away. There was sufficient adhesion between the plunger surfaces and the liquid to produce the desired oscillation amplitude.

With each surface, thread, tube and flat sheet, the change in the adhesion of the drop to the surface could be observed. Only a small force was required to remove the drop from the thread. In one interesting sequence of the SL-3 data the astronaut tried to shake the drop off a tube, demonstrating its adhesiveness. A drop adheres very strongly to a flat surface. Large perturbations were applied to a sessile drop and they did not even produce a displacement of the line of contact between the interface and the surface. The adhesion between the sessile drop and a tube, and a needle can be observed in Figure 11.

In another sequence of the Fluid Mechanics Series, the astronaut made a low-g drinking cup. He could drink from the cup and add water in much the same manner you would in one-g. The cup was made by inverting a small can inside a larger can, so as to form an annular container. The liquid orients in the bottom of the cup and was strongly held in that position. Interface shapes in containers of various shapes have been investigated in designing propellant tanks that preferentially orient the liquid over the outlet. The shape of an interface and the perturbation required to displace the liquid from an

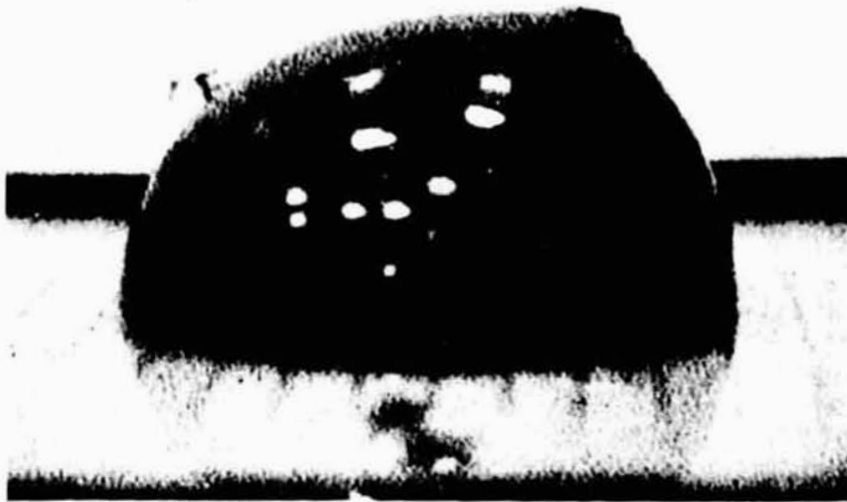


Figure 10. Sessile drop (the tube is freely resting on the drop surface).

ORIGINAL PAGE IS
OF POOR QUALITY

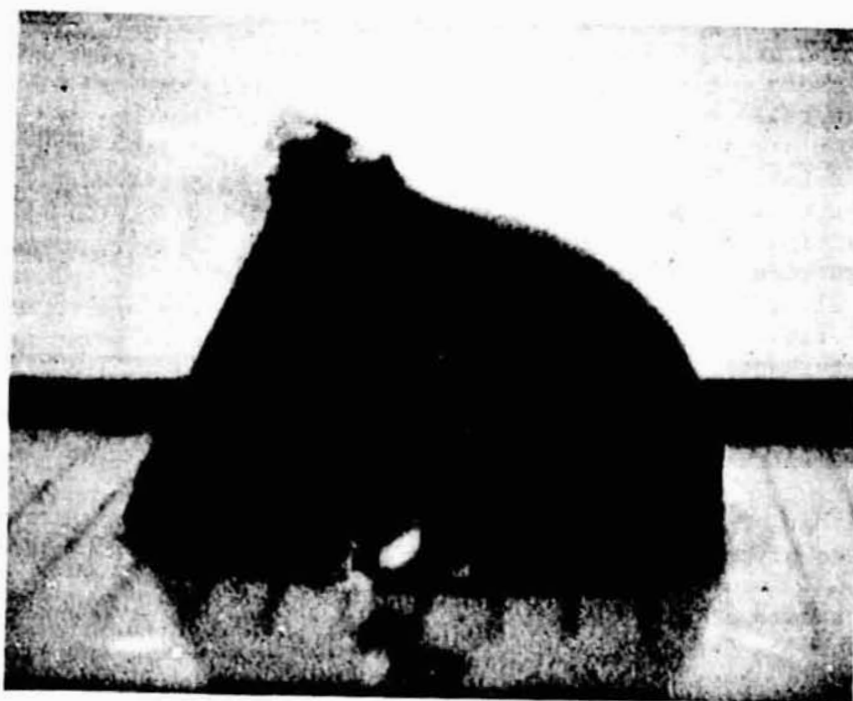
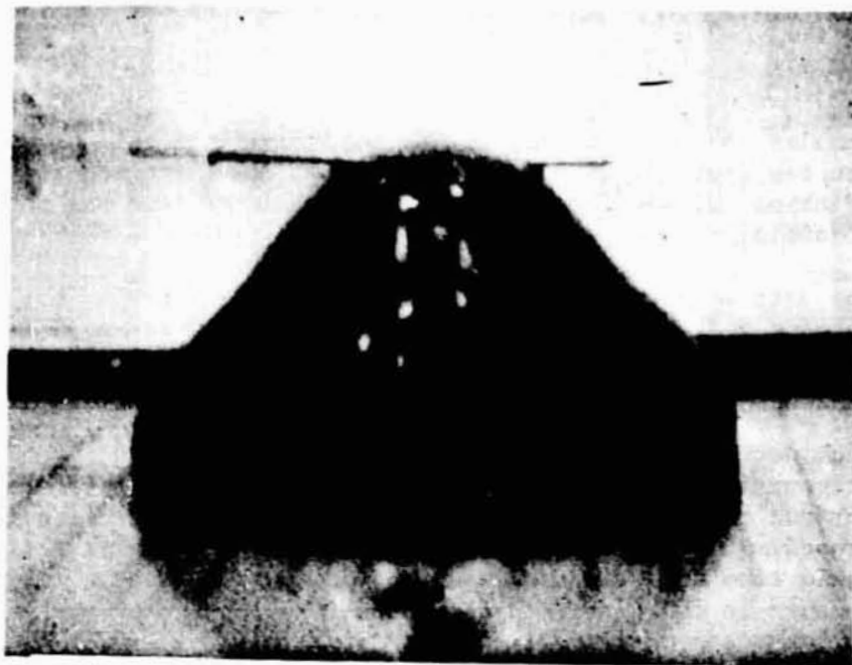


Figure 11. Adhesiveness of liquid drop to a needle (top) and a tube (bottom)

annular container is one of the configurations that have been studied (Ref. 26). Since the shape of the interface in the drinking cup could not be observed, a correlation was not possible.

The astronaut suggested a refinement to the drinking cup, by showing a drawing of his design (Figure 12). As he admitted, the cup is not too efficient because a large amount of its volume is taken up by the central lump.

Much work has been done in developing a means by which the internal geometry of a propellant tank can be modified so that surface tension forces will preferentially orient a liquid propellant over the tank outlet in low-gravity (Ref. 27). We would like to offer our solution to the problem here (Figure 13) because it does demonstrate how the shape an interface assumes in low-g can be used.

Three thin sheet vanes are placed in the cup. The profile of one vane is shown in the cross-sectional view. Holes are placed in the vanes so liquid will transfer from one sector to another of the cup. An equilibrium interface shape is reached when the pressure within the liquid is uniform. Therefore the sharp corners formed by the vanes and the cup will produce regions of lower pressure within the liquid, so they must fill with liquid to establish equilibrium. Since the vane is wider near the lip of the cup (the outlet) a larger amount of liquid will have to position in that region to achieve an interface with a uniform curvature. So the liquid in the cup, even when the volume is small, will tend to position near the lip of the cup so it can be drunk. The vanes will act as slosh baffles to suppress disturbances to the liquid. Very little of the internal volume of the cup is occupied by the vanes, so efficient use is made of the volume. A device using these general concepts will be used in the propellant tanks of the Viking Orbiter (Ref. 28).

Whether or not there is a need for a low-g drinking cup in the space program is debatable.

In a demonstration of the wetting of a liquid in the Fluid Mechanics Series, drops were placed on three different surfaces: plastic, metal and paper. The drops were difficult to see because of their size, but with the descriptions provided by the astronaut the relative wetting was demonstrated. On the plastic surface the drop had a hemispherical shape and a contact angle near 90 degrees, as was seen in other sequences. A similar drop

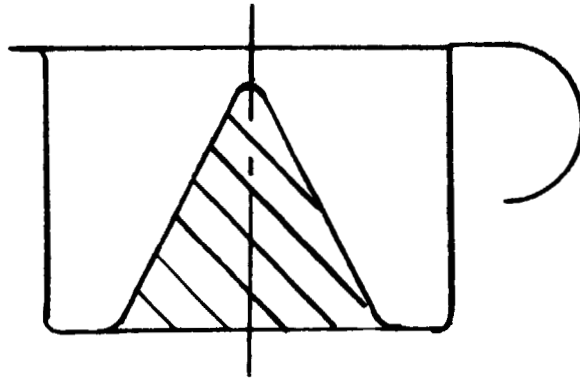


Figure 12. Low-g Drinking Cup as designed by William R. Pogue

ORIGINAL PAGE IS
OF POOR QUALITY

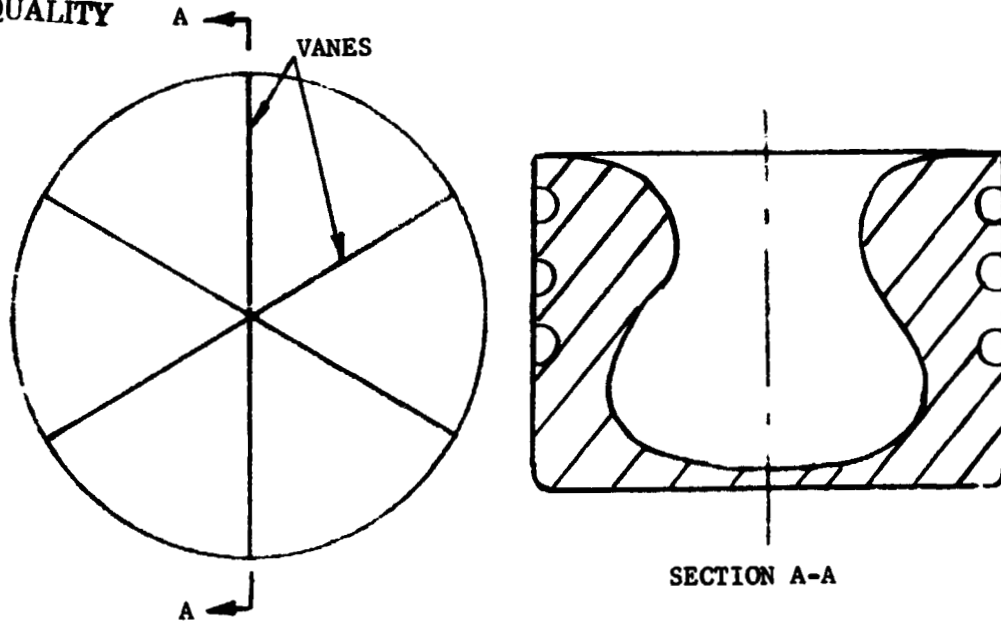


Figure 13. Low-g Drinking Cup as designed by Martin Marietta Corp.

was formed on the metal surface. It would be expected that the contact angle would be somewhat less on the metal than it was on the plastic surface, but the image was not good enough to perceive the difference. As discussed in Chapter II, the reason for the difference in contact angles is due to the differences in the energy of the surface. The higher the energy of the solid surface in comparison to the liquid surface, the smaller the contact angle.

When the water was placed on the paper surface, more spreading of the water and a lower profile to the drop was observable. The contact angle of the water on the paper was smaller than it was with the other surfaces, but paper has a lower surface energy than both metal and plastic. However, the mechanism involved here is no longer just wetting of a surface because water was being absorbed by the paper. Since the surface was filled with water the interface of the drop was essentially in contact with water, for which there is no such thing as contact angle. Eventually the entire drop would be absorbed into the paper.

SUMMARY

In this section of the report, those portions of the data in which static interface shapes could be observed were discussed. The theory that establishes the shape a gas/liquid interface will assume in low-g was presented and the influence of a surface in contact with the liquid was considered. Calculated interface shapes of a drop on a thread correlated with the observed interface shapes. The significance of the capillary area in determining the minimum energy interface configuration when more than one possible interface exists was shown. The data demonstrates that contact angle is highly dependent on the surface material and can not be readily correlated.

B. Oscillating Drop

Another of the objectives of the Fluid Mechanics Series of demonstrations was to investigate the oscillation of a liquid drop. Using the acquired data, oscillation frequencies could be correlated. Data that indicates an effect of oscillation amplitude on frequency was also obtained. Damping rates were significantly greater than predicted by theory, due to non-linear effects.

When a drop of liquid is perturbed under low-gravity conditions it will oscillate about its equilibrium interface shape, the sphere. If the drop is perturbed in the proper manner it can be caused to oscillate in various modes. The shape of the drop as it goes through one-half cycle of oscillation is shown in Figure 14. Shown are the four lowest modes of oscillation. The first mode is the basic harmonic mode of the drop. A drop tends to oscillate in this mode whenever it is disturbed. If the drop is perturbed at the proper frequency the second and higher modes can be excited.

The effect of viscosity on the oscillation has been evaluated (Ref. 30) and a parameter to define the point at which critical damping occurs is identified as follows:

if $\frac{\sigma r}{\rho \nu^2}$ is greater than 1.7 damped oscillations occur,

if $\frac{\sigma r}{\rho \nu^2}$ is less than 1.7 the motion is critically damped and a perturbed drop will not oscillate, but slowly return to its equilibrium shape.

For the drops being analyzed here the parameter is on the order of 10^4 so damped oscillation did occur.

Oscillation Frequency of a Spherical Drop

The frequency of oscillation of a liquid drop was analyzed by Lord Rayleigh in 1879 (Ref. 31). For any given mode of oscillation, determined by the integer l , the frequency is given by

$$f = \sqrt{\frac{l(l-1)(l+2)\sigma}{3\pi\rho V}} \quad (9)$$

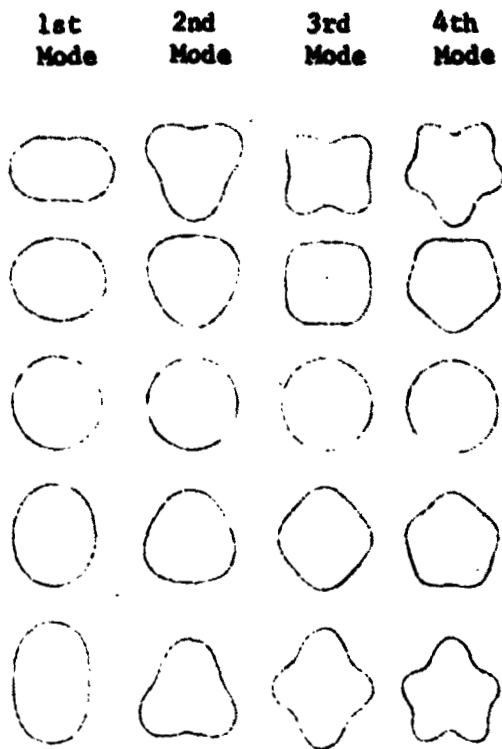


Figure 14. The four lowest modes of an oscillating drop (from Ref. 29)

ORIGINAL PAGE IS
OF POOR QUALITY

Where the frequency f is in Hertz.

When $l = 2$ the frequency is that of the first mode of oscillation. Equation (9) is then

$$f = \sqrt{\frac{8\sigma}{3\pi\rho V}} \quad (10)$$

The oscillation frequency is determined by the surface tension, which is the restoring force, and the mass (density times volume) of the drop.

A comprehensive analysis of the oscillation frequency and damping of a liquid drop can be found in Reference 32. The effects of the viscosity of the drop and the surrounding fluid, and the effect of the presence of surface active agents are considered.

In the Fluid Mechanics series a number of oscillating drop demonstrations were accomplished. In one sequence the drop was restrained on a thread to prevent it from drifting away. This enabled the camera to be positioned close to the drop, giving an image size about 40% of the film frame width.

Syringe plungers were used to apply the perturbation to the drop. The plungers were brought into contact with opposite sides of the drop. The drop adhered to the 1.25 cm diameter disks on the ends of the plungers. By pulling the plungers away from the drop, the drop was elongated until it eventually broke away from the plungers. At the point of detachment of the surface, the drop was elongated but also had a spurt in the surface where the plunger made contact (Fig. 15). This spurt quickly withdrew into the surface of the drop under the action of surface tension. The perturbation produced by the withdrawal of the plungers from the surface of the drop was sufficient to cause a fairly large amplitude oscillation. In earlier attempts to oscillate a drop in the Fluid Mechanics Series, wires and needles were used to apply the perturbation. Since there was very little adhesion between the surface of a needle and the water, the oscillations produced were of very low amplitude.

In this sequence, in which the drop was restrained on the thread, most of the tests were with water drops of 50 and 100 cc volume. The drops were lightly tinted with marker pen ink to improve their visibility. In one test, a drop with about one percent soap added to it was oscillated. In another the drop had an internal air bubble. A list of the tests in this series is

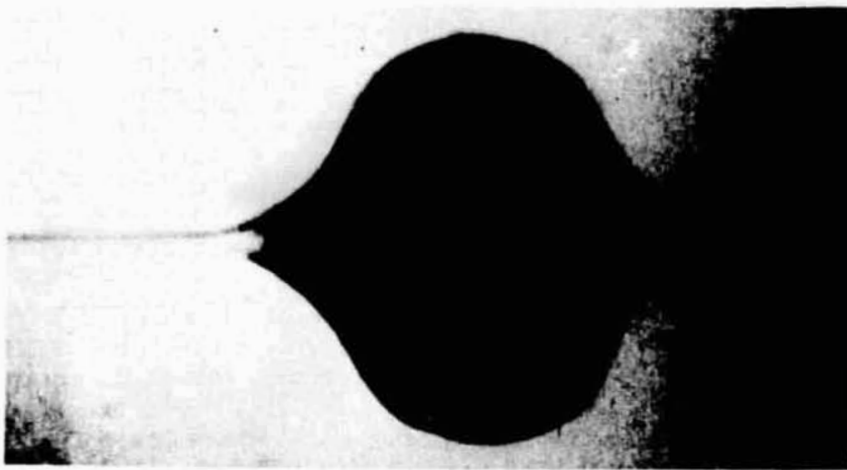
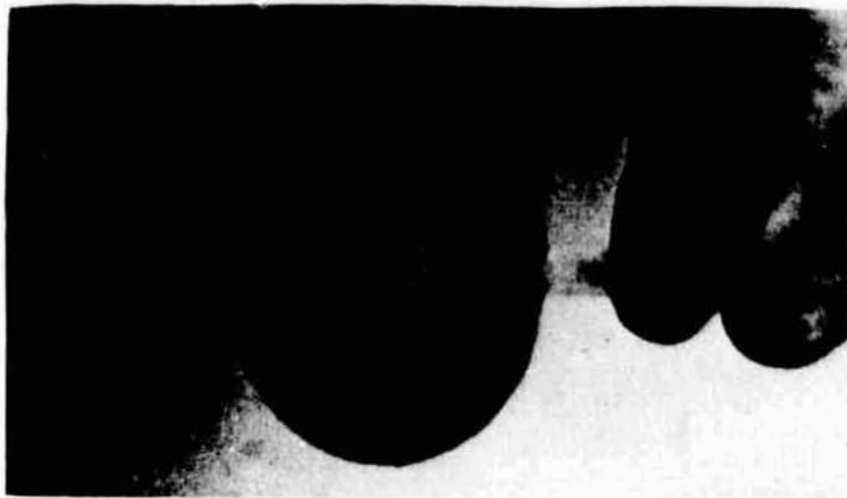


Figure 15. First mode oscillation of a drop. Top photo is just before pulling away plunger, next is just after. Others are spaced every one-half cycle.

ORIGINAL PAGE IS
OF POOR QUALITY

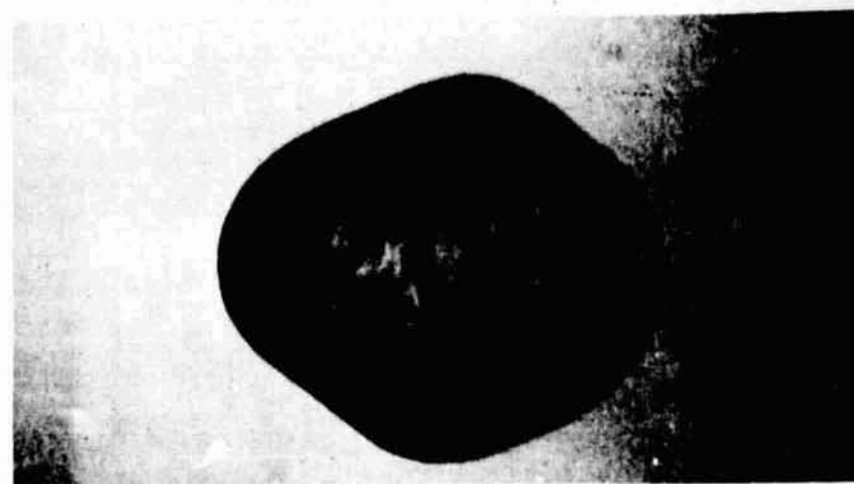
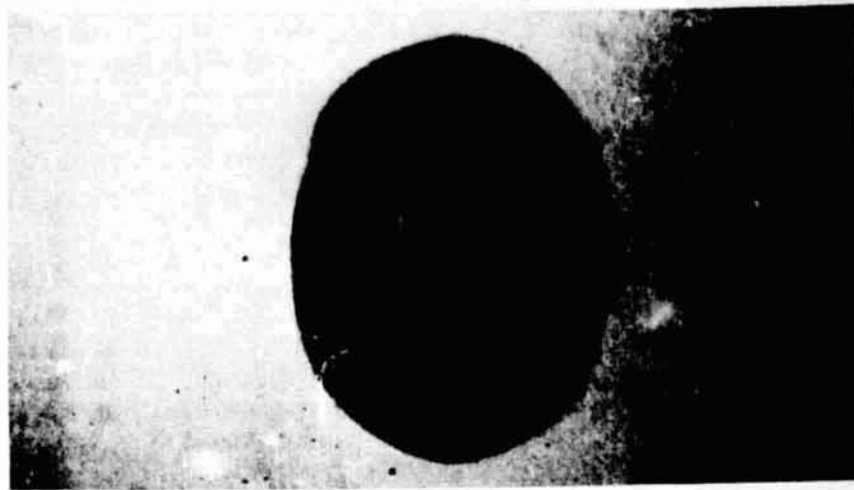
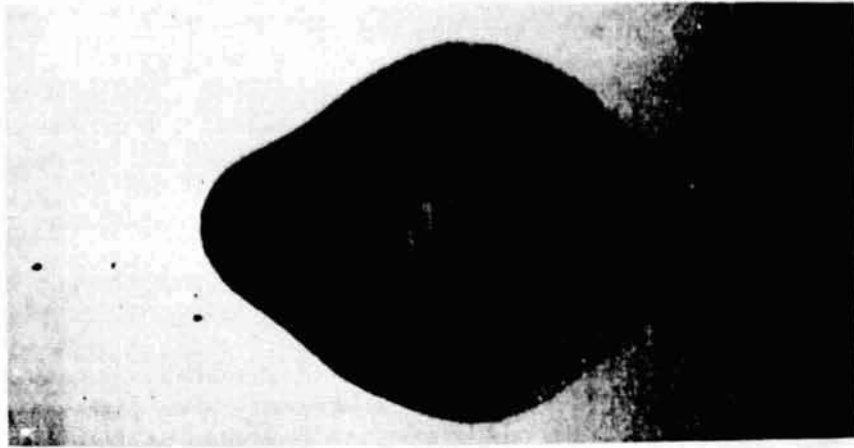


Figure 15. Continued

presented in Table 2. When the volume was stated on the sound track it is listed on the table. The duration is the period of time that the drop was allowed to oscillate, which gives some indication of the quality of the data for any particular test.

The 50 and 100 cc drops were oscillated in two different ways, referred to as symmetric and asymmetric. Symmetric oscillation of the drop was produced by simultaneously pulling both plungers away from opposite sides of the drop (Figure 15). First mode oscillations were produced in this manner. When first one plunger was pulled away and then the other was pulled away about one-half cycle later, asymmetric oscillations were produced (Figure 16). The asymmetric oscillation corresponds to the second mode. Based on equation (9) the frequency at the second mode ($l = 3$) is 1.94 times the frequency at the first mode ($l = 2$), so pulling the plungers in that manner does excite the second mode. Both a side view (plungers pulled on the plane of view) and an end view (plungers pulled perpendicular to the plane of view) of the symmetric oscillations are in the film data (Figure 17).

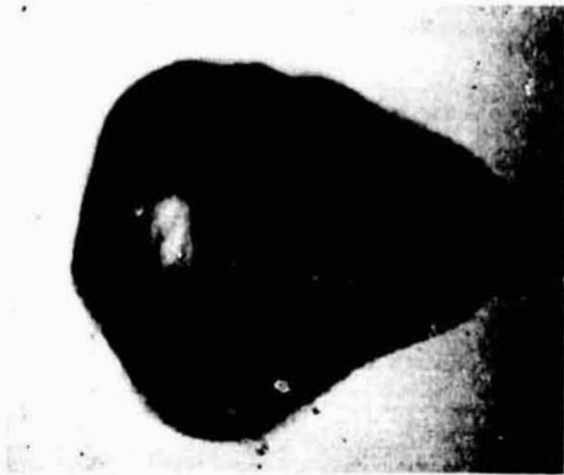
The oscillations produced by the plungers, due to the nature of the perturbations, could not be pure first or second mode. Only if the drop was displaced to a shape as shown in Figure 14 would pure oscillation in that mode occur. Due to the elongation and the spurts produced by the plungers, higher modes of oscillation were produced in addition to the basic first or second mode that was excited. The basic mode had a larger amplitude so it could always be observed, even though the other modes were present. In addition, the higher modes damped out at a faster rate, as will be discussed later, so they disappeared within a few cycles leaving just the basic modes.

Actually the picture presented by Figure 14 is somewhat simplified. For each mode there are $2l + 1$ different oscillations, all having the same frequency (Ref. 33). There is the basic axisymmetric mode and others are degenerate modes that are three dimensional in form. The manner of perturbation probably also excites the degenerate modes.

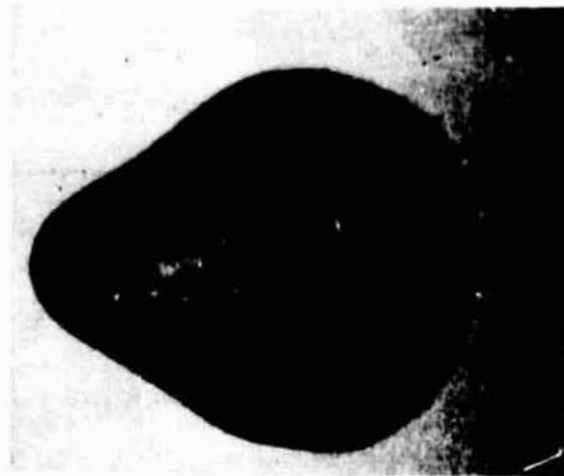
While the second mode of oscillation can be induced by pulling the plungers as described, the period of time that it persists is limited. The drop has a natural tendency to oscillate in the first mode, its basic harmonic frequency. Therefore the second mode persisted for a short time, usually long enough to measure the frequency, and then damped out. As the second mode decayed,

Table 2 Oscillating Drop Tests (Drop on thread)

Number	Volume, cc	Type of Oscillation	Duration, sec
1	50	Symmetric	41
2	50	Symmetric	19
3	50	Symmetric	9
4	50	Perpendicular to Plane of View	14
5	50	Perpendicular to Plane of View	25
6	50	Asymmetric	5
7	50	Asymmetric	3
8	50	Asymmetric	6
9	50	Asymmetric	19
10	50	Asymmetric	47
11	100	Symmetric	46
12	100	Symmetric	24
13	100	Perpendicular to Plane of View	31
14	100	Asymmetric	33
15	100	Asymmetric	39
16	100	Asymmetric	36
17	100	Asymmetric	11
18	--	Drop with Air Bubble	28
19	--	Drop with Air Bubble	28
20	--	Soap Solution	45



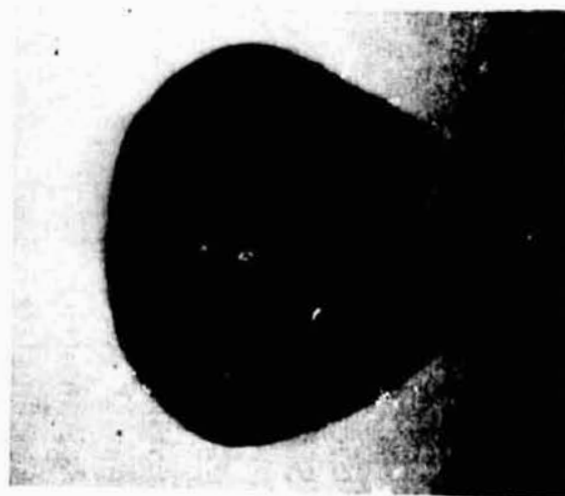
(a)



(d)



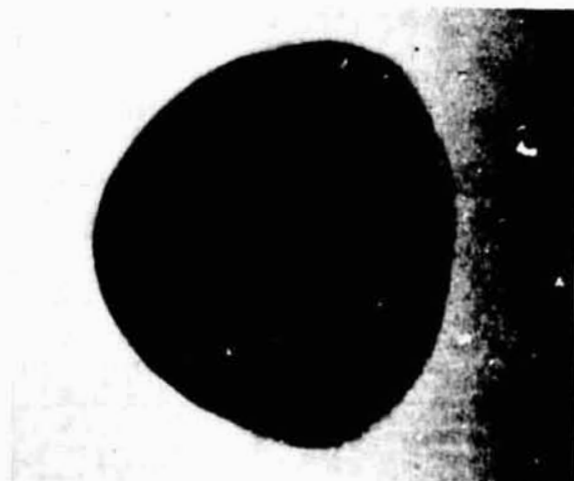
(b)



(e)



(c)



(f)

Figure 16. Drop oscillating at second mode frequency, pictures spaced every one-half cycle

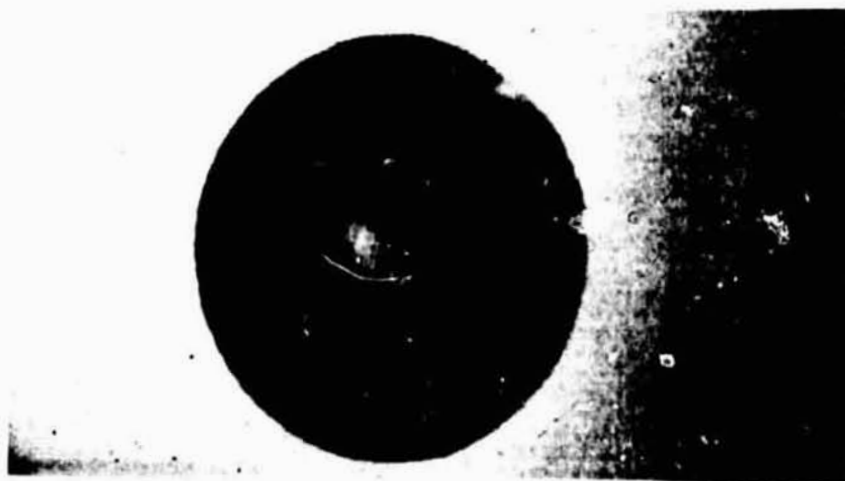
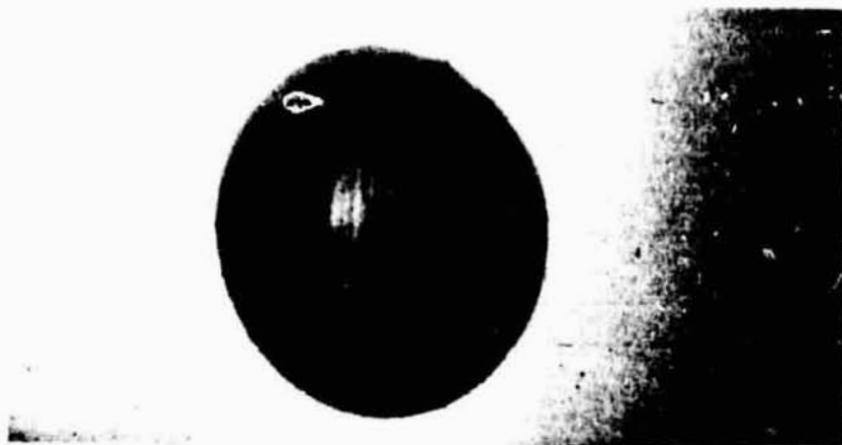


Figure 17. First mode oscillation of drop, perturbed perpendicular to plane of view. First photo - plungers against drop, others are spaced one-half cycle apart.

ORIGINAL PAGE IS
OF POOR QUALITY

there was a period during which both the first and second mode were present, giving the drop a very erratic oscillation. Finally the second mode disappeared, leaving only the first mode oscillation.

The measured frequencies of oscillation were correlated using equation (9) and the results are presented in Table 3. A very good correlation was obtained for the first and second modes of oscillation of the 50 and 100 cc drops. The stated drop volumes were used. Measurements of the drop volume from the film confirmed the stated volumes. A density of 1 gm/cc was used. As discussed in Chapter II, the marker pen ink is only a mild surface active agent, causing a slight reduction in the surface tension of water for the concentrations used. A value of 70 dynes/cm was used for the surface tension. Depending upon the duration of the test, the frequency of oscillation could be measured fairly accurately by counting cycles and film frames, and converting to Hertz using the frame rate of 24 frames per second. The uncertainty in the measured and calculated frequencies is estimated to be 5% and was neglected by considering two significant digits.

The tests in which the second mode was induced with the 50 cc drop were not too successful. In only 2 of the 5 attempts was second mode oscillation obtained. When it was induced it only persisted for a few cycles and then became muddled with the first mode that was beginning to appear. The second mode oscillation of the 100 cc drop was more successful.

The volume of the drop with the internal air bubble was not stated on the sound track so it had to be measured by scaling from the diameter of the disk on the end of the plunger (1.25 cm). The formation of the air bubble inside the drop is part of the film data so the drop could be measured before and after the air was added (Figure 18). Measured values of 50 cc of water and 10 cc of air were obtained. One cycle of oscillation of the drop with the internal air bubble is shown in Figure 19.

A direct correlation of the oscillation frequency is not possible using equation (10) because it does not account for the internal air bubble. However, if the physical significance of the terms in equation (1) are accounted for, a correction factor can be applied to the equation and a fairly good correlation can be obtained. The mass of the drop appears in the denominator of the equation. Adding air to the drop does not significantly

Table 3. Correlation of Oscillation Frequencies.

Volume, cc	Type of Oscillation	Measured Frequency	Calculated Frequency, Hz
50	Symmetric	1.1 (9)*	1.1
50	Asymmetric	2.0-2.1 (2)	2.1
100	Symmetric	0.78 (3)	0.79
100	Asymmetric	1.5 (4)	1.5
60	Drop With Air Bubble - Symmetric	0.82 (2)	0.87
50	Soap Solution - Symmetric	0.71 (1)	0.70

*Number of Tests

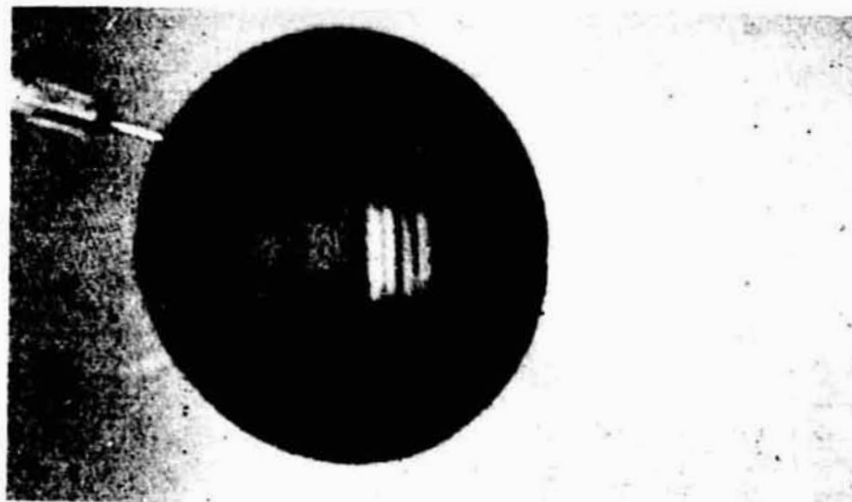
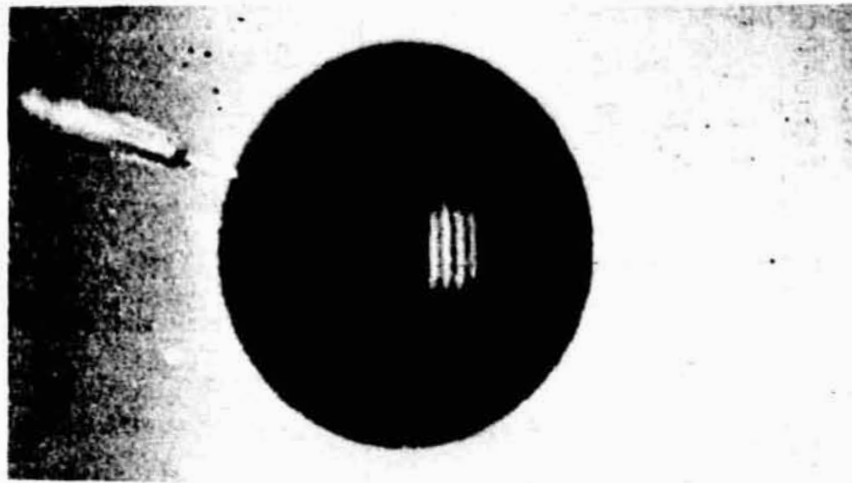


Figure 18. An air bubble is added to a drop before it is oscillated.

ORIGINAL PAGE IS
OF POOR QUALITY

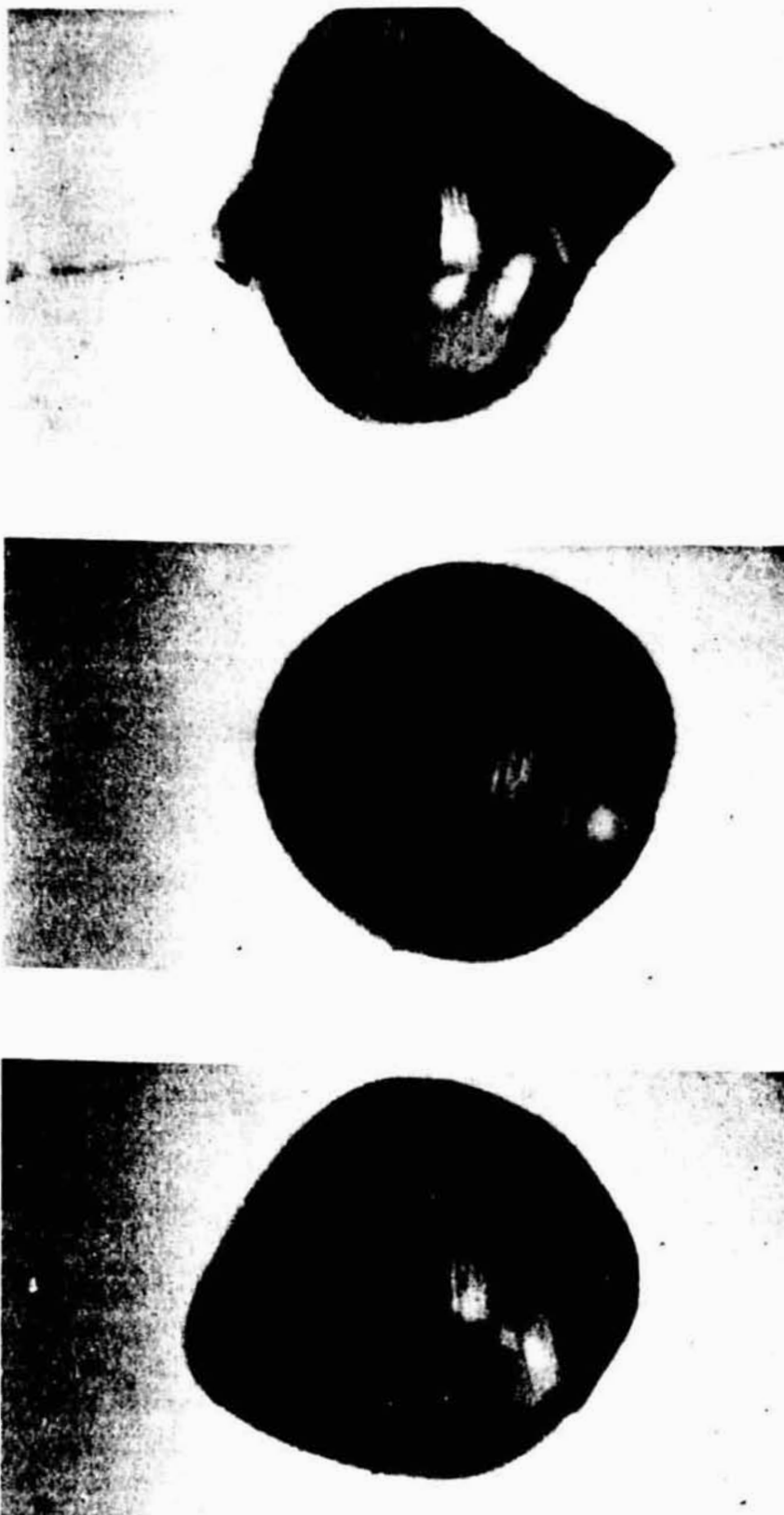


Figure 19. Oscillation of drop with internal air bubble. Top photo is immediately following pull away of the plungers, others follow every one-half cycle.

change the drop mass, so the mass of 50 grams was used there. Surface tension can be expressed as ergs per square centimeter, energy per unit area. The surface tension energy in the equation is based on the surface area of a sphere. With an internal air bubble the area of the outer surface of the drop has been increased and the internal area of the bubble has been added. Therefore the surface tension term was modified by the ratio of the surface area of a sphere (A_s) to the total surface area of the drop and air bubble (A_c). The change in the capillary area of the drop (discussed in Section A) is taken into account.

$$f = \sqrt{\frac{8\sigma}{3\pi\rho V} \left(\frac{A_s}{A_c} \right)} \quad (11)$$

The correlation obtained is fairly good considering the uncertainty in the volume of the drop and bubble, and the resulting uncertainty in the surface areas.

Adding soap to water reduces the surface tension and therefore the frequency of oscillation. The volume of the soap drop was not stated on the sound track, but it was measured as 50 cc. A surface tension of 29 dynes/cm was used in obtaining the correlation. The measured frequency was based on only seven cycles because the oscillations damped out rapidly, so its accuracy is somewhat low. Photos of this drop as it oscillates are shown in Figure 20.

In another sequence in the Fluid Mechanics Series, thirteen drop oscillation tests were performed using the same drop. The drop was free-floating in all these tests. Both plungers were pulled away from the drop simultaneously, exciting the first mode in all tests. A different type of plunger, having a round ball on its end, rather than a flat disk, was used in these tests. The liquid adhered more strongly to these plungers, so the amplitude of the perturbation was larger than that of the tests described above. There was a mirror in the background, oriented so that it also gave an end view of the drop. However, the size of the image of the drop was small, only 6% of the film frame width. Details of the drop oscillation could not be seen and the image in the mirror was worse (Figure 21). The volume of the drop was not stated on the sound track, so this data could not be correlated using equation (9). A drop volume of 32 cc was calculated using the measured frequency in that equation.

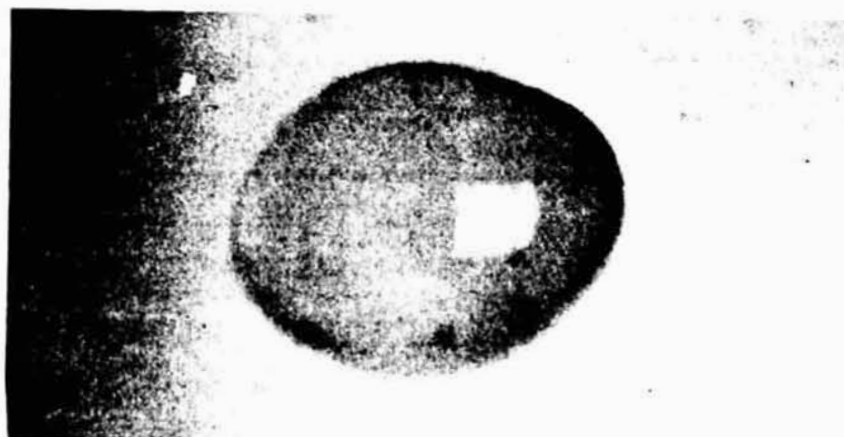


Figure 20. Oscillating soap drop. Top photo is immediately following pull away of plungers. Pictures are spaced one cycle apart in time.

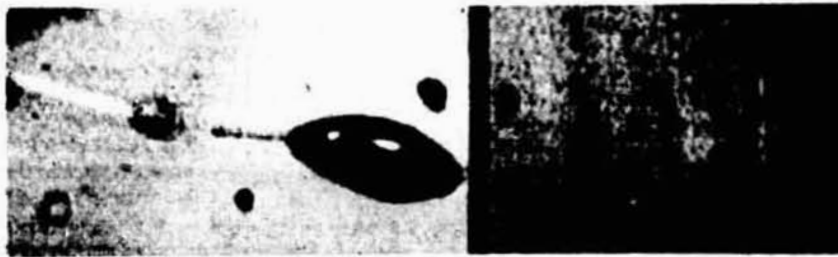


Figure 21. Oscillating Drop. Plungers pulled away and lower photos are one-half cycle apart.

ORIGINAL PAGE IS
OF POOR QUALITY

Each of the tests is listed in Table 4 with its duration. The range of the measured frequencies are listed, with the minimum being the initial value during the test and the maximum being the final value.

While no correlation of frequencies was possible, some other interesting effects were noted. An effect of amplitude on the oscillation frequency of a drop has been noted in ground based tests and analyses. The analytically derived variation is shown in Figure 22 (Ref. 29). The amplitude ratio is defined as the ratio of the two major axes of the drop. Here only the maximum values at the peak of the oscillation are used. As the amplitude ratio increases, the period of the oscillation is increased. It takes a longer time for the drop to displace to a large amplitude than it does to displace to a small amplitude. As the amplitude ratio approaches one, the period approaches that given by Rayleigh's equation (equation (10)). Rayleigh's equation was derived based on the assumption that the amplitude of the oscillation is small. As Figure 22 shows, large amplitudes are required before a significant change in the oscillation period can be detected (e.g., an amplitude ratio of 1.2 produces a one percent change in period). This curve is only known to be applicable to first mode oscillation.

In general it can be seen from the data in Table 4 that there was about a five percent variation in frequency from start to finish of the test. The initial amplitude ratio was about 1.5. So the data appears to lie somewhat about the curve in Figure 22.

As the amplitude of oscillation of a drop decays from its initial amplitude, each successive value of period and amplitude should fall on the curve in Figure 22. An attempt was made to show this trend with the data from two of the tests. The data points are shown on Figure 22. The lowest measured value of frequency was used to define the Rayleigh frequency. Since the image was small, the accuracy of the amplitude measurement is not good. Again, the data indicate that the effect of amplitude is somewhat greater than predicted by the theory.

This effect is due to the nature of the perturbation applied to the drop. The plungers distorted the drop and induced higher modes of oscillation that were most pronounced when the amplitude of the oscillation was large. The curve in Figure 22 is only applicable to a pure first mode oscillation, with the drop having the form shown in Figure 14. It has been shown that if

Table 4. Oscillating Drop Tests (Free Floating Drop)

Test Number	Test Duration (sec)	Frequency (Hz)	
		Minimum	Maximum
1	17.8	1.20	1.28
2	21.6	1.22	1.29
3	14.9	1.26	1.32
4	19.4	1.29	1.35
5	6.5	1.30	-
6	17.6	1.35	1.38
7	23.7	1.36	1.41
8	20.7	1.33	1.41
9	22.8	1.32	1.39
10	38.9	1.33	1.41
11	18.5	1.41	-
12	25.6	1.36	1.41
13	17.3	1.37	1.43

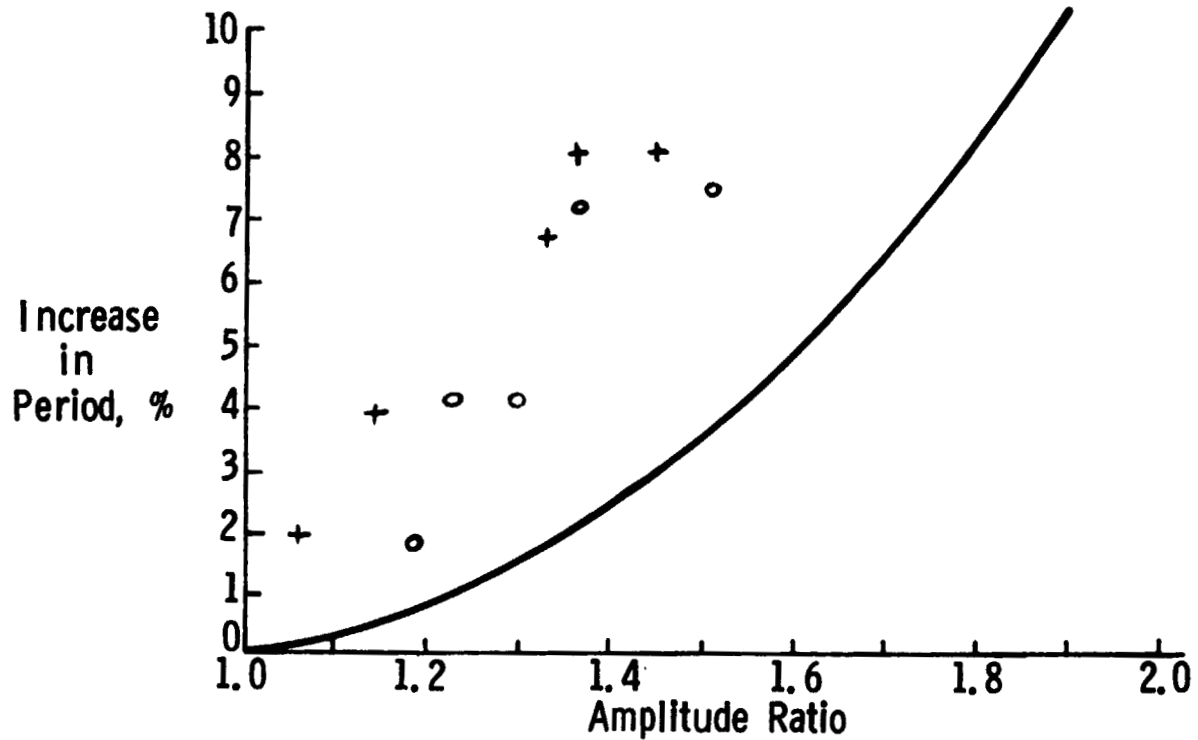


Figure 22. Effect of Oscillation Amplitude on Period

the form of the drop is different from that given by Figure 14 as it oscillates, a greater increase in amplitude ratio will occur (Reference 29). The curve in Figure 22 represents a minimum energy level of first mode oscillation.

Another interesting thing can be noted in the data listed in Table 4. There is a gradual increase in the measured frequencies with each successive test. Volume is the only likely suspect, since a decrease in volume would cause an increase in frequency. As the plungers were pulled away from the drop, the spurts pulled out from the surface pinched off into small drops. In many of the tests small drops could be seen after the plungers were pulled away. The astronaut could also be observed diligently trying to collect up all these small drops on the plungers so they could be returned to the drop before the next test. Using equation (10) the sensitivity of the frequency to the volume can be derived:

$$\frac{df}{dV} = -\frac{1}{2} \sqrt{\frac{8\sigma}{3\pi\rho V^3}} \quad (12)$$

Substituting in the known variables, it is found that

$$\frac{df}{dV} = -0.022 \text{ Hz/cc} \quad (13)$$

A change of frequency of 0.15 Hz, the net change over the thirteen tests, corresponds to a 6.8 cc change in volume out of a total 32 cc drop volume. While it is not obvious from the film, a small amount of liquid must have been lost from the drop with each test. The drop volume gradually decreased and the frequency of oscillation increased.

Another portion of the Fluid Mechanics Series in which oscillating drops appear is the coalescence demonstrations. The coalescence of two drops provides the perturbation to induce a fairly large amplitude oscillation. The image is large and the volume of the drops is stated for two of the six tests, however the astronaut says that the volume is "around 30 cc". Another problem involved in using this data is that grape and strawberry drink were used to color the drops. Both of these additives are strong surface active agents, as discussed in Chapter II, reducing the surface tension to values between 50 and 60

dynes per centimeter. Due to the uncertainty of both volume and surface tension, no reliable correlations were obtained.

Oscillating drops appear in other places in the Fluid Mechanics Series and SL-3 data, but the sequences usually suffer from one or more of the following deficiencies: the period of time which the drop was allowed to oscillate was too short, the drop was rotating or had a non-uniform perturbation, or the volume of the drop was not known.

The best oscillating drop sequence was the one in which the drop was on a thread. It provided the best data quality, the variables were fairly well known and a consistent correlation could be obtained.

Damping Rate for Oscillating Spherical Drop

Damping is the dissipation of energy due to viscous forces. Sir Horace Lamb derived the basic equations for the damping rate of an oscillating spherical drop in 1881 (Ref. 34). The oscillation amplitude is assumed to decay in an exponential manner.

$$a = a_0 e^{-\beta t} \quad (14)$$

where a_0 is the amplitude at a time zero and a is the amplitude after time t has elapsed. The damping coefficient β determines the rate of decay. From Lamb's analysis, the damping coefficient is a function of the liquid viscosity and the radius of the drop.

$$\beta = \frac{(l-1)(2l+1)\nu}{r^2} \quad (15)$$

where l indicates the mode.

When $l = 2$ the damping rate for the first mode is obtained.

$$\beta = \frac{5\nu}{r^2} \quad (16)$$

Equation (14) is used to derive an expression that will allow the damping coefficient to be calculated from parameters that are measured from the data. Time is a function of the frequency of the oscillation and the number of cycles, n.

$$t = \frac{n}{f} \quad (17)$$

therefore,

$$\beta = \frac{f}{n} \ln \frac{a_0}{a_n} \quad (18)$$

where a_0 is the amplitude at the 0th cycle and a_n is the amplitude at the nth cycle. The amplitude is always the peak amplitude of the oscillation. It is the difference between the overall displacement of the drop and its static diameter. As time approaches infinity, the amplitude goes to zero (not to the drop diameter). All of these parameters, amplitude, frequency and number of cycles, can be measured from the film data.

Damping rate is much more sensitive to the test conditions than is oscillation frequency. The theory of equation (15) is only applicable to the internal dissipation of energy of low amplitude oscillations of a single mode.

Due to the nature of the perturbation applied to the drop (plungers pulled away from surface of drop) higher modes of oscillation were excited. When both of the plungers were pulled away simultaneously the first mode oscillation had the highest amplitude and the other modes had a relatively low amplitude. Calculated values of the damping coefficient of the first six modes are listed in Table 5 for two drop volumes, 50 and 100 cc. As can be seen, the damping coefficient for the higher modes is significantly larger than the coefficient for the first mode. Due to their smaller amplitude and high damping rate, the higher mode oscillations could only be readily observed for a few cycles. As the oscillations continue the higher modes gradually disappeared, leaving the first mode as the only observable mode. With the 50 and 100 cc drops, the higher modes could no longer be observed after about 10 cycles. When it was intended to excite the second mode, by pulling one plunger and then the other, the second mode persisted for about 15 cycles and then gradually

TABLE 5. CALCULATED DAMPING COEFFICIENT

l	50 CC DROP β (SEC)	100 CC DROP β (SEC)
2	.0092	.006
3	.026	.017
4	.051	.032
5	.083	.053
6	.123	.078
7	.170	.110

TABLE 6. MEASURED DAMPING COEFFICIENT

VOLUME (CC)	TYPE OF OSCILLATION	β (SEC)
50	SYMMETRIC	0.18 (2)*
50	ASYMMETRIC	0.38 (1)
100	SYMMETRIC	0.088 (1)
50	SOAP SOLUTION - SYMMETRIC	0.38 (1)

*NUMBER OF TESTS

changed to first mode. Only the first mode had sufficient amplitude and duration to permit measurement of the damping rate. The measured damping coefficients, Table 6, were found to be much larger than the values predicted by theory.

There are two reasons for the larger damping rate. One is that the higher modes of oscillation interact with the first mode, increasing the viscous shear and therefore the damping rate. The modes do not damp independently, but interact. Another significant effect is the dissipation of energy due to the motion of the liquid interface with respect to the thread. Due to the hysteresis of contact angle at the thread (as discussed in Section A of this chapter) considerable energy is required to displace the interface along the thread.

The first of these problems can be minimized by ignoring the first portion of the test, when the higher modes were prominent. After about 10 cycles the higher modes were not visually apparent, but their effect on the damping rate could persist for a much longer period. The only way to completely avoid the effects of higher modes on the damping is to use a method of perturbing the drop that only excites the first mode.

The amplitude of the oscillation was small after the more pronounced effects of the higher modes had disappeared. It became difficult to resolve the small difference between the displaced drop and its static diameter with sufficient accuracy. One of the most significant problems in making this measurement is that the oscillation axis may be moving with respect to the plane of the film. Since the image is only two dimensional the rotation of the drop is perceived as a change in amplitude.

An accurate measurement of the decay in amplitude of a pure first mode oscillation could not be accomplished with any of the oscillating drop data. In those tests in which the drop was restrained on a thread, the quantitative effect of the thread on the damping rate could not be established. The measured values of damping coefficient are only valid for a drop on a thread and oscillations with many modes present.

Surface active agents are another factor which can increase the damping rate. This is one of the conditions under which surface tension driven flow or the Marangoni effect can be produced. (Another is discussed with respect to the Ice Melting demonstration). When there is a surface active agent on the surface of a drop, the oscillations cause gradients in the

concentration of the surfactant. As the drop elongates increasing the surface area, the concentration of the surfactant is decreased where the drop has deformed the most. Decreasing the concentration of the surfactant increases the surface tension of the liquid in that region of the drop. Near the center of the drop the surface tension remains at the low value imposed by the surfactant. The Marangoni effect is that liquid will flow along a surface from the region of low surface tension to the region of high surface tension. This flow opposes any further increase in surface area and thereby increases the damping. Similarly, contractions in the surface area are also opposed.

The effects of surfactants on a liquid surface can be represented by an inextensible film over the surface. The film does not permit any local expansion or contraction of the surface. The damping of a surface with an inextensible film can be compared to a surface of a pure liquid to determine the maximum effect of surfactants. If density and viscosity are the same the ratio is given by Ref. 32):

$$\frac{\text{Damping coefficient with inextensible interface}}{\text{Damping coefficient with pure liquid}} =$$

$$\frac{2(2\ell^2 + 2\ell + 5)}{(2\ell + 1)^2} \quad (19)$$

where ℓ defines the mode of oscillation. When $\ell = 2$, for first mode oscillation, the effect is the most significant with the ratio equal to 1.36. At higher modes of oscillation the ratio approaches one. The increase in damping due to a surfactant is not a substantial one.

Since the marker pen ink is a mild surfactant, it would not have had any effect on the damping rate. Perhaps the effect of the strong surfactants, such as the fruit drinks, would approach that described above.

Oscillating Sessile Drop

In the Fluid Mechanics series a single sessile drop was oscillated in a number of different ways. The drop was setting on a flat plastic surface. There was a quarter inch grid on the

surface below the drop to aid in measuring its size. The camera was located somewhat above the drop so the image does not allow the height of the drop or the contact angle to be measured accurately. It is estimated that the drop volume was 50 cc. The contact angle was near 90 degrees so the interface had the form of a hemisphere.

The measured oscillation frequencies for each of the tests performed with this drop are listed in Table 7. The means of perturbing the drop and the duration of the test (an indication of the data quality) are listed in the table.

In the first two tests a tube (soda straw sized) was slowly withdrawn from the top of the drop, with the tube oriented vertically. The interface distorted until the adhesion between the drop and the tube was overcome and then the interface retracted. This perturbation induced the oscillation of the drop. The form of the first mode oscillation of the sessile drop is similar to the first mode of a spherical drop. First it elongates in a direction perpendicular to the surface and then one-half cycle later it flattens and elongates in a plane parallel to the surface (Figure 23). Unless the amplitude of the oscillation is very large, the line of contact between the liquid interface and the solid surface remains fixed. The interface rotates about this line of contact, so the contact angle varies as the drop oscillates.

In test number 3 (Table 7) a syringe needle tangentially contacting the top of the drop was used to excite the oscillation. Using the adhesion between the needle and the surface, the drop was driven into oscillation at its second mode by moving the needle up and down a few times and then pulling it away. The second mode is similar in form to the second mode of the spherical drop, shown in Figure 14, considering just the upper half of the spherical drop. Again the contact line remained fixed and contact angle varied during the oscillation. From the measured sessile drop frequencies, the second mode is 2.3 times the first mode frequency, while the factor was shown to be 1.94 for the spherical drop. This is the first indication from the data that the presence of the surface has a significant effect on the oscillation of the drop.

In test 4 the syringe needle was parallel to the surface and was slowly pulled away from the drop in the vertical direction. First mode oscillation, of a lower amplitude than was achieved with the tube, was induced.

Table 7. Oscillating Sessile Drop Data

Test	Duration, sec	Frequency, Hz	Source of Oscillation
1	26	1.1	Tube, Vertical
2	23	1.1	Tube, Vertical
3	6	2.5	Syringe, 2nd Mode
4	20	1.1	Syringe
5	11	1.0	Unknown
6	29	1.0	Tube, Horizontal
7	7	2.5	Strike Surface
8	9	0.52	Lateral

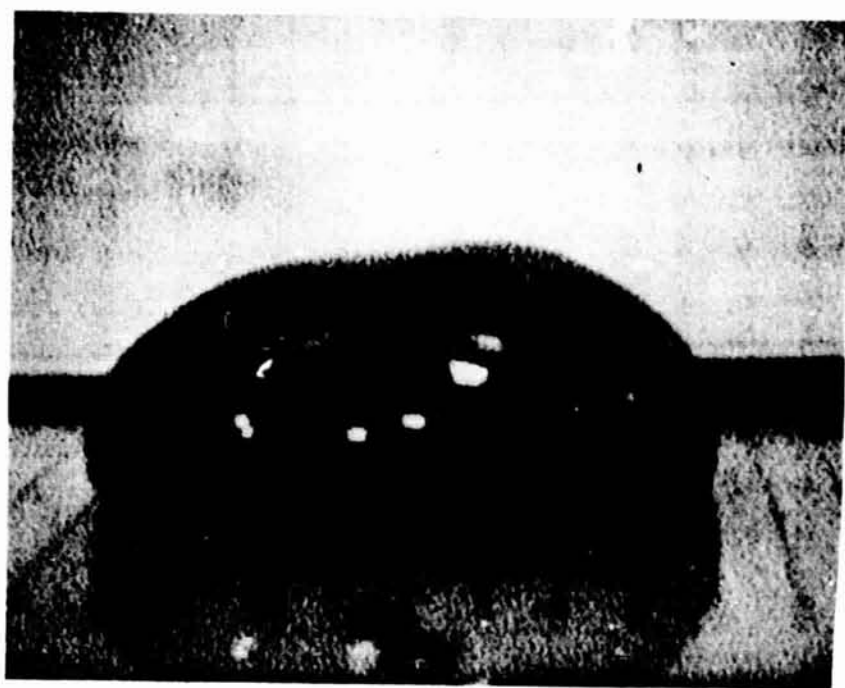
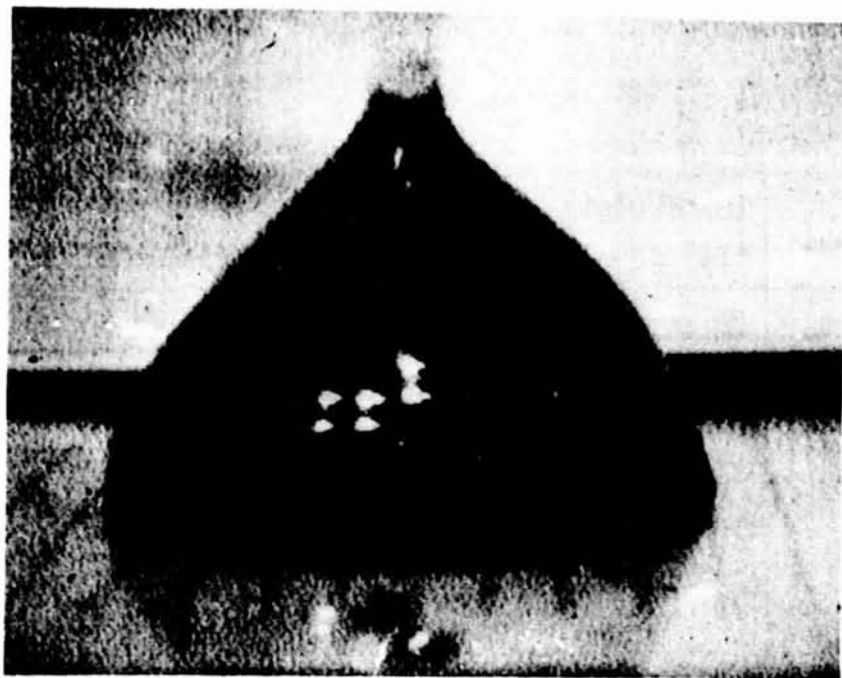


Figure 23. Tube as pulled out of sessile drop inducing oscillation.
Photos are every one-half cycle.

ORIGINAL PAGE IS
OF POOR QUALITY

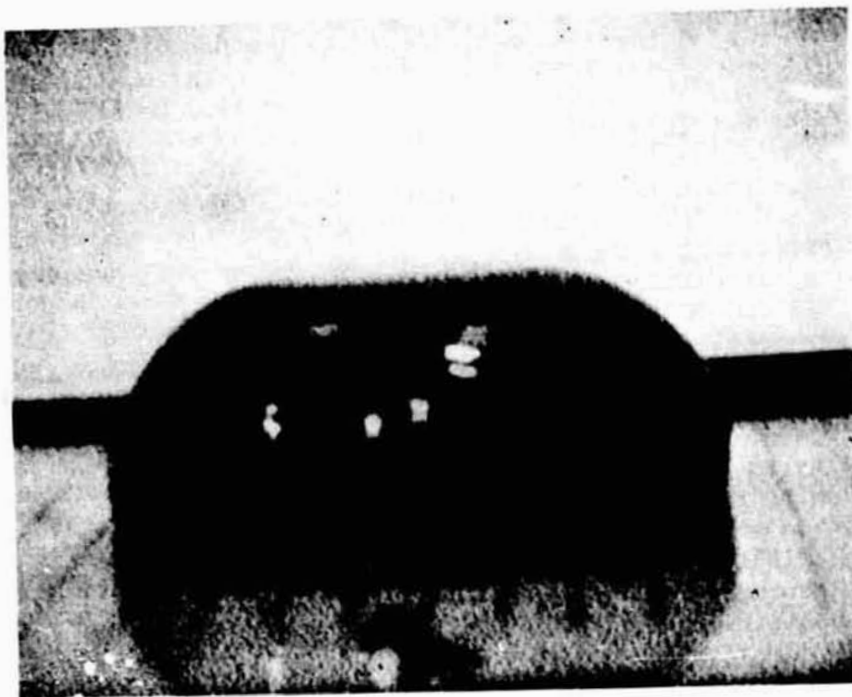


Figure 23. Continued

Following test 4 a needle was passed through the drop laterally a few times. While no gross movement of the contact line could be observed, the image was not good enough to determine if small shifts in the contact line occurred. It has been observed in ground based tests that a contact line moves in a series of small localized shifts of the line along the surface (Ref. 35). Next the tube was passed through the drop a number of times. In some cases small shifts in the contact line could be observed. None of these sequences provided any useful oscillation data.

At the beginning of test 5 there is an interruption in the film data so the source of the perturbation can not be observed. Based on the amplitude of the oscillation it appears that the tube was used again. In this test and the following test (test 6) the frequency of the first mode is 0.1 Hz lower than it was in tests 1 and 2. The accuracy of the data is sufficient to resolve this change in frequency. Apparently this was due to the disturbances applied to the drop following test 4. Perhaps the contact line of the drop was not in its equilibrium configuration due to the resistance of the contact line to movement. The disturbances applied to the drop allowed the contact line to displace and relieve some tension within the drop. In subsequent tests the net surface tension force was somewhat less and the frequencies were therefore lower.

High frequency oscillations were setup in the drop by striking the surface with a wrench. At first it was just gently tapped. The perturbation could be observed to travel from the base to the top of the drop. As this wave meets the top of the drop a small rounded spurt appeared (Figure 24). The high frequency oscillation damped out quickly and some erratic oscillation of the drop remained. The surface was struck several times and the force with which it was struck was gradually increased. Each time the appearance of the oscillation was similar to that described above, but the amplitude was greater. Following repeated hits on the surface, second mode oscillation could be observed. The frequency of this oscillation was the same, within the measurement accuracy, as that measured in test 3. Apparently the second mode is less sensitive to changes in the boundary condition at the contact line.

Following test 7 the tube was placed horizontally on top of the drop. The tube was rotated about an axis perpendicular to the surface with the drop acting as the pivot point (Figure 25).



Figure 24. Spurt formed by high frequency oscillation.



Figure 25. A tube is rotated on top of the drop.

ORIGINAL PAGE IS
OF POOR QUALITY

Surface tension forces kept the tube from sliding off the side of the drop. With the tube horizontal, it was pulled vertically away from the drop. As this was repeated a few more times, a variation in the wetting of the tube and therefore the adhesion between the drop and the tube could be observed. The most adhesion was achieved when the tube was pushed deeply onto the drop, allowing a larger area to be wetted by the liquid.

A lateral oscillation was induced by shifting the surface abruptly. It was moved laterally about 2.5 cm in 0.3 seconds. Due to inertia the motion of the drop lagged the motion of the surface (Figure 26). When the drop did follow, movement of the contact line could be observed as it was pulled along behind the drop. The drop continued to laterally oscillate, without any further movement of the contact line at a frequency of 0.52 Hz.

No theory to predict the oscillation frequency of a sessile drop could be found in the literature search. An adaptation of the equation for the spherical drop was considered as a means of calculating the frequency. A correlation with the above described sessile drop tests was not attempted because of the poor image. However, in the Liquid Floating Zone demonstration there is some much better oscillating sessile drop data. Sessile drops were formed on 2.22 cm diameter disks and in some of the tests the disks were moved so as to induce first mode oscillation of the sessile drop. The disk diameter was used to scale the drop dimensions. Since the drop was fixed in position with respect to the disk, dimensions perpendicular to the plane of the image are no problem. The image is large (Figure 27).

This data has been correlated with some success by LMSC (Ref. 9) and Dr. Carruthers (Ref. 7). They used equation (10) with the radius of a spherical drop substituted for the volume as follows:

$$f = \sqrt{\frac{2\sigma}{\pi^2 \rho r^3}} \quad (20)$$

The sessile drop has the form of a truncated sphere, so the radius of that sphere was substituted into the equation. Predicted frequencies were up to twenty percent greater than the measured frequency.

Equation (11) was used to try to improve the correlation. That equation was used with some success in predicting the oscillation

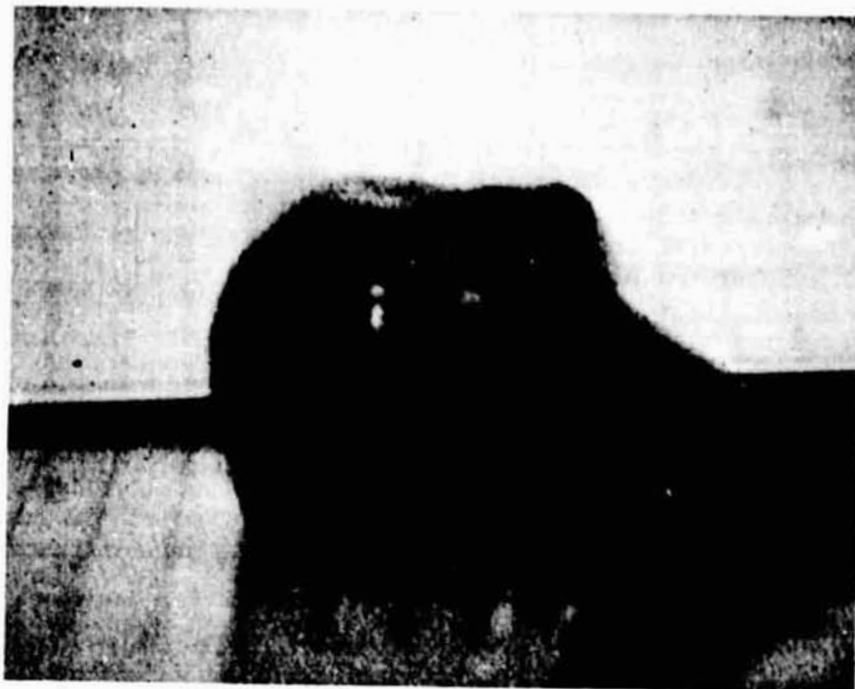


Figure 26. Rapid lateral motion of surface causes drop to lag movement.

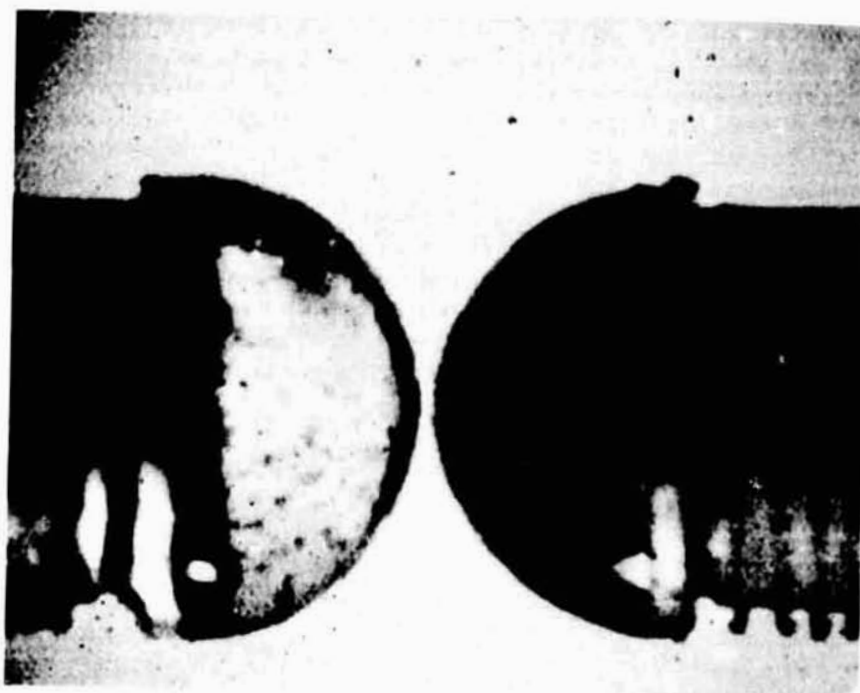


Figure 27. Two sessile drops for Liquid Floating Zone demonstration.

frequency of the drop with an internal bubble. In comparing the sessile drop with a spherical drop, the mass is considered to have the same effect in both cases. The effect of surface tension is modified by considering the capillary area defined in section A. For the spherical drop, the capillary area is simply the surface area (A_s). For the sessile drop, equation (7) for A_c was used to account for the surface of the drop that is exposed to the air and the surface in contact with the disk. The contact angle is the angle formed by the surface where it meets the edge of the disk. It was found that the ratio of the two areas (A_s/A_c) had a value greater than, but near to one. The concept of surface energy discussed in section A predicts that this ratio is always greater than one. Since its value is near one the influence of the area ratio on the calculated frequency is small. Frequencies calculated using this approach did not correlate as well as did equation (20) above. The boundary of the liquid and the solid has a significant effect on the sessile drop oscillation frequency that can not be directly accounted for by using the equations for the oscillation of a sphere. Equation (20) provides a reasonable approximation if the radius used in the equation is as defined.

SUMMARY

The better quality oscillating drop data correlated very well with the theory. Drops of two different volumes, with two different values of surface tension, and at both first and second mode frequencies were correlated. By a simple modification of the equations, the effect of an internal air bubble on oscillation frequency was predicted. The effect of the amplitude of oscillation on the frequency was also shown. No correlation of damping rates was possible because of the nature of the data. Since higher modes of oscillation were present, much higher damping coefficients were measured. Theory to correlate the oscillation frequency of a sessile drop is not available, but an approximate frequency can be calculated from the equation for an oscillating sphere.

C. Coalescence

A demonstration of coalescence was also a part of the objectives of the Fluid Mechanics Series of demonstrations. The influence of the drop sizes and velocities was to be evaluated. Coalescence appears many places in the data but a series of six tests provided the best quality data. In each of these six tests complete coalescence occurred, while in some of the other data bouncing of two drops was observed. Measured parameters fit within the proper categories for coalescence as established in ground-based testing.

When two drops of liquid collide several types of interaction are possible (Ref. 36).

- 1) They may bounce apart, contact of the two surfaces being prevented by the intervening air film;
- 2) They may coalesce and remain permanently united;
- 3) They may coalesce temporarily and separate, apparently retaining their initial identities;
- 4) They may coalesce temporarily, with the subsequent separation accompanied by satellite drops; or
- 5) With very high energy collisions, spattering may occur, in which numerous tiny droplets are expelled radially from the periphery of the interacting drops.

The type of interaction that does occur with any collision depends primarily upon the size of the drops and their velocities. Angular momentum, electric fields and other factors can also have an influence.

Drop collisions appear a number of places in the fluid mechanics demonstrations. They appear in the SL-3 demonstrations and a number of places in the Fluid Mechanics Series. In the rotating drop sequence, after the drop had broken into two drops, the rejoining of the drops sometimes appears in the data. In the Liquid Floating Zone demonstration two sessile drops were brought together allowing them to coalesce. Coalescence of air bubbles within the zone was also demonstrated.

The best data is a series of six coalescence tests that were conducted as part of the Fluid Mechanics Series. In each test

one drop was statically positioned on a thread. The other drop was free-floating and was maneuvered so as to impact the static drop. The parameters that were measured for each test are identified in Figure 28 and they are listed in Table 8.

It was assumed that the centers of both drops were in a plane parallel to the plane of the film. When the initial contact of the drops could be observed, it appears that this assumption is justified. For the faster moving drops, which have a smeared image on the film, this may not be the case.

The drops have different colors so their mixing following coalescence could be observed. Strawberry drink was used to give the red color and either grape drink or marker pen ink to give the black color. In one case no colorant was added to the moving drop. As discussed in Chapter II the fruit drinks are strong surfactants, reducing the surface tension of the water to a value of about 55 dynes/cm.

The astronaut states that the drop volume is around 30 cc during test 1. The black drop was oscillating in the first mode as it approached the red drop. Just prior to contact, the black drop was elongated in a direction toward the red drop and was beginning to retract. Based on the path of the moving drop, it came very close to missing the stationary drop, with the oscillation helping to bring their surfaces closer together at the point of impact.

Selected pictures of the coalescence for test 1 are shown in Figure 29. Large amplitude, first mode oscillation was induced by the coalescence. Immediately following coalescence, there was a sharp boundary between the two differently colored liquids. As the oscillations continued the two colors can be observed to slowly mix. The mixing could be observed for about 40 seconds.

Two new drops of the same size and color were made for the second test. In this test the impact of the drops was more direct than it was in test 1. Again, first mode oscillation was produced and the mixing of the drops could be observed. A photo sequence of this test is shown in Figure 30.

In test 3 the static drop was the product of the coalescence in test 2. The remainder of the tests (tests 3 through 6) all use a static drop that was the product of the previous coalescence. A small drop, with a low velocity, coalesced with the static drop, as shown in Figure 31. Prior to coalescence the small drop

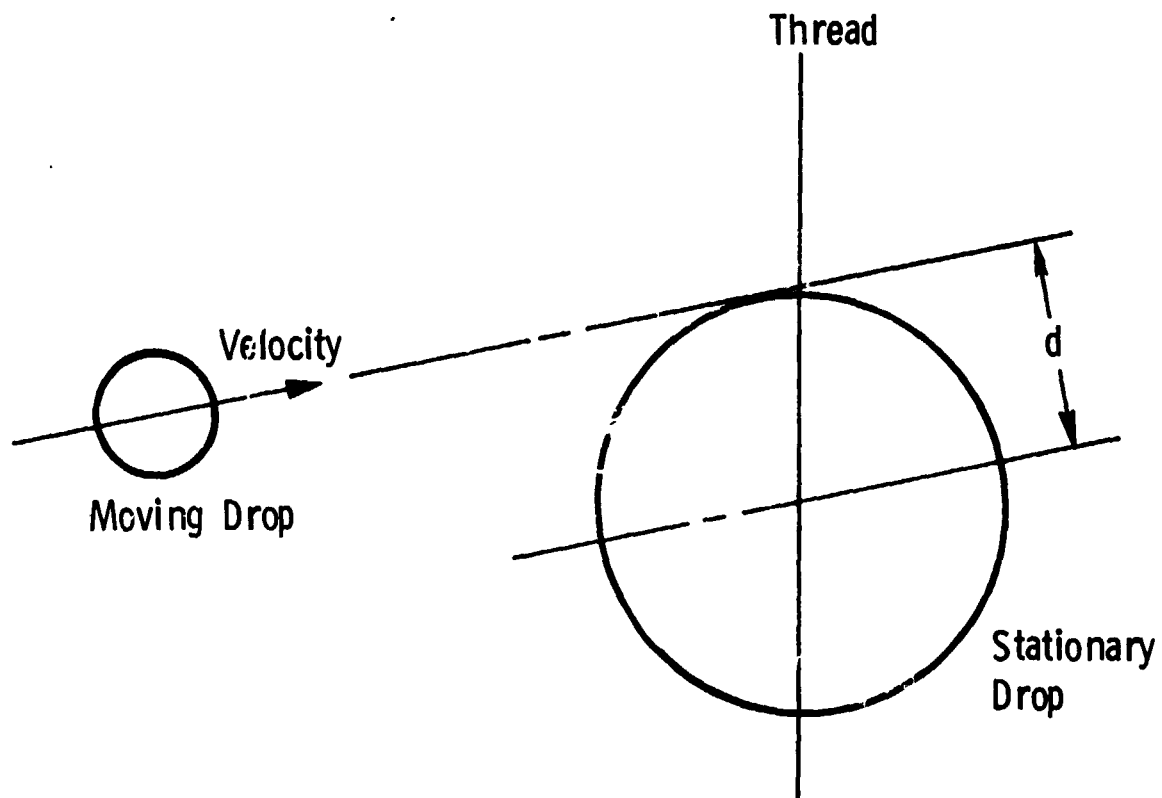


Figure 28. Drop configuration for coalescence demonstration.

Table 8. Coalescence Data

Test No.	Stationary Drop		Moving Drop			Distance Between Line of Centers, cm
	Volume, cc	Color of Water	Volume, cc	Color of Water	Velocity, cm/sec	
1	30*	Red	30*	Black	1.5	3.7
2	30*	Red	30*	Black	2.1	2.3
3	60	+	7	Black	2.4	2.7
4	67	+	3	Black	23.0	2.3
5	70	+	3	Black	14.0	2.4
6	73	+	7	Clear	1.4	1.9

*Per Sound Track

+Result of Previous Coalescence

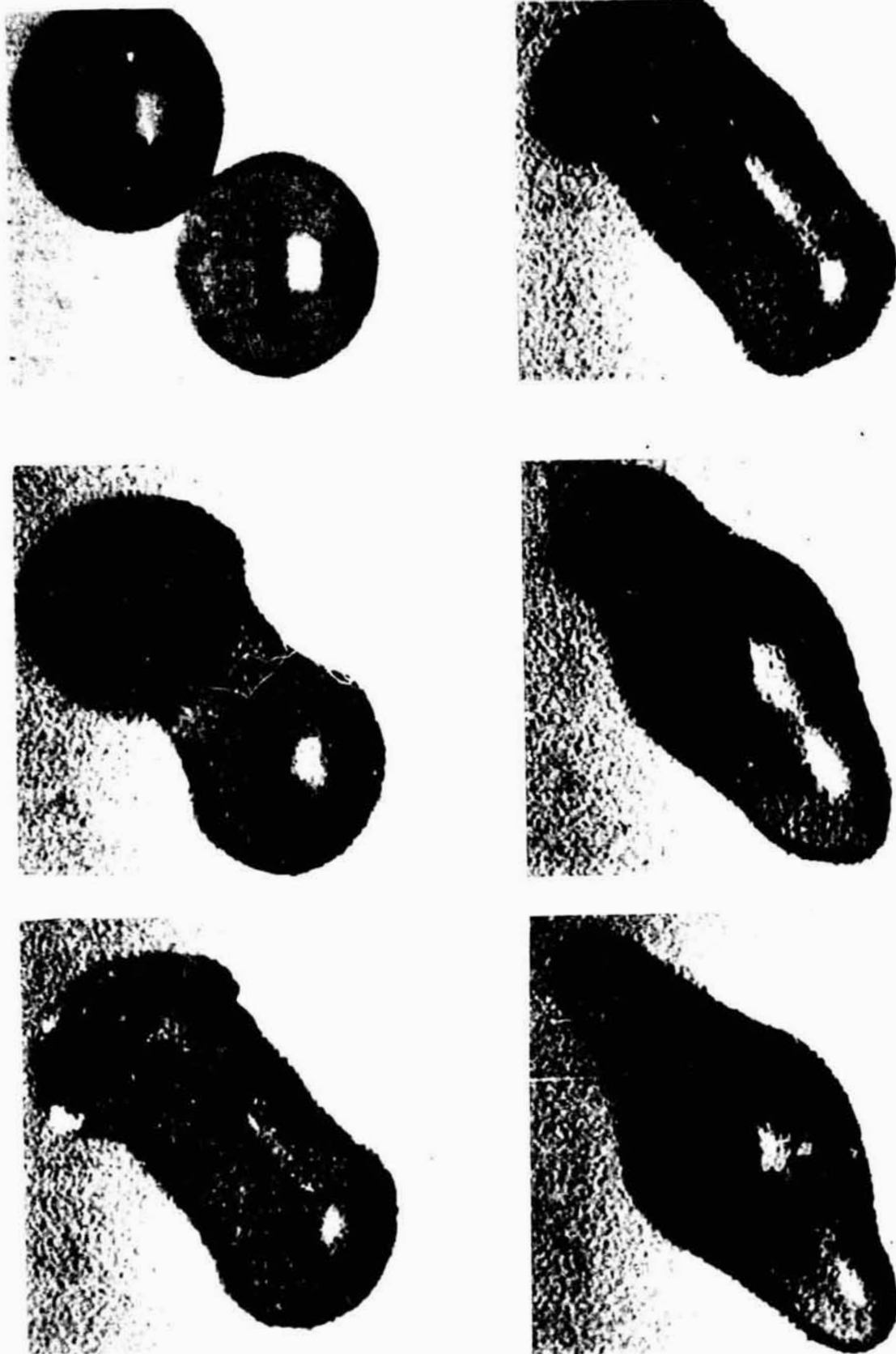


Figure 29. Coalescence - Test 1

ORIGINAL PAGE IS
OF POOR QUALITY

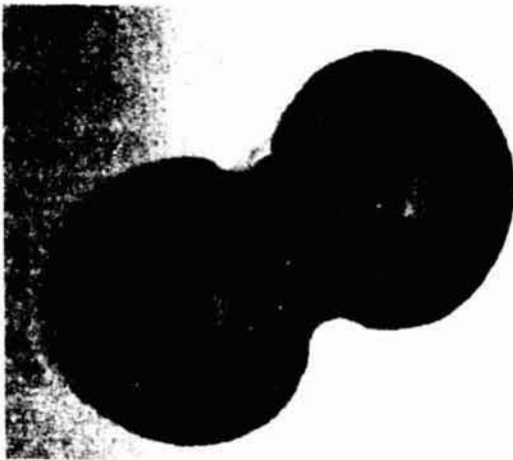
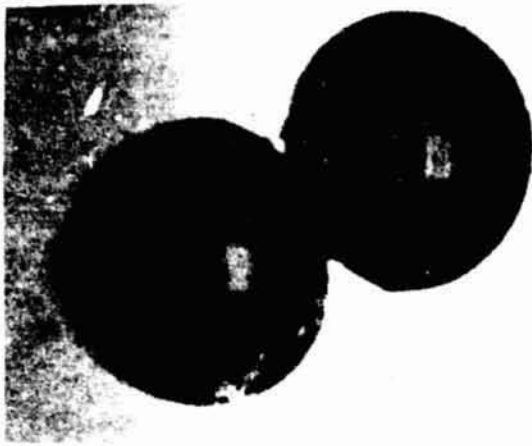


Figure 30. Coalescence - Test 2

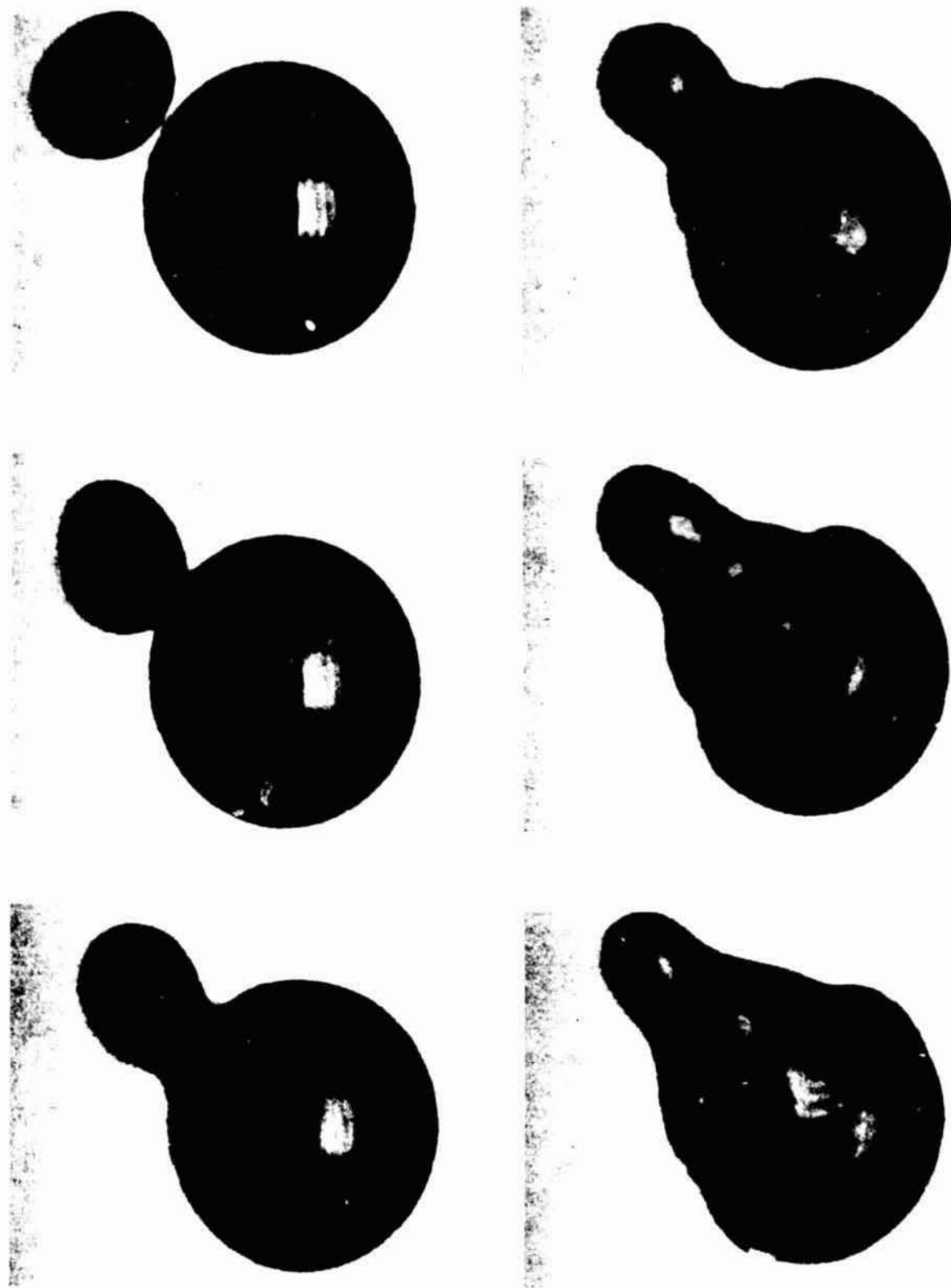


Figure 31. Coalescence - Test 3

was oscillating as it moved. Due to their relative sizes, second mode oscillation was induced by this coalescence.

The moving drop had a high velocity in test 4. Smearing of the drop image due to the film data format is obvious in Figure 32. After the small drop impacted the static drop coalescence occurred but the drops almost parted again. The static drop was rotated by the impact and was pulled off of its thread. Capillary waves could be observed traveling around the larger drop following impact. It is not shown in Figure 32, but the small drop was pulled completely into the larger drop as it continued to rotate. Erratic oscillations were induced by this coalescence.

In test 5 the small drop had a fairly high velocity. Again the large drop was rotated by the impact and pulled off the thread (Figure 33).

Test 6 is similar to test 3. The velocity of the drop was low and second mode oscillation was induced by the coalescence (Figure 34).

Two parameters have been used to categorize the coalescence of drops. One is the Weber number, the ratio of inertia force to surface tension force.

$$W_e = \frac{\rho r u^2}{\sigma} \quad (19)$$

where r is the radius of the moving drop and u is its velocity in this application. The other is a dimensional parameter

$$\left(\frac{d}{r_1 + r_2} \right)^2 \quad (20)$$

where d is the minimum distance between drop centers defined in Figure 28 and r_1 and r_2 are the radii of the two drops. These two parameters are listed for each test in Table 9.

Figure 35 (Ref. 36) shows a relation, derived from test data, between these two parameters for the case where both drops are the same size. Similar relations can be derived for drops of unequal sizes. The tests that established these curves and other data found in the literature is based on drops, the largest of which is 1.5 mm in diameter. The Skylab tests were performed with drops between 1.8 and 5.2 cm in diameter, so some care must be used in correlating this data.

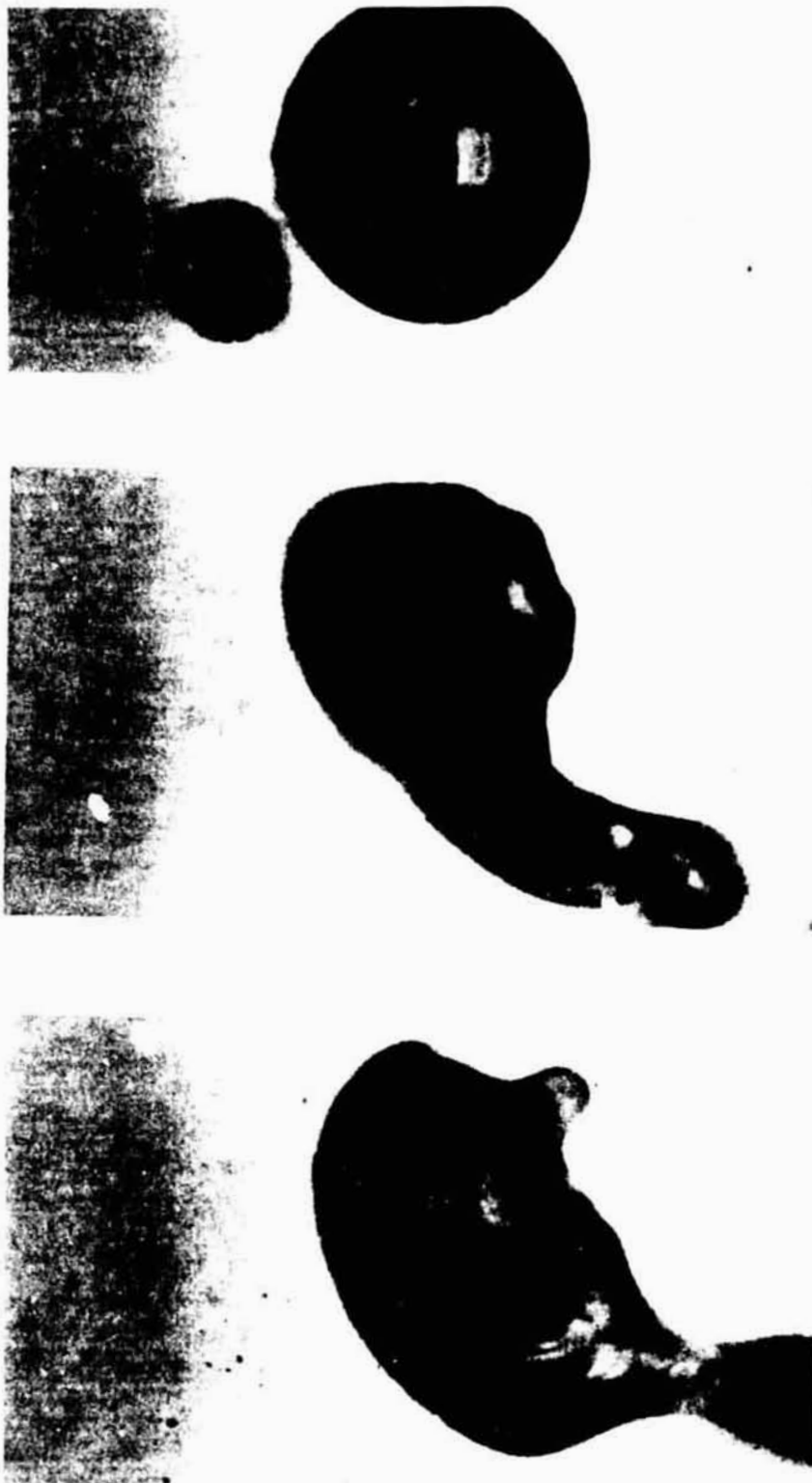


Figure 32. Coalescence - Test 4

ORIGINAL PAGE IS
OF POOR QUALITY

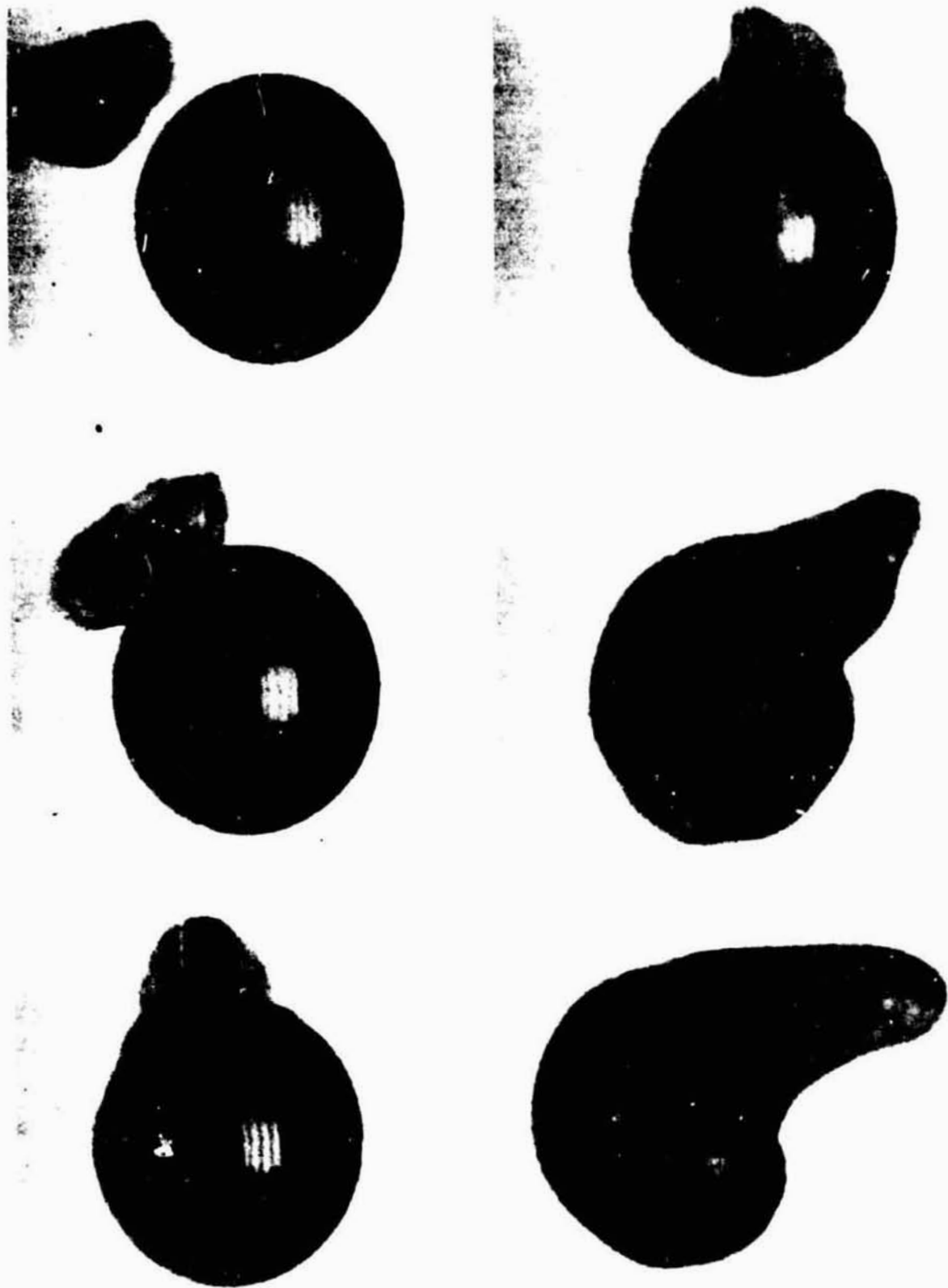


Figure 33 Coalescence - Test 5

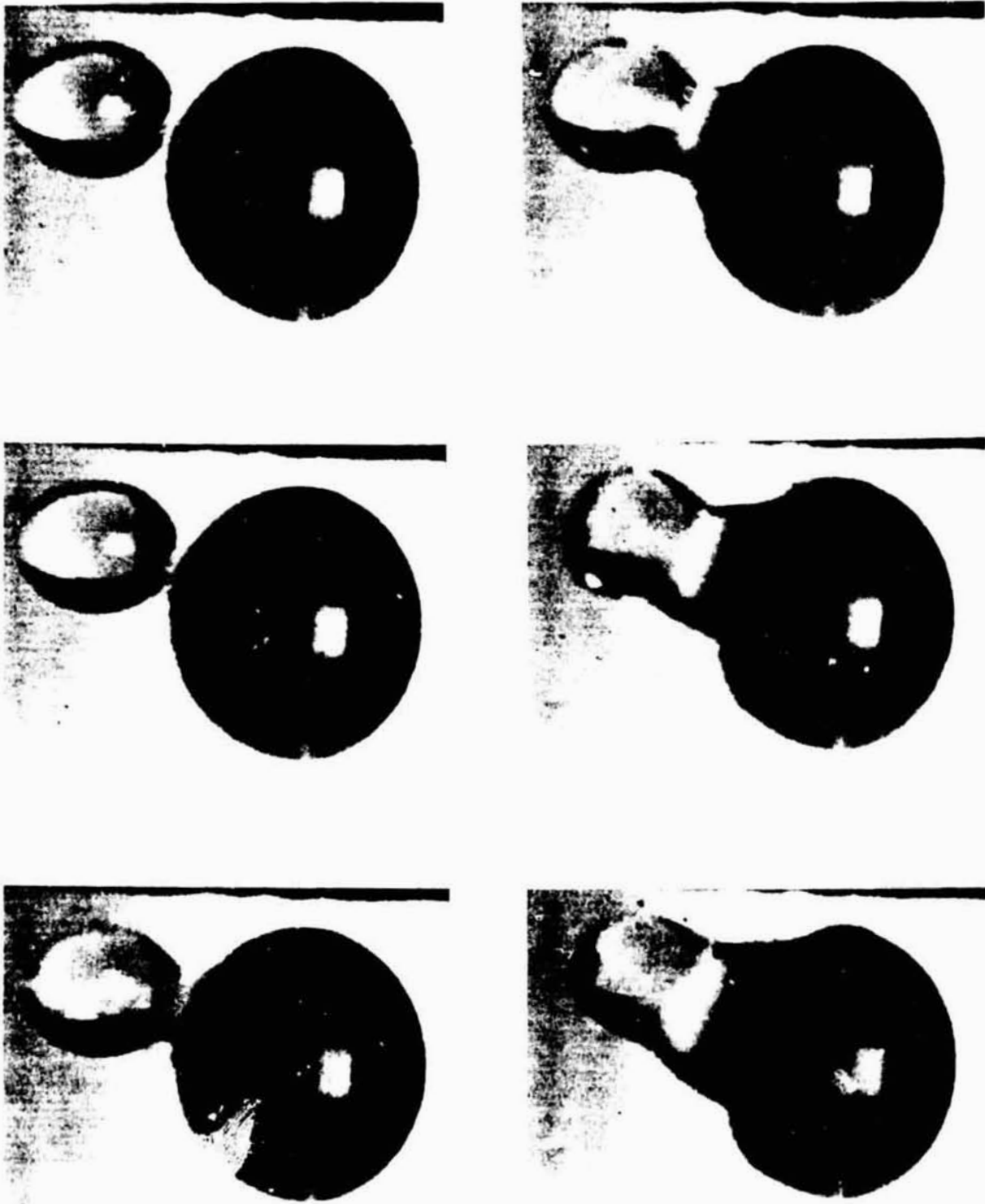


Figure 34. Coalescence - Test 6

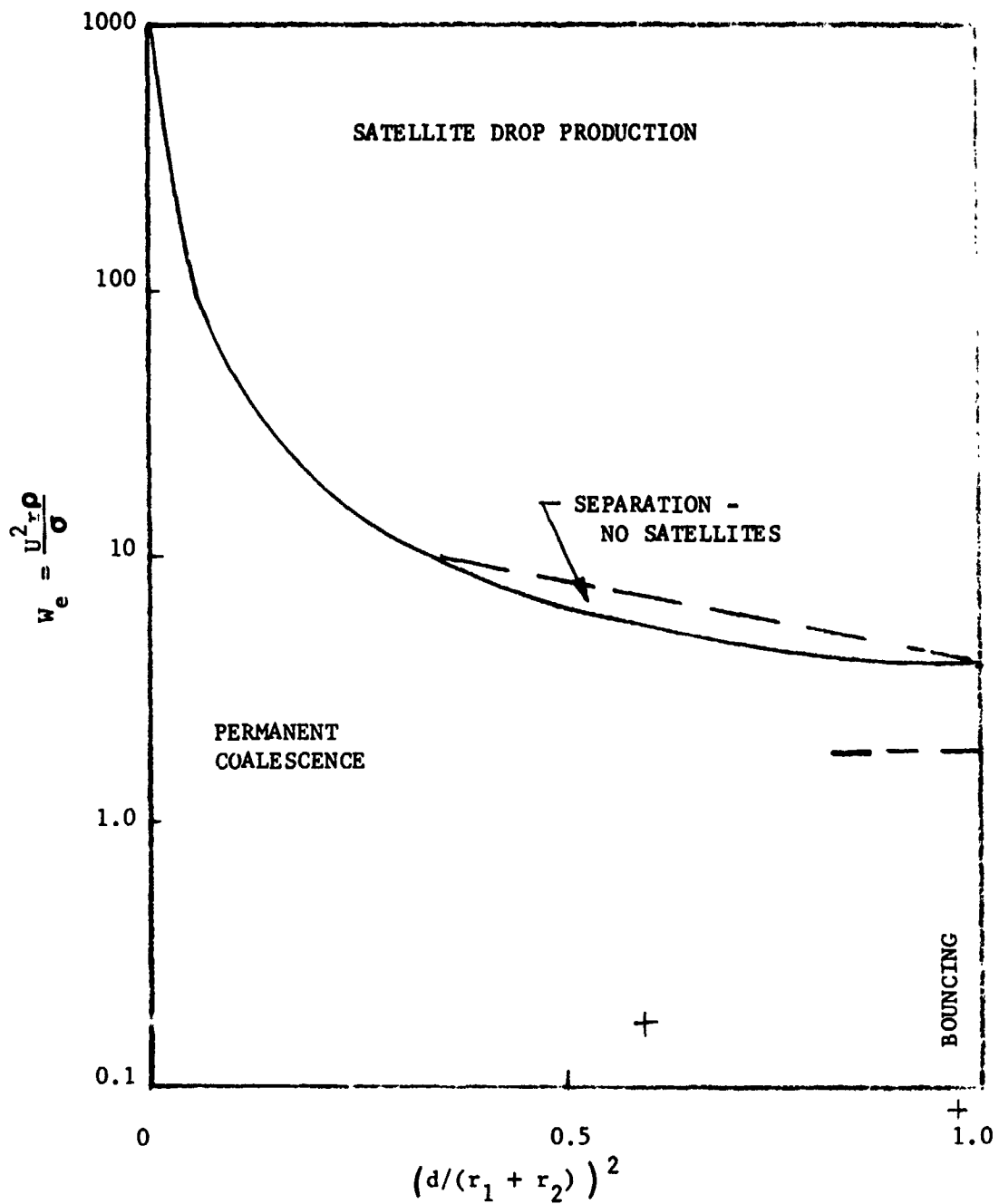


Figure 35. Regimes of Interaction for Equal Sized Drops (from Ref. 36)

TABLE 9. COALESCENCE PARAMETERS

Test Number	Weber Number	$\left(\frac{d}{r_1 + r_2}\right)^2$
1	0.09	0.96
2	0.17	0.60
3	0.14	0.75
4	9.5	0.67
5	3.5	0.70
6	0.04	0.50

The data points from test 1 and 2, the two tests in which the drops are equal sized, are shown on Figure 35. Test 1 falls into the region in which the drops should have bounced off one another.

Bouncing of the drops occurs when their relative inertia is low and they meet at a glancing angle. For equal sized drops the Weber number must be less than 2.0 and the parameter

$\left(d/(r_1 + r_2)\right)^2$ must be near to one. Under such conditions the layer of air between the drops cannot be expelled fast enough, so the drops do not make contact. There is a sequence in the Fluid Mechanics Series in which two drops impact but bounce off one another. The quality of the image was not good enough to measure the necessary parameters.

One reason that coalescence did occur in test 1 is that the moving drop was oscillating. The oscillations brought the surface of the drop closer to the stationary drop than is indicated by the location of the drop center. Figure 35 and the dimensional parameter do not account for the oscillations. The relatively large mass of the drop could also be a factor. It has been observed in ground based tests that increasing drop size (up to 1 mm diameter) tends to reduce the critical value of Weber number, below which bouncing occurs.

Test 2 falls well within the permanent coalescence regime.

Curves similar to Figure 35 were not available to compare the regimes of interaction for drops of unequal size. It would be expected that tests 3, 5 and 6 would fall into the permanent

coalescence region. In test 4 the moving drop almost separated from the static drop following the initial coalescence. It would be expected that this test must fall very close to the "Separation - No Satellites" regime.

D. Rotating Drop

Liquid drops were rotated with the objective of determining their shape as they rotate and to cause fission of the drop. In a unique series of tests, the existence of a "peanut" shape for a rotating drop was demonstrated. Very little experimental or analytical evidence as to the existence of this form was available prior to these tests. In one test the drop was rotated fast enough to cause spontaneous fission into two drops. The data from the six tests performed provide an indication of the relation between the angular rotation rate and the distortion of the drop.

If a free-floating drop is rotated in a low-g environment, surface tension forces can balance centrifugal forces to establish an equilibrium interface shape. Plateau was the first to experimentally investigate the interface shape of a rotating drop in 1833. He used two immiscible liquids of the same density, one to simulate the drop and the other to simulate the surrounding medium (Ref. 37). Lord Rayleigh analyzed the shape of a rotating drop in 1914 (Ref. 38) and more recent work by S. Chandrasekhar (Ref. 39) and D. K. Ross (Ref. 40) has refined that analysis.

In all the above work the equilibrium shape was established to be of the form of an oblate spheroid that tended towards a torus at the maximum distortion. The curves in Figure 36 show one-fourth of the cross-section of the drop with the b/r axis being both the axis of rotation and symmetry. When the rotation rate is increased the drop flattens along the b/r axis. Curve 5 is the last interface shape that still encloses the origin. Further increases in angular rate give a pure toroidal interface shape. At each point on the surface of the drop the curvature of the interface is such that the capillary pressure balances the hydrostatic pressure due to centrifugal force as follows:

$$\sigma(K - K_0) = 1/2 \rho r^2 \omega^2 \quad (21)$$

where K is the interface curvature (as defined in Section A) at a point on the surface the distance r from the axis of rotation and K_0 is the curvature at the axis of rotation. From the axis of rotation the increase in the capillary pressure with radius (due to the increase in curvature) matches the increase in hydrostatic pressure due to rotation. If the proper expression for the curvature is placed in equation (21) it can be solved to yield the interface shape.

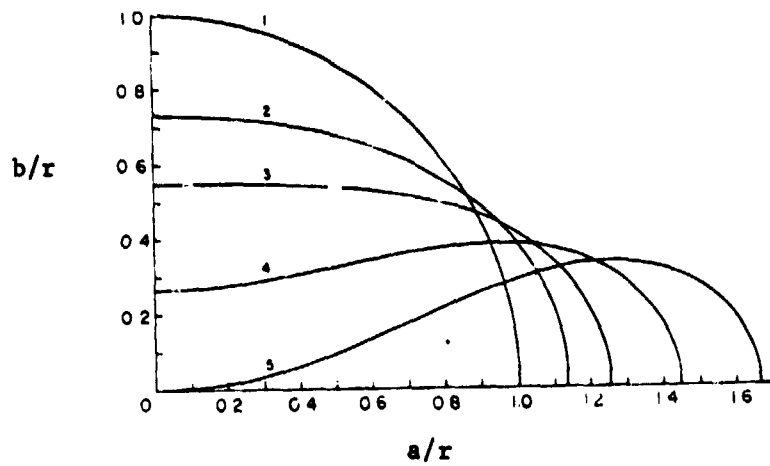


Figure 36. Interface shape for a drop of the toroidal form

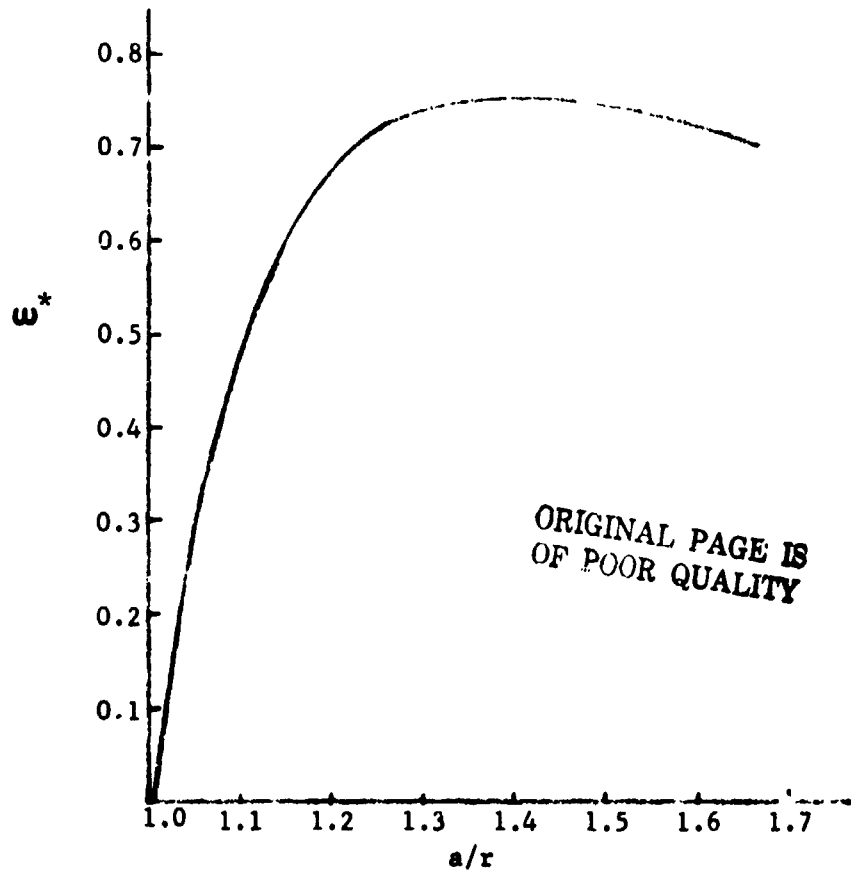


Figure 37. Variation of ϵ^* with drop distortion

A parameter ω^* is used to nondimensionalize the rotational rate, where

$$\omega^* = \sqrt{\frac{\rho \omega^2 r^3}{8\sigma}} \quad (22)$$

and r is the radius of the drop when it is spherical.

When $\omega^* = 0$ curve 1 is obtained. For curve 5, $b/r = 0$, $a/r = 1.6701$ and $\omega^* = 0.7071$.

A plot of ω^* versus the distortion of the drop (a/r) shows that ω^* is double valued when it is greater than 0.7071 (Figure 37). The value of ω^* increases with distortion until it reaches a maximum of 0.7540, beyond that point ω^* decreases as the distortion continues to increase. Since the dimensional angular rate is directly related to ω^* its variation with distortion is the same. The angular momentum of the drop is single valued however, always increasing with increasing distortion.

In Section A of this report it was shown that there are two possible interface shapes for a drop on a thread: the drop could be centered on the thread or it could be tangent to the thread. While both interfaces had a uniform curvature and satisfied the contact angle boundary condition, only one interface for any given set of conditions is possible based on energy considerations. The drop will tend to be in its minimum energy configuration. A similar consideration arises with the rotating drop. One interface configuration has been shown. Pressures due to capillary and centrifugal forces are balanced to define an interface shape. The possibility of another interface shape, which could have a lower energy must be considered. For the rotating drop, the kinetic energy due to rotation must be added to the surface energy of the drop to determine its total energy.

The stability of a drop can be analyzed. If a small perturbation is applied to the drop and it returns to the same configuration, the drop is stable and is in the minimum energy configuration. If it is found to be unstable, another configuration with a lower energy must exist. Both S. Chandrasekhar (Ref. 39) and D. K. Ross (Ref. 41) have analyzed the stability of the toroidal form of the rotating drop, but their results do not agree. According to D. K. Ross the toroidal form is stable if ω^* is less than the maximum value of 0.7540. He states that at larger values the drop will be unstable and a new equilibrium shape emerges. According to S. Chandrasekhar at values of ω^*

of about 0.5 (he uses a slightly different notation so these are only approximate values) the drop will be unstable if viscous forces are present, and unconditional instability occurs at ω^* of about 0.70. He states that "one may anticipate that at this point a stable sequence of triaxial forms branches off". The toroidal shape was obtained in Plateau's experiment for all values of angular velocity because the viscous liquid that surrounds the drop damps out any disturbances, making the toroidal form stable.

There appears to be much similarity between the stable rotating forms of a drop held together by gravitational forces (Ref. 42) and this case, a drop held together by surface tension forces. The analysis of the self-gravitating drop appears to be much more developed than for the surface tension drop.

From the literature search, the field of lunar geology yielded the only indication of the other possible form of a rotating drop (Refs. 42, 44, and 45). Some glass globules ejected from meteoroid impacts were found to have a peanut or dumbbell shape. The cross-section of this shape is similar to that in Figure 36, except that the a/r axis appears to be an axis of symmetry. Apparently the glass globules were rotating after ejection and they solidified in that form. Measurements of the glass drops were used to predict the angular velocity that would yield such an equilibrium shape.

In Reference 36 the coalescence and subsequent breakup of drops due to rotation was investigated. Following coalescence the drops were about to break apart again and have a peanut shape, similar to the glass globules discussed above. However, the breakup due to angular momentum was analyzed based on the toroidal form.

To summarize the existing literature of the rotating drop, the analysis has concentrated on the toroidal form. It has been shown that it is not the only form a rotating drop can assume. Other than a few hints, such as the lunar glass drops, very little has been done to define the shape and behavior of other forms.

In a unique demonstration on Skylab, the peanut shape was shown to be an equilibrium form for the rotating drop. Six individual tests were conducted in the Fluid Mechanics Series and the peanut form was obtained in each.

A number of different methods were used to rotate the drop, as shown in Figure 38. A ring with peripheral holes was taken up to Skylab for the purpose of rotating drops. It was hoped that a drop could be rotated by blowing through the ring, but it was not successful. The drop could not be kept centered in the ring. Rather, brute force methods were used, such as inserting a tube into the drop and stirring it, and striking the edge of a drop a number of times with the needle of a syringe. While these methods did induce rotation, the most successful method made use of two food cans with three strings between them. The strings were twisted in the center and the drop tended to position at this point as shown by Figure 39. Attempts to displace the drop from the centered position were opposed by the strings, as shown by the center and right photos of Figure 39. The cans and strings were rotated, allowing the string to stir the drop. A controlled amount of angular momentum could be applied to the drop without producing any lateral translation. Any attempt to further increase the angular momentum of the drop by reinserting the strings usually caused the drop to break apart. The syringe needle was the best method of increasing angular momentum because it could be inserted into and withdrawn from the drop without producing excessive perturbations.

In a low-g environment, with a minimum of dissipation due to viscous drag of the air, the drop continues to rotate in an equilibrium form. The typical equilibrium form achieved in these demonstrations is shown in Figure 40. The drop is rotating clockwise in the plane of the picture.

An evaluation of the forces acting on the peanut form of the rotating drop indicates that the drop is not symmetrical with respect to its long axis. Some typical cross-sections are shown in Figure 41. Consider the cross-section passing through the axis of rotation. Cross-sections near the ends of the drop are close to circular. The drop is not symmetric with respect to any of the axes.

The parameters measured from each rotating drop are shown in Figure 41. They are the angular velocity (ω), the elongation perpendicular to the axis of rotation (a), and the compression along the axis of rotation (b). The measured parameters for each of the tests are listed in Table 10. The duration is the period of time that the drop was allowed to rotate.

The volume of the drops was not stated on the sound track. Using the measured frequency of oscillation, the volume of the drop



(a) Blow ring



(b) Stir with straw



(c) Strike with needle



(d) Food cans and strings

Figure 38. Methods of Rotating Drops



Figure 39. The drop tends to center on the threads, even though disturbed as it is in right photos.

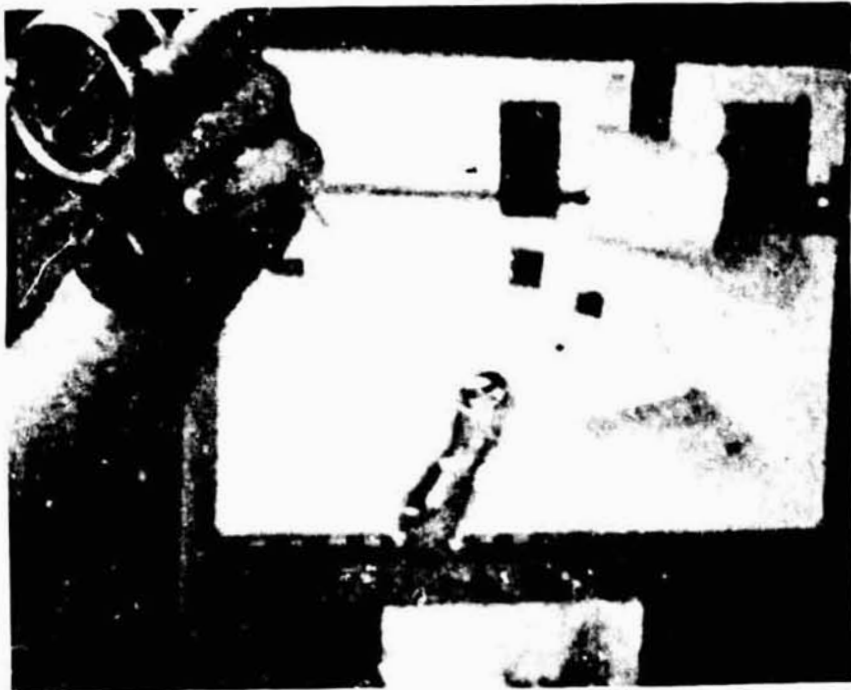


Figure 40. Peanut shape assumed by rotating drop.

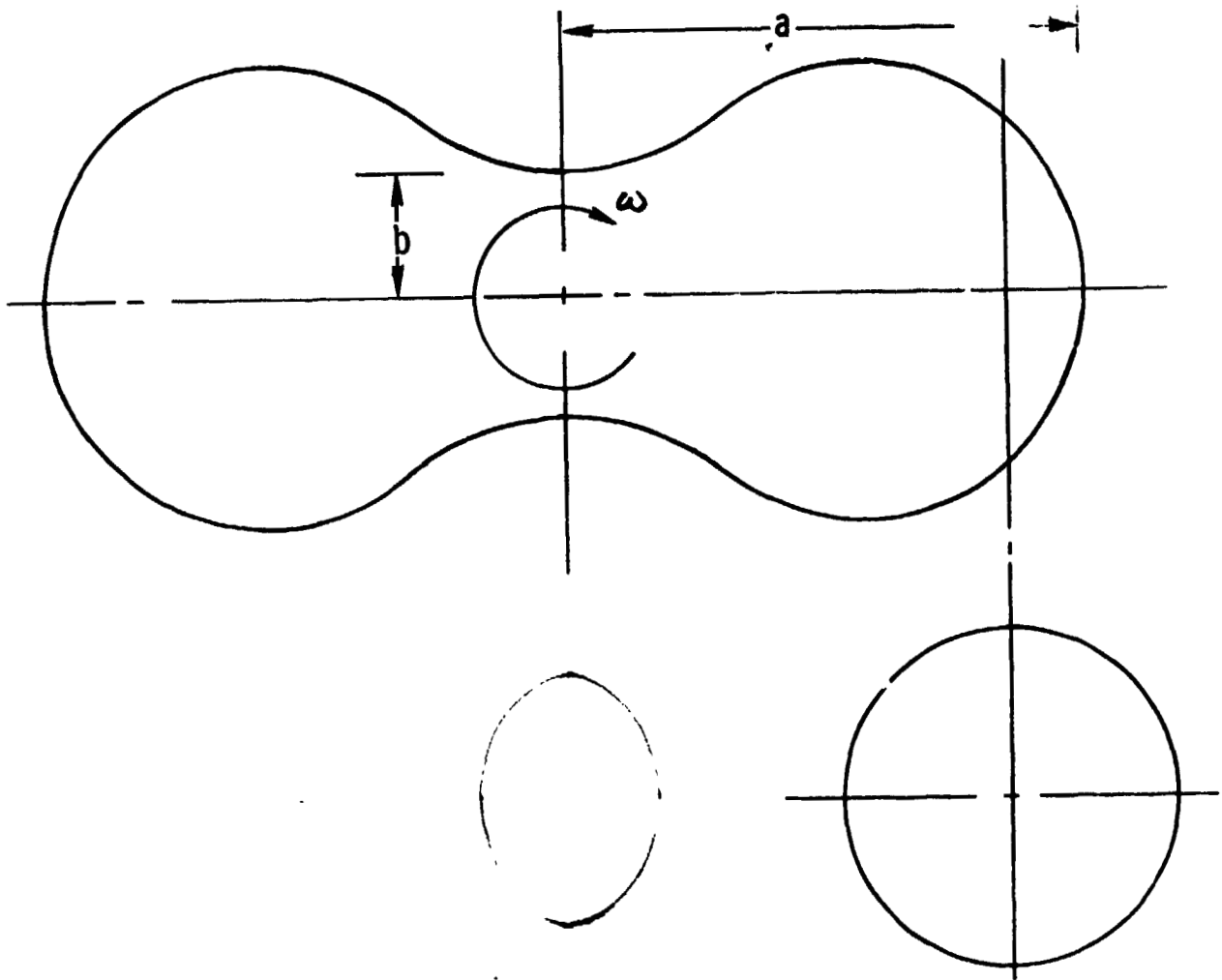


Figure 41. Rotating Drop Configuration

ORIGINAL PAGE IS
OF POOR QUALITY

Table 10. Rotating Drop Data

Test No.	Duration, sec	Drop Volume, cc	Rotation Rate		a/b
			ω , rpm	ω^*	
1	20	35	33.5	0.42	1.6
	37	35	25.0	0.32	3.5
2	8	35	27.0	0.34	2.6
3	25	91	27.2	0.55	3.2
	7	91	25.3	0.51	3.4
4	58	91	28.3	0.58	3.7
5	17	91	24.4	0.50	4.3
6	31	71	19.4	0.35	∞

for tests 1 and 2 was calculated. By scaling the dimensions with respect to the food cans used in rotating the drop, the other volumes were calculated. The ratio a/b was used to define the elongation since both dimensions could be directly measured at any point in time. This eliminates the dependency of the elongation parameter on the drop volume.

A syringe needle was used to rotate the drop in test 1, a tube was used for 2 and the cans and strings were used for the remainder of the tests.

Test 1 demonstrated how angular momentum and angular frequency can vary. After allowing the drop to rotate at a steady rate for 20 seconds, the needle was passed through the drop a few more times to increase the angular momentum of the drop. The drop elongated, but the angular rate decreased. From this test it can be concluded that the variation of ω^* and drop elongation for the peanut shape is similar to that for the toroidal shape. The parameter ω^* is double valued. After a maximum value, the rotation rate decreases as distortion increases. In the first part of the test the drop had a prolate spheroid form (watermelon). After the increase in angular momentum the drop necked down at the axis and assumed the peanut shape. This data point must lie beyond the maximum value of ω^* . In both parts of the test the shape and rotation rate were not varying with time.

The angular rate obtained in test 2 falls in between the two rates of test 1. Again the shape and rotation rate were static. The drop midsection was cylindrical in shape indicating that the value of ω^* must be close to the point at which necking at the axis begins to occur.

In test 3 the angular momentum was again increased during the test. Before and after the increase the drop had the peanut shape. The drop was still elongating, so it was not at steady state at the end of the test. Again the second data point provided by this test must be beyond the maximum value of ω^* .

In tests 4 and 5 the peanut shape was again assumed by the rotating drop. The elongation was decreasing and the angular rate was increasing in test 4 as the drop achieved its equilibrium configuration, again showing that ω^* is double valued.

Test 6 is the most unique of the tests. After applying the angular momentum to the drop it rotated for a period of 31 seconds. During this period the drop was elongating, in the

peanut shape, and the rotational rate was slowing. Fission of the drop, splitting it into two equal sized drops, occurred (Figure 42). Since it took such a long period for fission to occur the value of angular momentum applied must have been very close to the critical value for fission to occur.

The data points from the six tests are plotted in Figure 43. Also shown in the figure is the curve for the toroidal shape of the rotating drop. If the volume of the 35 cc drop was actually greater and the volume of the 91 and 71 cc drops was less, a fairly smooth curve could be drawn through the data points. Even though there is some uncertainty in the drop volume, there is sufficient accuracy to draw some conclusions about the peanut shape of the rotating drop.

- 1) The curve of ω^* versus drop elongation is double valued. After a maximum value, ω^* decreases as elongation increases.
- 2) The slope of the ω^* versus elongation curve is greater following the maximum value of ω^* than it is for the toroidal shape.
- 3) The peanut shape appears to be the minimum energy configuration for the range of angular rates of the tests. This is based only on the fact that all the points lie below the curve for the toroidal shape. The energy of the drop depends upon the surface energy and the kinetic energy. The moment of inertia and the surface area of the drop must be known before an exact comparison can be made.
- 4) None of the rotating drops were of the toroidal form so very little could be learned concerning the transition from that form to the peanut form. As discussed above, stability analyses indicate the smallest value of ω^* for this transition is about 0.5. The drop in the first part of Test 1 falls the closest to the transition point, while the other drops were well within the peanut regime. A value of ω^* of 0.42 was measured for that test, but there is some uncertainty in the drop volume.

ORIGINAL PAGE IS
OF POOR QUALITY

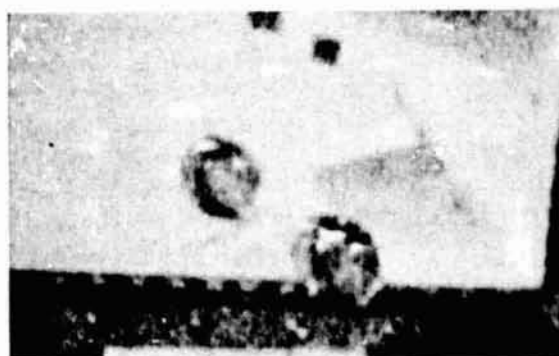
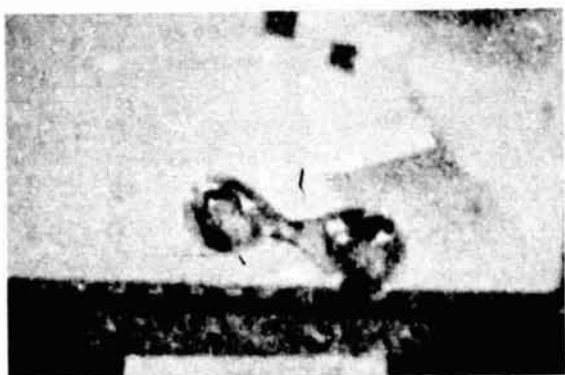


Figure 42. Fission of a Rotating Drop

ORIGINAL PAGE IS
OF POOR QUALITY

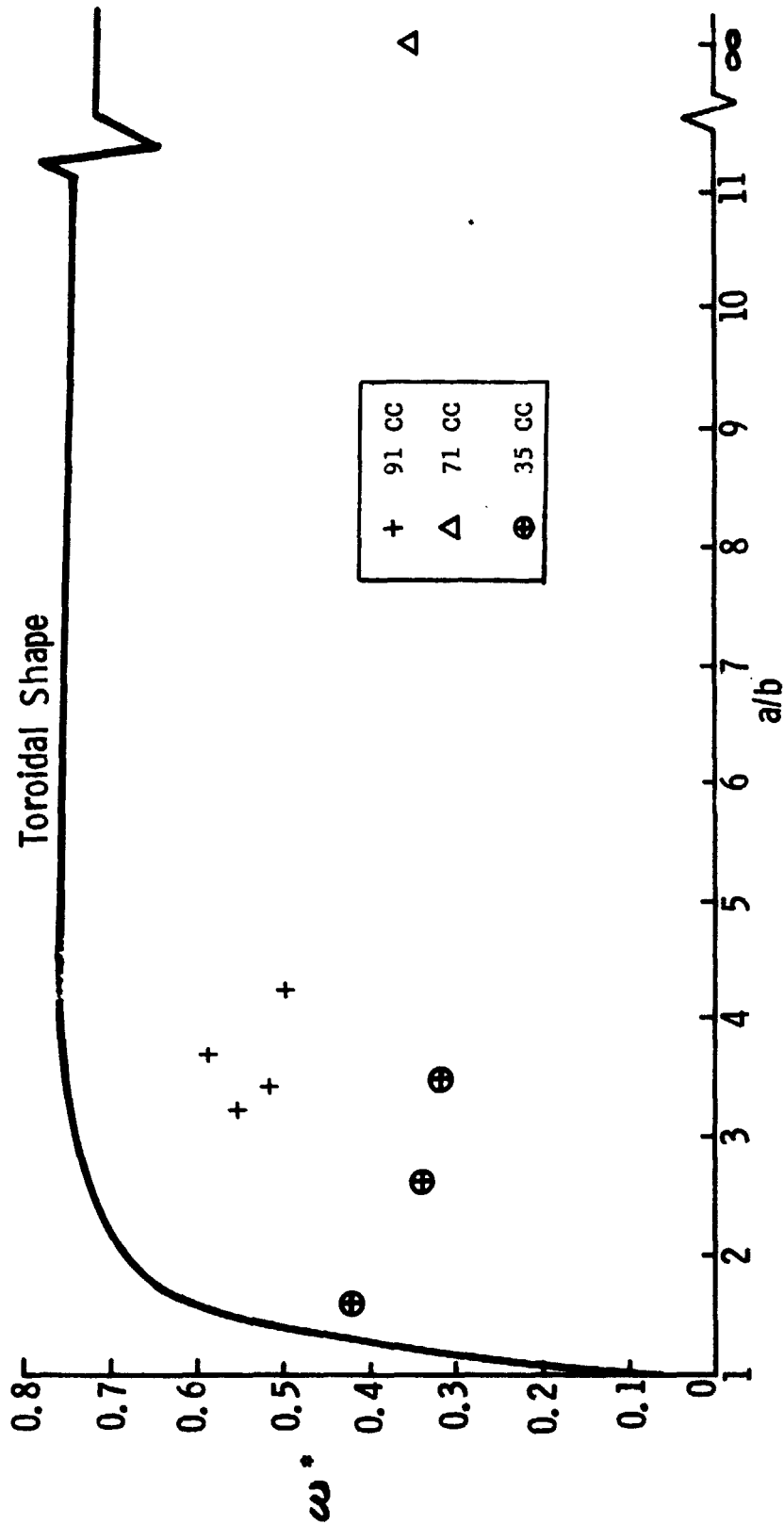


Figure 43. Comparison of demonstration data and toroidal theory.

E. Immiscible Liquids

The objective of the Immiscible Liquids demonstration was to demonstrate their behavior in low-g. The rate of coalescence of a dispersion of the two liquids was to be established. It was found that the rate of separation of the immiscible liquids was very slow. No significant separation was observed over a period of 10 hours.

Two liquids are immiscible when they are mutually insoluble. A dispersion of two immiscible liquids can be formed if they are strongly mixed. If the densities of the two liquids are different, the dispersion will quickly separate in one-g. In low-g, the force of gravity will not be present to separate the two liquids and the dispersion will behave quite differently. Such dispersions can be formed in one-g with certain liquids, especially if their densities are nearly equal, and are referred to as emulsions (Ref. 46).

A small experiment module was used to demonstrate the behavior of immiscible liquids. The module consisted of three vials: one with 25% oil and 75% water, one with 50% oil and 50% water, and one with 75% oil and 25% water. The oil could be separated from the water using the centrifugal force produced by swinging the module on the end of a string. A dispersion could be formed by shaking the module.

In the film data the manipulation of the test module was demonstrated. The liquids were shown after being separated and after dispersion (Figure 44). In one sequence, the module was held in front of the camera for a period of four minutes after shaking. The module was photographed over a period of 10 hours, using a 35 mm camera, to record any separation of the liquids.

Lacy and Otto (Ref. 10 and 11) present a detailed description and analysis of the Immiscible Liquids demonstration. Their second paper is similar to the first except that some photo densitometer measurements, made from the photographic data, are added to the analysis. They performed the same experiment in one-g and demonstrated that separation of the two liquids took place in less than 10 seconds. Their analysis of the data concluded that the dispersion was at least 3.6×10^5 times more stable in low-g than it was on earth. (The dispersions were less separated after 10 hours in low-g than they were after 0.1 second in one-g).

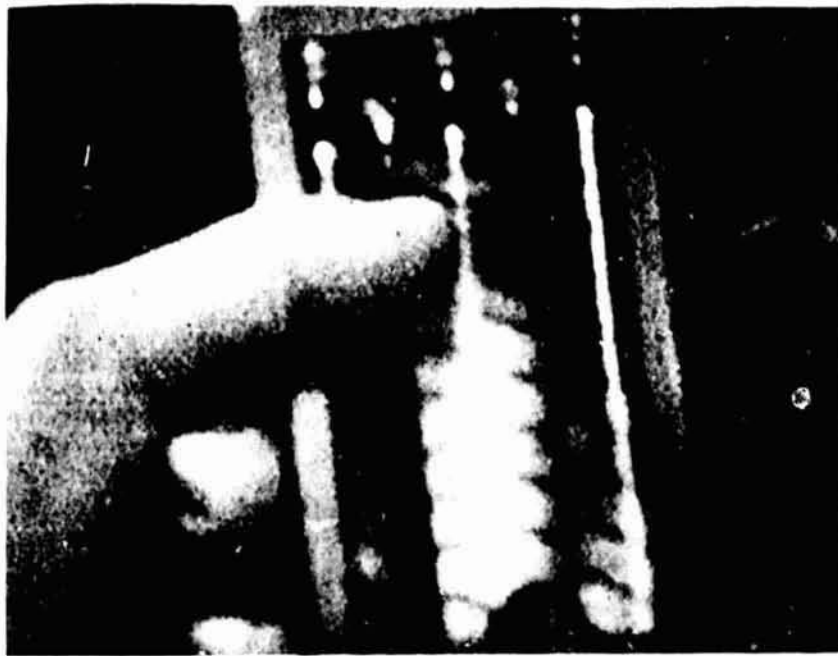


Figure 44. The module with three vials for the Immiscible Liquids demonstration is shown following centrifugal separation (above) and after mixing (below).

ORIGINAL PAGE IS
OF POOR QUALITY

When gravitational forces are small, the mechanism for separation of the dispersion is very different. One liquid can separate from the other only by coalescence. If drops of one liquid do come into contact and do coalesce, separation can proceed at some slow rate. Therefore the motion of the drops in the dispersion and probability of coalescence become important factors. The presence of surface active agents can have a significant effect on the rate of separation (usually slowing it).

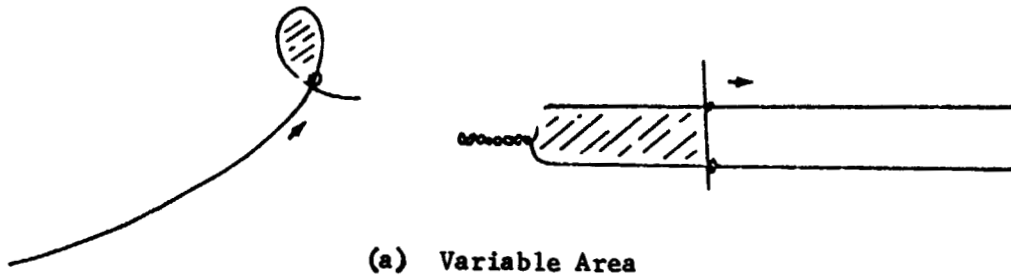
The demonstration did not yield any data on the mechanisms of separation in low-g. Astronaut Pogue did observe a "cellular structure that grew coarse during the elapsed 10 hours". Apparently separation was taking place at a slow rate, but it could not be detected from the photographic data.

F. Liquid Films

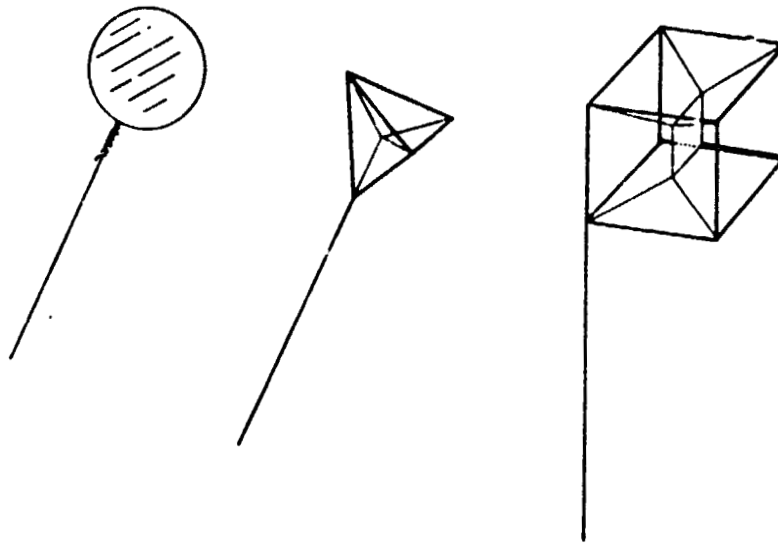
The objective of this demonstration was to construct thin liquid films in low gravity and to observe and record their formation, characteristics and time to rupture. While the form of the films was the same as in one-g, they contained a large volume of liquid (especially those formed on the three-dimensional wire frames). For this reason, their lifetime was increased in comparison to similar demonstrations on Earth.

Skylab mission SL-4 astronaut Gerald Carr conducted a series of demonstrations using both plain water and a soap solution to form a number of liquid films. Three types of wire frames were used: variable area, two-dimensional; fixed area, two-dimensional; and fixed volume, three dimensional (Figure 45). Both water and soap solution films were formed with the variable area frames, while the fixed area and volume frames utilized only the soap solution.

There were two film formation methods attempted. The first used the variable area frames to increase the surface area of a small liquid drop (1/8 to 1 cc) until the film that formed had burst. An expanding loop was used to draw films of both plain water (Figure 46) and soap solution (Figure 47). A maximum film diameter of 7.6 cm (3 in) was observed for "plain" water, while the astronaut was able to draw the soap solution out to the limit of loop expansion. The second variable area frame was a rectangle with two extended legs and a fourth movable side that slides along them. Only soap solution was expanded in the rectangle, a smaller drop (estimated to be about 1/8 cc) yielded a film area of about 45 cm².



(a) Variable Area



(b) Fixed Area and Volume

Figure 45. Wire Frames Used in Liquid Film Demonstration (from Ref. 12)

ORIGINAL PAGE IS
OF POOR QUALITY



Figure 46. Film Formed with "Plain" Water



Figure 47. Film Formed with Soap Solution

ORIGINAL PAGE IS
OF POOR QUALITY



Full of Soap Solution



Some Solution Removed by Shaking

Figure 48. Cube Wire Frame with Soap Film and Bulk Liquid Soap Solution in Center

The second film formation method consisted of dipping the frames in a container of soap solution and jerking them out to form a film rather than remove a significant quantity of liquid. In fact, on several trials with the cube wire frame, astronaut Carr pulled it out slowly, and it contained a considerable additional volume of liquid, as visible in Figure 48. Once the films were formed, the frames were held stationary and changes occurring in the films up to rupture were observed and timed. During trials in which bulk liquid soap solution was contained in the frame, the astronaut was able to essentially remove the bulk liquid by shaking the frame. The films then assumed minimal surface configurations similar to those noted in ground laboratory tests.

The three frames used in the inertia method (jerk from a container of soap solution) were a fixed area loop, a tetrahedron and a cube. Films on the loop lasted up to 1-1/2 minutes, with those on the complex shapes, tetrahedron and cube, changing constantly as parts of the film network ruptured and surface tension caused the remaining films to readjust. Astronaut Carr commented that the most stable configurations for the 3 dimensional frames occurred when films did not contact one another, i.e., when they covered adjoining or opposite exterior faces.

Extensive analyses of liquid films and their governing phenomena have been performed in the field of surface chemistry. Although the mechanism of film rupture is not well understood, it can be stated that undisturbed films usually rupture only after some degree of thinning (Ref. 46). Thinning of films is generally accomplished by two means: drainage and evaporation. However, stability of a film is governed by its elasticity and resilience.

There are two types of liquid drainage that occur in films. The first is due to gravity, it is negligible in "thin" films (1-5 μ thick) and has no bearing on the Skylab films since, although some were quite thick, they were created in a zero-gravity environment. The second drainage mechanism is due to the curvature of the film where it contacts the wire frame. This curvature causes a lower pressure at the film edge and so pumps liquid from the center of the film to the film/wire interface. Therefore the rate at which a film thins is inversely proportional to its minimum width or diameter.

Evaporation is a significant film thinning agent only when the surfactant film covering the bulk liquid is very thin. This surface film acts as a retardant to evaporation, becoming more effective as the surfactant layer thickens. The actual rate of evaporation is also affected by the vapor pressure of the liquid in the film and the conditions of the atmosphere in which the film is created.

Pure liquids do not produce a stable film, since they offer no resistance to rupture. Elasticity of a film is a measure of its ability to withstand a temporary area expansion without rupture. As the surface area increases, the surfactant concentration is lowered and therefore the surface tension is raised locally. This increased surface tension resists rupture and by the Marangoni effect (as mentioned in Section B) reinforces the thickness of the film. From this explanation, it is obvious that pure liquids have no elasticity, since the surface tension is constant throughout the liquid layer. It should further be noted that a saturated solution also has no elasticity, again due to uniform surface tension throughout the layer, (Reference 47). The logical conclusion, then, is that maximum film stability occurs when the concentration of the solution is somewhere between zero and the maximum; and this is, in fact, the case.

The resilience of a film is a function of both the rate of diffusion of the surfactant back to a surface that has been extended and therefore undergone a rise in surface tension, and the rate at which the Marangoni effect thickens the film at this weak point. A more resilient film will thicken before the surface tension returns to the surfactant-influenced equilibrium level; while if the surface tension lowers before the film is again a uniform thickness, the area remains weak and a likely site for initiation of film rupture.

The shape assumed by several films that join along one or more sides is governed by surface tension. In a two dimensional case, the equilibrium condition is 3 films joined at angles of 120° . For three dimensional cases, the shapes produced are somewhat more complex, but still governed by the principle of equal surface tension in all legs leading from the junction.

In summary the most important properties for film stability are:

- 1) low equilibrium surface tension,
- 2) moderate rate of attainment of equilibrium surface tension by surfactant diffusion, and
- 3) high surface viscosity, which tends to retard drainage and therefore maintain thicker films.

The soap solution liquid films formed on Skylab show a considerable increase in longevity over those formed of a similar solution in ground (1-g) experiments. However, tests by Wesley Darbro of NASA-MSFC have shown no significant improvement in stability over ground films that were rotated to at least partially negate the effects of gravity drainage, (Ref. 12). The Skylab zero gravity environment appears to have little or no effect on the other drainage and stability mechanisms of soap films. In fact, much larger and longer lasting films have been formed on earth using other solutions (Ref. 37).

The second important result was the formation of films containing significant amounts of bulk liquid on the three dimensional wire frames. Darbro discusses the impact of this bulk liquid on the film minimum surface in Ref. 12.

An additional comment should be made on the two dimensional films made with the expanding wire loop. Since pure water has no elasticity (as explained earlier) it is extremely doubtful that it would be possible to form a pure water film. It is suspected that some contaminant acted as a surfactant and thus made the formation of a "plain" water film possible.

G. Ice Melting

The objective of this demonstration was to observe the interface between each of the phases as the ice melted and to evaluate the rate of melting in low-g. Compared to one-g, the mechanism of melting is much different in low-g. The liquid does not drain away from the ice but surrounds it. This insulating layer of liquid influences the rate of heat conduction to the ice. Gravity driven convection would not be present, but surface tension forces are one possible source of low-g convection.

An ice cylinder was photographed with a 16 mm camera as it melted in this demonstration. The ice was initially 3.0 cm in diameter, 6.1 cm in length and had a volume of 43.2 cc. It was formed on a wooden stick located on the axis of the cylinder. About every ten to fifteen minutes, the camera was started, operated at 2 frames per second for a few seconds and then stopped. The data quality is poor because the camera was slightly out of focus. It took about 190 minutes for the ice to completely melt. Pictures of the ice cylinder as it melted are shown in Figure 49.

As the ice melted, the water surrounded the ice, with surface tension, the ice and the stick determining the interface shape. An interface configuration in which the curvature of the surface is uniform and therefore the liquid pressure is constant (as described in Section A) is always established. After some melting had occurred the surface had the form of an ellipsoid, being elongated by the ice. Most of the liquid collected on the sides of the ice cylinder to make the ellipsoidal form, removing liquid from the ends of the cylinder. Since the small area of ice at the ends of the cylinder was more directly exposed to the surrounding air, the ends of the ice melted faster than the sides. The length to diameter ratio of the liquid interface gradually changed as the ice melted, from a value of 2.0 for the ice cylinder to 1.2 for the liquid drop. The drop always had some elongation due to the presence of the stick, in the same way a thread elongated a drop (section A). The ratio of the drop diameter to the stick diameter was 24:1, which was large enough to permit the drop to be centered on the stick and not sit tangent to the stick. Since the preferential interface shape is highly sensitive to contact angle, this data point can not be directly compared with the drop on a thread data in Section A.

Ice Cylinder

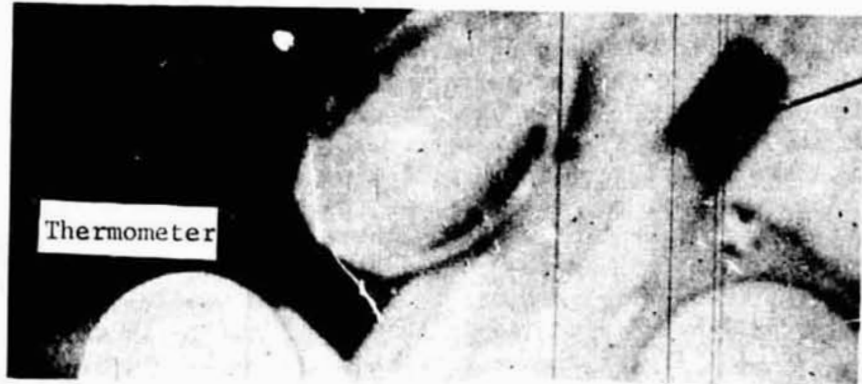


Figure 49. Ice Melting Demonstration

There is another less pronounced effect on the shape of the interface and the liquid surrounding the ice. As the ice first began to melt, the liquid interface was very close to the ice at the ends of the ice cylinder. Therefore the temperature of the liquid surface must have been colder at the ends of the ice cylinder than it was along the sides, where there was a thicker layer of liquid. Since there was a temperature gradient along the liquid surface there must also be a surface tension gradient. Surface tension is primarily a function of temperature, with surface tension decreasing with increasing temperature for most liquids. Therefore the surface tension was greater near the ends of the ice cylinder than it was along the sides. "If for any reason differences of surface tension exist along a free liquid surface, liquid will flow toward the region of higher surface tension", (Ref. 48) as Marangoni described the phenomena that bears his name. Therefore, liquid will flow from the sides of the ice cylinder to its ends. Continued movement of the liquid tends to reduce the temperature gradient and establishes circulation within the liquid. As the length of the ice cylinder reduced, there was more liquid over the ends of the cylinder. The temperature gradients along the liquid surface will gradually reduce and the Marangoni flow will eventually cease.

The phenomenon of Marangoni flow is further described and some simple experiments demonstrating it can be found in Ref. 49. A survey of the literature of the Marangoni effects can be found in Ref. 50.

None of the effects of the surface tension driven flow could be directly observed in the film data. Nor does the data permit an evaluation of the magnitude of the Marangoni effect. Some type of suspended particles would be necessary to make the circulation visible and any change to the interface shape due to the flow could not be discerned. Since a temperature gradient of approximately 20°C was present between the ice and air, it must be assumed that Marangoni flow was occurring. Temperature gradients of $4^{\circ}\text{C}/\text{cm}$ have been shown to produce liquid surface velocities of $1\text{ cm}/\text{sec}$ in alcohol (Ref. 49).

The liquid surrounded the ice, tending to insulate the ice from the surrounding air. How well the liquid insulates the ice depends upon the magnitude of the conduction and convection heat transfer within the liquid. The Marangoni flow could be making a significant contribution to the convection heat transfer.

Convection heat transfer can also be induced by mechanical vibrations referred to as "G-Jitter" (see Chapter II). The vibrations can produce velocity fluctuations and shear stresses within the liquid, which can produce convective heat transfer (Ref. 18). Forced convection, due to the air flow of the ventilation system, must also be considered as a possible source of heat transfer.

Drs. Otto and Lacy (Ref. 14) made a detailed evaluation of the ice melting data. They performed an identical experiment in one-g and found that the ice melted in 130 minutes. In one-g the liquid drained away from the ice leaving the surface of the ice exposed to the surrounding air, so the mechanism of heat transfer is quite different from the low-g case.

Using a simplified model of the ice cylinder, they analyzed the heat transfer in the one-g and low-g case. For the low-g case, they conclude that conduction and radiation heat transfer provided the heat of fusion of the ice. However, the accuracy of the data and the heat transfer model do not permit assessment of small convective effects. Convective heat transfer in low-g is not well understood and much work needs to be done to establish its mechanisms and magnitudes (Ref. 18).

H. Foams

A foam is a mixture of gas and liquid with a definite structure. The bubbles of a foam are arranged such that three films come together forming angles of 120 degrees between each film. (This is attributed to Plateau, 1861.) The behavior of a foam, its stability, drainage and the influence of surfactants is similar to that of liquid films described in section F.

Dynamic and static methods are used to measure the stability of foams. One of the dynamic methods is to bubble gas through the liquid that is capable of foaming. After an initial period during which the height of the foam column above the liquid gradually increases, this height becomes constant. Bubbles are bursting at the top of the column at the same rate they are being formed at the base of the column. The height of foam is like a property of the liquid, being only dependent upon the flow rate of the gas (Ref. 47).

While it was not intended as such, this dynamic measure of foam stability was demonstrated in Skylab. Following the Ice Melting demonstration (section G) soap was added to the liquid drop that formed from the ice cylinder. As air was injected into the drop, a foam was formed (Figure 50). The volume of the foam gradually increased as air was added. As air continued to be added the foam reached a static diameter and no further increase in size was observed. On the surface of the foam, bubbles were observed erupting and small drops flying away as air was added. The mechanism of bubble collapse and formation of a jet at the surface of the foam must be the same as discussed for cavitation (Section L).



Figure 50. Adding air to a soap and water solution increases the volume until it reaches a static size (lower photo).

ORIGINAL PAGE IS
OF POOR QUALITY

I. Low-g Transfer of Liquids

One method of successfully transferring a liquid from one container to another in a low-g environment was demonstrated. The test liquid for this demonstration was blood. This demonstration was not part of any of the fluid mechanics demonstrations, but was found in the collection of Skylab video tape data.

A sample of blood had just been withdrawn from one astronaut by another (O. Garriott). The blood was in a large syringe and was being transferred to an evacuated bottle (Figure 51). The camera was zoomed in as the transfer began so the image is fairly large.

The needle of the syringe was inserted into the bottle, piercing a diaphragm. It extended part way into the bottle. Blood immediately began to be drawn from the syringe to the bottle, since the bottle was at a pressure somewhat below ambient. As the flow of liquid began, a drop could be observed forming at the tip of the syringe. The drop continued to expand until it contacted the wall of the bottle. At this point there was a volume of liquid, located near one end of the bottle, dividing the gas into two separate volumes. Liquid continued to transfer as the two gas volumes compressed. The volume of gas near the diaphragm of the bottle was the smaller of the two. Each volume must have had the same pressure with the liquid acting as a piston between them.

The quality of the image is not good enough to observe the shape of the liquid interface. It would be expected that it would be concave and hemispherical in form. No turbulence or geysering of the liquid could be observed. The interface on each side of the liquid volume moved toward the ends of the bottle as the transfer continued. The astronaut applied some pressure to the plunger of the syringe to achieve complete transfer of the liquid.

There is little difference between the transfer in low-g and one-g. The pressure within the bottle was selected so that the addition of a given volume of blood reduced the pressure differential to zero. In one-g the liquid will fall to the bottom side of the bottle, so there will always be a single gas volume. While the two separate gas volumes did not influence the proper transfer, it does demonstrate one of the problems that can arise in the low-g transfer of liquids.



Figure 51. Transfer of blood from syringe to evacuated bottle.

ORIGINAL PAGE IS
OF POOR QUALITY

When small quantities of liquid and small containers are being used, evacuating one container to achieve transfer is a simple approach. On a larger scale, structural considerations and vaporization of the liquid usually rule out this method of transfer. If the receiver container must be vented during the transfer, the location of the gas becomes very critical.

The plunger of the syringe eliminated the problems that might arise in the supply container in low-g. The volume between the plunger and the wall of the syringe was initially completely full of liquid. As liquid left the syringe the plunger followed, so no gas could enter the syringe. Liquid was always over the entrance to the needle during the transfer. In the position of the liquid within the syringe was not controlled in such a manner, gas could become positioned so that it would be transferred instead of liquid. The receiver would then rapidly fill with gas and transfer would stop. Some means of orienting the liquid in the supply container must be provided.

J. Diffusion

The objective of this demonstration was to observe the rate of diffusion in a low-g environment. Diffusion by itself is difficult to observe on earth because the force of gravity also produces circulation within a fluid. Within the limitations of the data a correlation of the diffusion rate was obtained. A parabolic diffusion front was also noted.

Diffusion is a process by which a fluid can become uniformly mixed by the random motion of the molecules of the fluid. Differences in temperature within a fluid will be equalized by diffusion. When two different fluids are present, diffusion will uniformly mix the two.

The demonstration was conducted using a tube quite close in size to an average laboratory test tube, 1.3 cm I.D. and 15 cm long. This container was filled 3/4 full of water and the tea, mixed in about seven times the normal concentration, was carefully inserted, contacting the water. The tube was mounted next to a ruled scale so that the progress of the diffusion front could be measured. A clock was also located on the side of the test container. The tea used (the astronaut's normal drinking tea) came premixed with sugar. A camera was set up to take time lapse pictures of the demonstration, including container, scale and clock face.

Quality of the data obtained was somewhat degraded by the fact that the camera was out of focus (Figure 52). It was not possible to distinguish the position of the hands on the clock-face, so the single significant data point was the position of the diffusion front in the center of the container after 51.5 hours at the conclusion of the demonstration. This location was approximately 2 cm from the starting position of that front. The other noteworthy result was that astronaut Lousma reported at the end of the experiment that the diffusion front had assumed a parabolic shape, with a significant lag in diffusion at the container wall. This observation is also confirmed in the time lapse pictures.

The limited data described above was used in a simple one-dimensional analysis of diffusion by B. Facemire at NASA-MSFC (Refs. 13 and 51). The result is a complementary error function that calculates the concentration at a position X at time t as a fraction of the initial concentration. The only other input

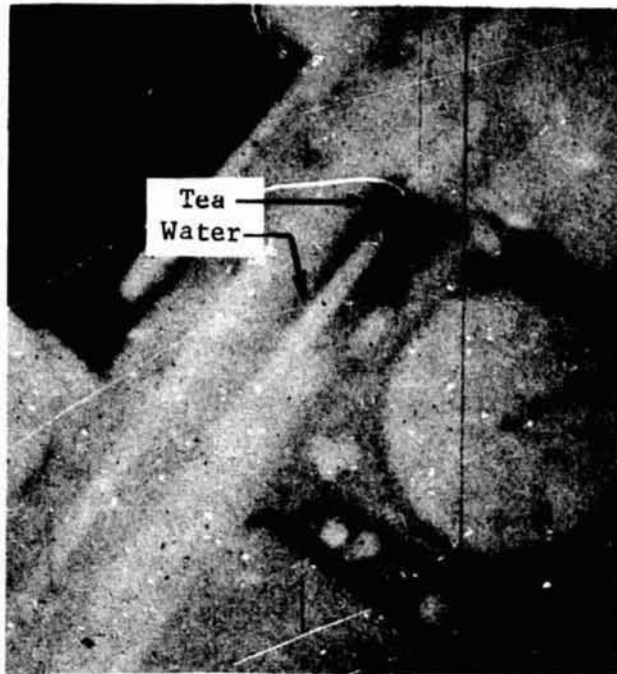


Figure 52. Diffusion Front Progress, SL-3
Liquid Diffusion Demonstration

ORIGINAL PAGE IS
OF POOR QUALITY

needed to perform the calculation is the diffusion coefficient of tea in water. Since this is not readily available, the coefficient for sugar in water was used since the tea did contain some sugar. What is being observed is the diffusion of whatever gives the tea its color, so the diffusion coefficient of that molecule should be used. Since the variation in the diffusion coefficient is small for many molecules in water, the coefficient for sugar is adequate.

The results obtained when the Skylab data was substituted in the above-described expression, using the sugar in water diffusion coefficient, correlated well with the visible concentration level found by refractive index measurements of tea solutions conducted at MSFC.

There are obvious effects at the wall of the container, as indicated by the parabolic shape of the diffusion front, that retard the rate of diffusion of the tea into the water. This retardation may be due to the differing nature of molecule collisions with the wall and molecule collisions with other molecules. Reference 51 speculates that the retarding force is electrostatic in nature. Due to the quality of the data obtained, further analysis was deemed to be impractical.

K. Liquid Floating Zone

The objective of this demonstration was to examine the stability of a liquid zone surface in low-g, under both static and dynamic conditions. An examination of the internal liquid circulation was also to be accomplished. A highly successful series of tests were performed in which the zone was rotated and oscillated in every possible manner. Two modes of instability were demonstrated, one of which had never been observed before. While the astronaut could observe the internal circulation, it could not be observed on the film data. This demonstration was expanded beyond its original objectives by astronaut Gibson to include other phenomena of the liquid within the zone, such as coalescence, the behavior of air bubbles, etc.

The Liquid Floating Zone is one method by which metals can be processed without a container in low-g. The zone is molten metal suspended between two coaxial solid rods. In a typical application a crystal is grown or a refined metal is solidified on one rod while the other rod provides the raw material. Heaters located around the zone melt the metal. In order to reduce concentration and temperature gradients the zone must be rotated as it is heated, so the dynamic behavior of the zone is a concern.

In this demonstration the zone was simulated with water suspended between two parallel disks 2.22 cm. in diameter. The disks were mounted on rods so that their spacing could be varied and each could be rotated.

Zones of 6, 14 and 20 cc were formed from two sessile drops. One drop was usually clear and the other was colored or had soap added to it. The zone was rotated three different ways; one rod rotated, both rods rotated in the same direction and both rods rotated in opposite directions. Two modes of stability were observed. One mode is axisymmetric (Figure 53), in which the zone pinched off as it was rotated. It was found that if the liquid is highly viscous (soap solution) the zone was always axisymmetrically unstable, for the zone lengths tested. The other mode has the form of a skip-rope (Figure 53). Misalignment of the disks or any off-axis perturbation caused this non-symmetrical mode to form.

A preliminary analysis of the stability of the rotating zone can be found in References 6 and 7. A more complete evaluation will be found in References 8 and 9 when they become available.

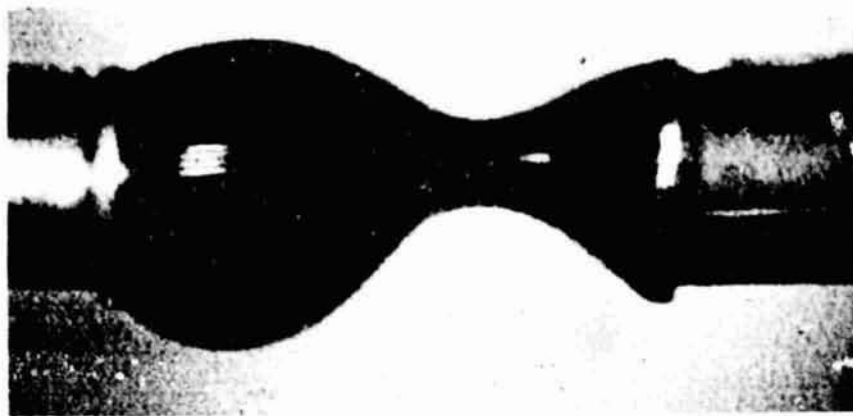


Figure 53. Unstable modes of rotating zone, axisymmetric above and unsymmetric below.

Other dynamic effects that were demonstrated were:

- 1) Coalescence of the zone from the sessile drops (Figure 54). This data is discussed in Section C. Liquid was transferred from one sessile drop to the other by pulsing one rod so that drops broke away and coalesced with the other drop (top photo in Figure 55).
- 2) Longitudinal oscillation of the zone. The entire zone was oscillated by axially perturbing one of the rods (center photo of Figure 55). An analysis of this data can also be found in references 7, 8, and 9. The data was found to correlate with the theory for capillary waves on a liquid surface only for the small zones.
- 3) Oscillation of the sessile drops (lower photo in Figure 55). This data is discussed in Section B.
- 4) Behavior of air bubbles in zone. Air bubbles were added to the zone. It was found that the larger bubbles coalesced quickly. The center photo in Figure 56 is only shortly after the upper photo. Some very small bubbles were formed in the zone and the effect of rotation was demonstrated. Due to buoyancy forces the bubbles were positioned along the center of rotation (bottom photo in Figure 56).
- 5) Mixing. By coloring the two sessile drops differently the mixing of the two liquids could be observed following coalescence and during rotation. Rope fibers were added to clear water for the same purpose (Figure 57). As the demonstrations were being performed the astronaut could observe the internal circulation patterns but they cannot be observed in the film data.
- 6) Ice melting. A cylinder of ice was placed between the two disks. The ice was smaller in diameter than the disks. Water was added to the surface of the ice to completely fill the zone (Figure 58). As the zone was rotated the ice cylinder aligned with the axis of rotation due to buoyant forces. The sequence does not show the complete melting of the ice.

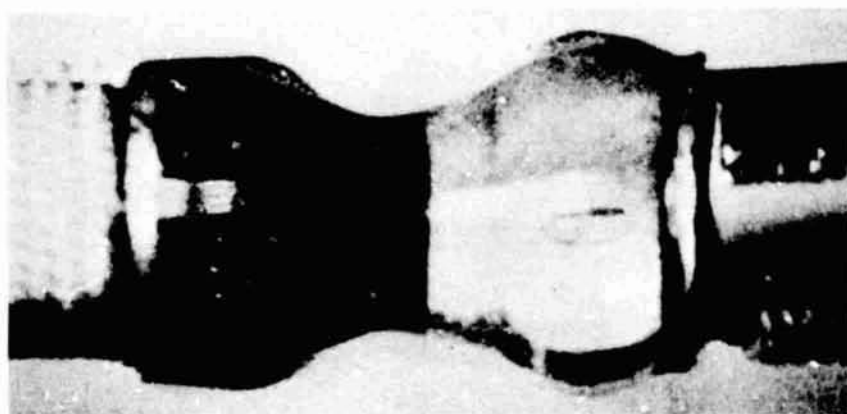
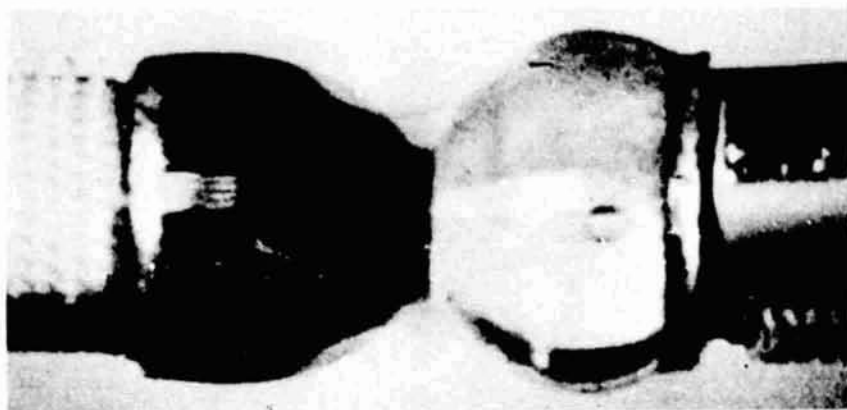
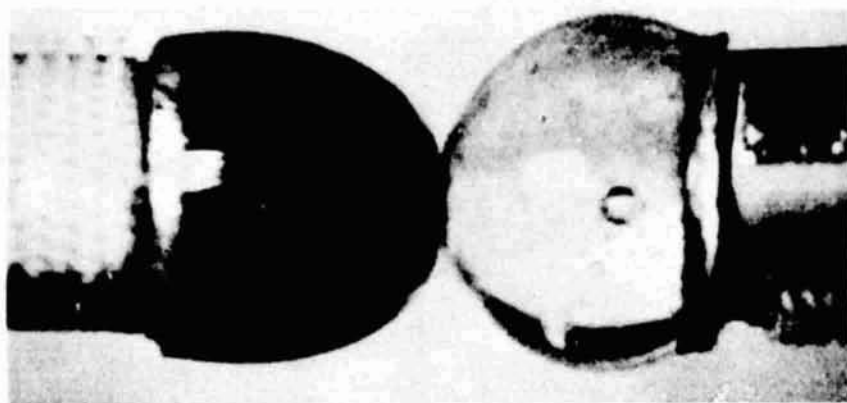


Figure 54. Coalescence of sessile drops from Liquid Floating Zone demonstration.

ORIGINAL PAGE IS
OF POOR QUALITY

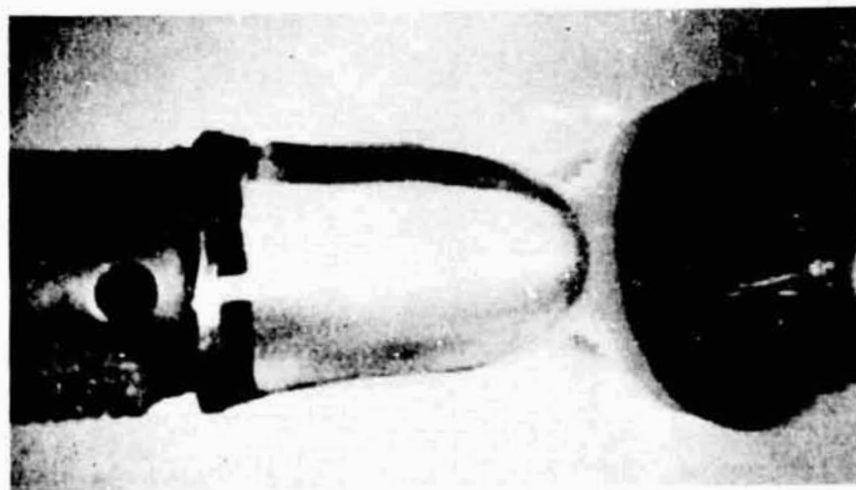
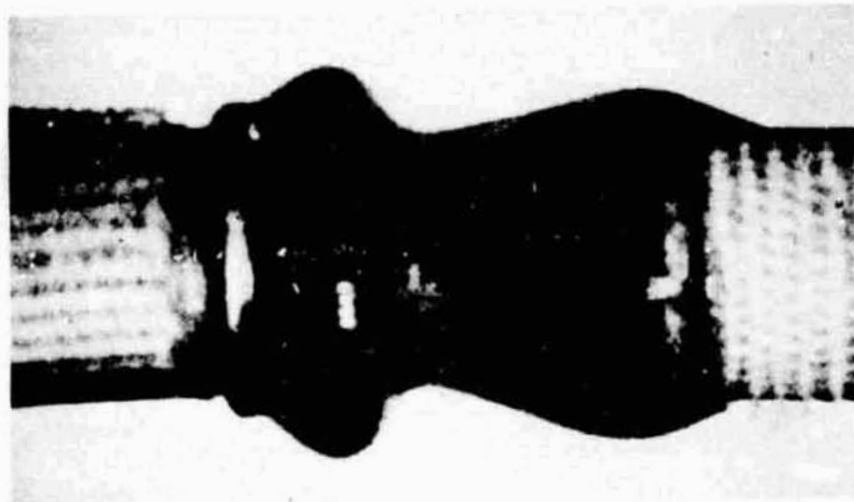
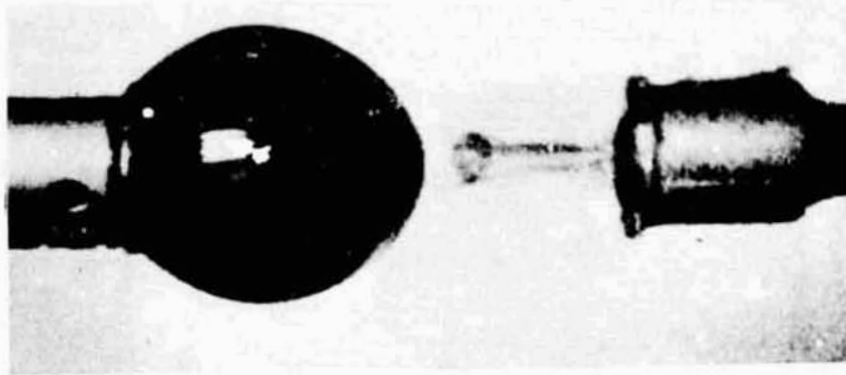


Figure 55. Drop dynamics in Liquid Floating Zone demonstration: shooting drop, lateral oscillation and oscillating sessile drop.

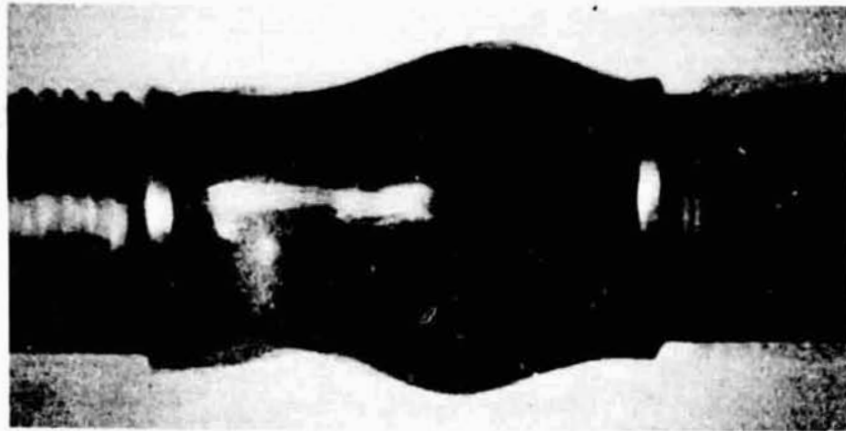
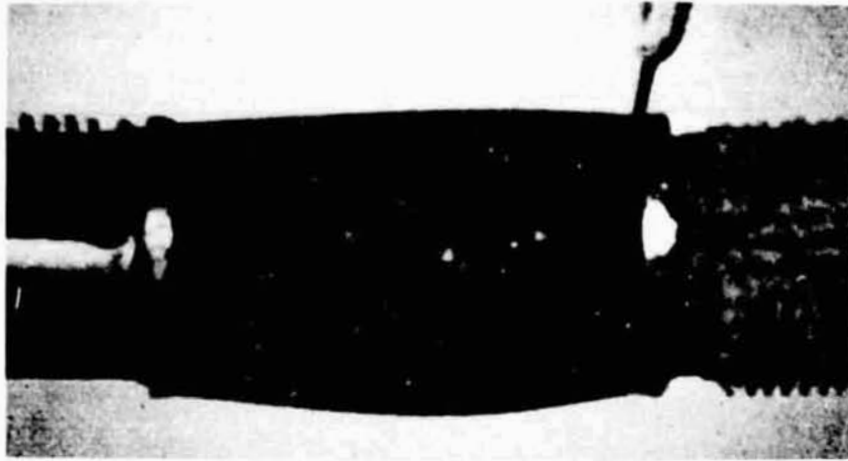


Figure 56. Bubbles within the Liquid Floating Zone

ORIGINAL PAGE IS
OF POOR QUALITY

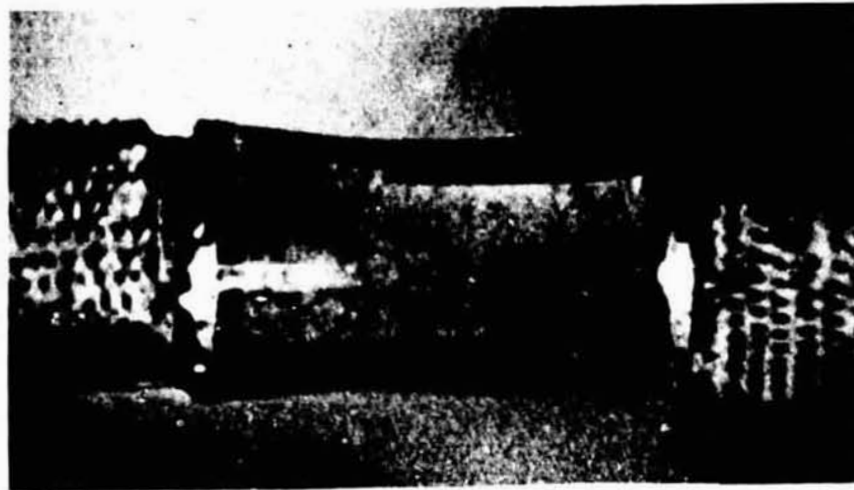


Figure 57. Rope Fibers in Zone

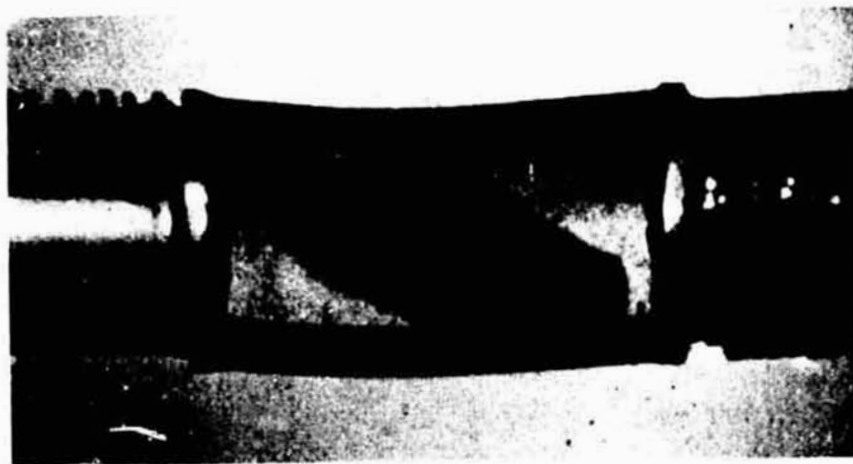


Figure 58. Melting Ice in Zone

ORIGINAL PAGE IS
OF POOR QUALITY

L. Cavitation

A bubble within a liquid can oscillate in much the same manner a liquid drop oscillates, as discussed in Section B. Both hydrodynamic and surface tension forces can act at the surface of a bubble. If the magnitude of the hydrodynamic forces exceed the surface tension forces at some point on the surface, the bubble can become unstable and collapse upon itself. A bubble can continue this action of collapsing, disintegrating and coalescing to restore its shape. Each time an unstable drop collapses a jet of liquid forms that shoots across the bubble. Such jets are the source of destructive forces of cavitation (Ref. 52). Reynolds first noted this in 1894 when water flowing through a constriction caused bubbles to form which collapsed, producing a hydraulic blow.

The phenomena of cavitation was inadvertently demonstrated twice in Skylab. One instance was when the oscillation of a drop with an internal air bubble was being demonstrated. The bubble and the drop had only a thin film separating them at one area on the surface. When this region was touched with the plunger the bubble ruptured. While the source of the instability of the bubble was not hydrodynamic forces as described above, the resulting collapse was the same as cavitation. A jet of liquid shot out of the drop at the point the bubble had been ruptured. The drop before and after the rupture of the bubble is shown in Figures 59 and 60.

As the velocity of the jet decreased, surface tension forces acted to retract part of the jet back into the drop, while some of the jet pinched off into individual drops. A column of liquid is unstable, under the effects of surface tension, when its length exceeds its circumference. The quality of the data did not permit an evaluation of the jet velocity or the instability of the jet.

In the other demonstration, air was added to a drop until it burst. When the bubble ruptured, the drop imploded and a jet of water shot out one side. In this sequence the jet could be seen pinching off into three small and one large drop. The drop is shown before and after rupture of the bubble in Figures 61 and 62.

In another sequence, a jet of water was formed by injecting water into a drop. A very long jet was formed in this case, reaching a length four times the original drop diameter. The



Figure 59. Drop with internal air bubble immediately before rupture.



Figure 60. Jet of liquid shoots out of view as bubble collapses.

ORIGINAL PAGE IS
OF POOR QUALITY

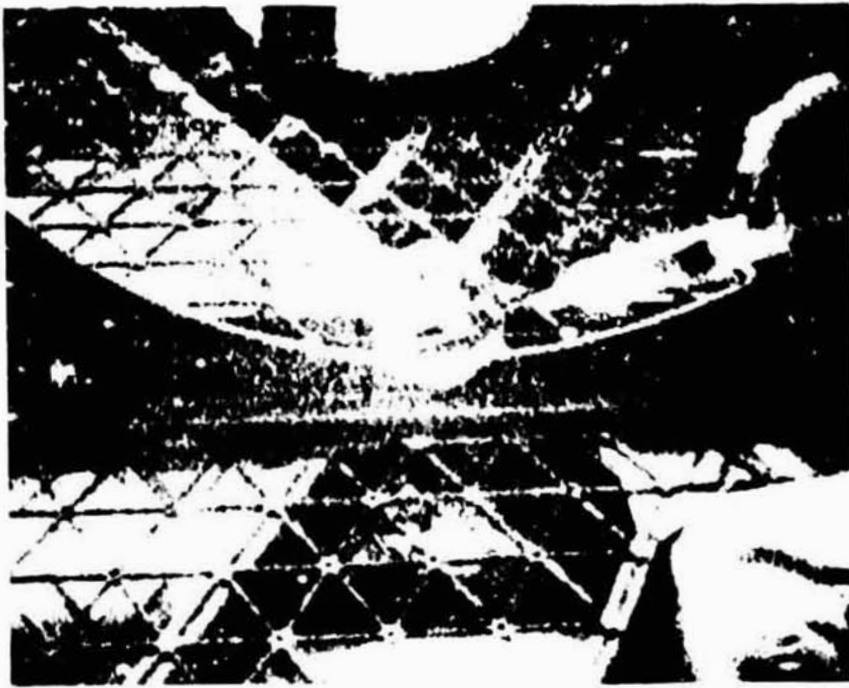


Figure 61. Air is being added with a syringe to a drop.



Figure 62. Collapse of the internal air bubble.

original drop was about 8 cm in diameter and the jet reached a length of 31 cm. As it formed, the jet had a velocity of about 26 cm/sec. Pinch-off of the jet into a number of drops was again observed (Figure 63).

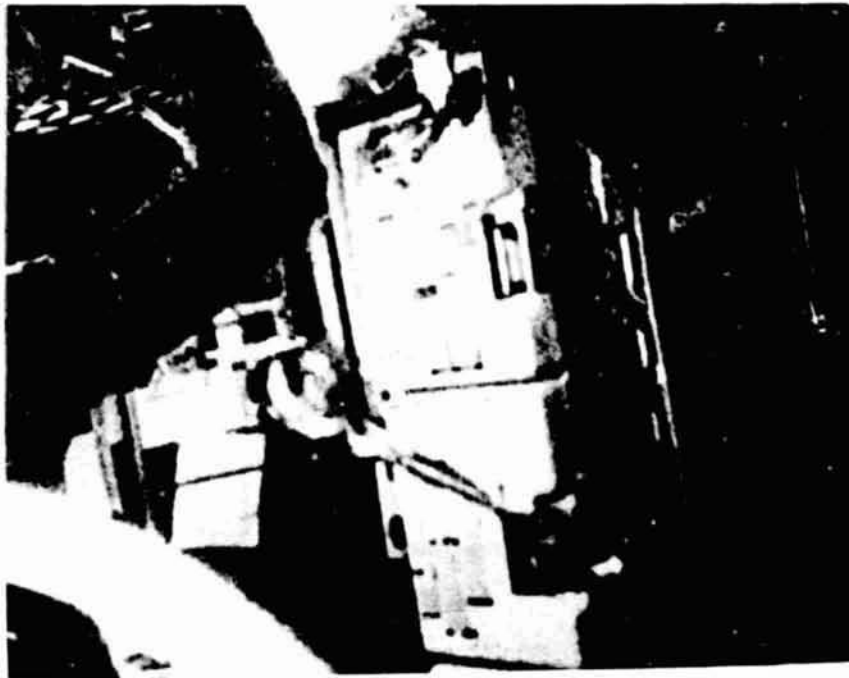


Figure 63. A jet of liquid is formed by injecting water into a drop.

ORIGINAL PAGE IS
OF POOR QUALITY

IV. APPLICATIONS SURVEY

A literature search was conducted to find the theory and analytical techniques applicable to the fluid mechanics phenomena observed in the Skylab demonstrations. This was a broad-based search covering many different fields of science. Most of the phenomena observed in the fluid mechanics demonstrations can be generalized to the behavior of the liquid drops or gas bubbles under some specified conditions. It became apparent in accomplishing the literature search that the application of the basic phenomena of drops and bubbles covers a wide range of disciplines. Most of the basic theory of drops and bubbles, such as the frequency and damping of an oscillating drop, was established around the end of the 19th century. In the current literature much the same phenomena are still being investigated, except that the added effects of electric fields, air flow, shock waves, surface active agents, vaporization, etc., are now being considered.

The phenomena observed in Skylab are not applicable only to a low-gravity environment. If a drop is very small or free falling the gravity force in one-g can be negligible in comparison to surface tension forces.

A colloquium, solely on the subject of drops and bubbles, was held at the California Institute of Technology in Pasadena, California in September, 1974. Papers presented at this colloquium ranged in subject matter from the behavior of the universe to the behavior of the nucleus of an atom, showing the wide range of applicability of the phenomena of drops and bubbles (Ref. 53).

In the following paragraphs the significance of the phenomena of drops and bubbles to various fields is briefly presented. Where the specific results of the Skylab fluid mechanics data analysis have some application, this is noted.

Astrophysics - A star can be treated as a drop of liquid. However, in this case, the force that holds the drop together is not surface tension, but gravity. The theory regarding the effects of viscous forces on oscillating drops is the same for self-gravitating and surface tension drops. The analysis of rotating, self-gravitating drops appears to be more advanced than the theory of rotating surface tension drops. Binary stars are believed to have been formed by the fission of a rotating star.

Since there are similarities, surface tension drops could be used to simulate and study the behavior of self-gravitating drops. Rotating drop experiments, such as those performed on Skylab, could simulate a star.

Cloud Physics - The objective of the science of cloud physics is to develop a model of a cloud, leading to an ability to understand, predict and possibly control the weather. Within a cloud, water droplets coalesce and break up under the influence of the forces of air flow and an electric field. The science of cloud physics has provided a considerable amount of information, both theoretical and experimental, on the dynamic behavior of a liquid drop. Compared to the drop sizes used in the Skylab demonstrations, the drops in a cloud are about 2 orders of magnitude smaller. A large drop in the field of cloud physics is 5 mm in diameter, with typical sizes for most analyses and tests being on the order of 100 microns. Since the drops in a cloud are small and free falling, their behavior is similar to a drop in low-gavity conditions.

Under low-g conditions the dynamic behavior of a drop can be simulated on a large scale. Oscillation frequencies, instead of being on the order of 100 Hz as they are for cloud sized drops, are slowed due to the larger size of the drop to around 1 Hz. High speed cameras are not required to view the phenomena. With the force of gravity and the effect of air flow eliminated from the test, just the basic behavior of the drop can be observed. Due to the larger size and slowed rates the phenomena can be directly observed as they happen and the duration of the test can be much longer.

The Skylab demonstrations provide a unique extrapolation of prior experimental results. Until the Skylab demonstrations, the largest drop used in an oscillating drop test was 5 mm in diameter (Ref. 54). In Skylab the largest drop was 5.8 cm in diameter, and larger drops could have been used. The results presented in Chapter III show that the same theory is applicable to all drop sizes. Coalescence theory is based on drops as large as 1.5 mm in diameter, while the Skylab tests used drops as large as 5.2 cm in diameter. With respect to coalescence, the Skylab data did not establish that the theory applicable to small drops can be applied to large drops. The rotating drop phenomenon has also been considered in the science of cloud physics, as discussed in Chapter III. The unique Skylab demonstration of the peanut-shaped rotating drop should contribute to the understanding of that phenomenon.

Geology - The spherical harmonics of the earth that establish its shape are the same in form as the modes of oscillation of a liquid drop. One of the most interesting geological items found in the literature search was the report of the discovery of solidified rotating drops on the moon. This was the only reference found in which the shape of the rotating drop was the same as that observed in the Skylab demonstration. (See Section D of Chapter III for details.)

Metallurgy - Metallurgists have been considering for many years the use of a low-gravity environment to improve the purity and structure achieved in the processing of metals. The need to use a container, which is always a source of contamination, can be eliminated by processing the metals as they free-float in low-g. Molten metals have a very high surface tension, ranging from about 300 to 1500 dynes/cm, so a large surface tension force is available.

Some experiments with molten metals were conducted in Skylab. In those experiments the effects of low-g on the melting, solidification, joining and brazing of metals was investigated (Refs. 55, 56, 57). Among the demonstrations, the liquid floating zone demonstration was specifically aimed at a containerless method of processing and refining metals.

Combustion - The ignition and combustion process within internal combustion engines and liquid rocket engines involves drops of the propellants. How these drops evaporate, atomize and behave in a shock wave are important to the efficiency of the combustion. Again, the basic dynamic behavior of a drop is essential to the understanding of more complex processes.

Chemical Processes - Drops and bubbles appear in many different forms in chemical processes. Emulsions, foams and aerosols consist of either drops or bubbles. The formation and behavior of such fluid mixtures is essential to the understanding of many processes. A few simple demonstrations of the behavior of emulsions and foams in the absence of gravity were conducted in Skylab. Detergency, the removal of foreign material from a surface by surface chemical means, is another example. The configuration assumed by a drop on a thread, demonstrated in Skylab, is one of the mechanisms of detergency.

Heat and Mass Transfer - Heat transfer involving a change of phase is a process of drops and bubbles. Nucleate boiling is the formation of a bubble on a surface. If a vapor can be made

to condense on a surface in the form of drops, rather than a film of liquid, the heat transfer rate to the surface is significantly increased. The static interface and dynamic behavior of a drop on a surface was demonstrated in Skylab. Contact angle was shown to be a significant parameter in determining the shape of the drop. Hysteresis of the contact angle influences the dynamic behavior of the drop.

Fluid Flow - Drops can be carried along by the flow of both gases and liquids. Again the basic behavior of drops and bubbles, as demonstrated in Skylab, is essential to understanding their behavior in fluid flow. How drops can rebound from surfaces and cause erosion is of concern. Collapsing gas bubbles in a liquid flow cause the destructive effects of cavitation. Cavitation was demonstrated on a large scale in Skylab.

Nuclear Physics - The nucleus of an atom can be simulated by a liquid drop. The binding energy of the nuclear particles is analogous to surface tension and a nucleus is incompressible, its density being independent of volume. The general features of nuclear energy levels are analogous to the oscillations of a liquid drop. A liquid drop model best simulates the fission of a nucleus. The stability of a nucleus can be considered as the stability of a drop to deformation: if the drop becomes unstable when deformed, fission occurs. The liquid drop model may be a key to determining the existence of heavy nuclei.

Aerospace - Fluids must be controlled within tanks on spacecraft so that liquid can be drained to supply life support systems and propulsion systems under low-gravity conditions. In many applications surface tension is used to preferentially orient the liquid within the tank or to prevent gas bubbles from entering the flow of liquid from the tank. One way in which this is done was demonstrated by the low-g drinking cup made by astronaut Pogue.

V. FUTURE EXPERIMENTS

When the Space Shuttle becomes operational in the 1980s, the performance of experiments in space will become somewhat routine. The opportunities to conduct experiments in space have been limited and will continue to be for a few more years. Some of the later Apollo missions provided some opportunities to perform some fluid mechanics experiments. The Skylab fluid mechanics demonstrations are presented in this report. These past efforts have demonstrated the feasibility and the advantages of performing fluid experiments in low-g.

In the Space Shuttle and its payload the Spacelab, true experiments will be able to be performed. Laboratory modules will be available that provide all the necessary apparatus, fluids, power and instrumentation. Currently the hardware for the Spacelab is being defined and the fluid mechanics experiments to be performed are being planned.

A distinguished committee of scientists* just completed (January 1975) a study to define what fluid physics, thermodynamics and heat transfer experiments should be performed in space (Ref. 18). Their report considers the current state-of-the-art and defines how low-g experiments could add to the understanding of the phenomena. The report states what phenomena should be investigated in low-g but does not describe how to perform the experiments. Their recommendations are briefly summarized here.

Critical Point Thermophysical Phenomena - Presently there is much interest in defining the properties of fluids near their critical point. In experiments on Earth, the force of gravity causes unwanted secondary effects, so low-g experiments are desirable. Properties such as the specific heat, dielectric constant, velocity of sound, viscosity and thermal conductivity would be measured at the critical point. These properties are believed to have an anomalous behavior near the critical point, but have yet to be measured accurately.

Fluid-Surface Dynamics and Capillarity - Experiments to verify the theories of many of the phenomena demonstrated on the Skylab are recommended here. Contact angle hysteresis, liquid interface shapes in low-g, surface waves in low-g, drop breakup and coalescence, and liquid films are the phenomena suggested for investigation.

*F. T. Dodge, H. N. Abramson, S. W. Angrist, I. Catton, S. W. Churchill, R. J. Mannheimer, S. Ostrach, S. H. Schwartz, and J. V. Sengers.

Convection in Reduced Gravity - In low-g, heat convection driven by buoyant forces is no longer significant, but there are other means by which convection can occur that should be investigated. Surface tension driven flow, thermoacoustic effects, mechanical vibrations, electric and magnetic fields, concentration gradients and chemical potentials would be considered as possible mechanisms of convection heat transfer.

Non-Heated Multiphase Mixtures - The behavior of foams, aerosols, immiscible liquid dispersions and bubbles should be investigated in low-g. The formation, behavior and stability of these mixtures could be studied without the pronounced effect of gravity.

Multiphase Heat Transfer - The long low-g periods available in space are ideal for the study of boiling, condensation, solidification and other phase change heat transfer processes. By eliminating the effect of gravity, the more subtle effects of surface tension, the liquid meniscus, liquid wetting, electric, magnetic and acoustic fields, etc. on multiphase heat transfer can be investigated.

The above summary only presents the general categories of experiments and mentions a few examples within each. The report itself mentions the many possible variations to the experiments. Each experiment has many parameters that could be varied.

A recent article (Ref. 58) also considered what future fluid mechanics experiments should be conducted in space. In this case the experiments were directed towards the science of cloud physics. The concept of a Cloud Physics Laboratory, which would be a Space Shuttle Payload, is described. The list of experiments has a lot of similarities with the above described report, except that they are directed specifically toward cloud physics phenomena. The article does not discuss the objective or approach of the experiments, but is directed more towards the concept and application of the Cloud Physics Laboratory.

It appears that there will not be any problem in finding experiments to be performed in space. The problem will be to determine relative priority of the suggested experiments, based upon their possible contribution to technology.

What was learned from the Skylab fluid mechanics demonstrations that should be applied to the procedures used in future fluid mechanics experiments?

The demonstrations showed that once the behavior of liquids in low-g is understood, their behavior can be used to advantage in handling and manipulating the liquid. Gravity forces are handy to have, since the liquid usually will be found in the bottom of a container. With gravity absent, surface tension forces must be put to use. Surface tension forces are handy to have since the liquid usually will be found in its minimum energy configuration. By using this principle, the adhesion of a liquid to a surface can be used to store, transfer, perturb, move and position a liquid. The astronauts developed a number of techniques and simple tools to handle liquids. The Skylab film data shows how they learned to make use of the surface tension forces.

The two Student Experiments that were to investigate fluid mechanics phenomena failed due to the failure of bladders that acted as liquid reservoirs (Refs. 59, 60). In the case of the wicking experiment, it appears that the bladder actually interfered with the proper operation of the experiment. As was shown by the Fluid Mechanics Series demonstrations, elaborate means of containing the test liquid are not necessary. The objective of the wave motion student experiment was achieved in the demonstrations by oscillating a free-floating liquid droplet. The objective of the wicking experiment could have been achieved by merely inserting the tubes into a large free-floating drop of liquid.

The other things learned from the demonstrations concern problems that most likely would be remedied by the proper conduct of a true experiment. The properties of the test liquid must be known and controlled. Since the surface tension of water can be drastically changed by a small amount of contaminant, it is not a good liquid for capillary experiments. Alcohol has a low surface tension and is a solvent, so it readily wets surfaces, is less sensitive to contaminants and will give repeatable results in capillary tests. Since future experiments will be performed in some sort of laboratory, hazardous test liquids such as alcohols and freons could be kept under control.

Pure liquids should be used when the more classical theories are being correlated. Liquids with known amounts of surfactant present and known properties should be used to experimentally determine the effects of the surfactants.

The volume of liquid used in the test must be accurately measured.

An accurate measure of damping coefficients will require a more sophisticated test method than was used in the demonstrations. First, a better method of setting the system into oscillation is required, be it a drop or liquid surface in a container. For drops, acoustical forces have been suggested (Ref. 61) as a way of applying a perturbation. Using such a method, the drop could be driven into oscillation in the desired mode, without inducing higher modes of oscillation. If a good quality image was obtained, 16 mm film data would be adequate for measuring the change in oscillation amplitude with time. A two dimensional image would be acceptable if no motion out of the plane of view was induced by the means of producing the oscillation. The idea of using a thread to tether the liquid drop was satisfactory for the demonstrations, but such an approach would be unacceptable for an experiment.

Acoustic forces could also be used to improve the technique for a rotating drop experiment. A drop can be rotated by aligning the acoustic sources so that they produce a torque. The angular momentum of the drop could be increased in small increments, stopping frequently to observe the deformation as a function of angular speed.

Many coalescence experiments have been performed on earth. Apparatus to form drops of given sizes and velocities could be adapted from proven methods (Refs. 36, 62, 63, 64).

Methods of making the flow of liquid visible (e.g., glass beads, Schlieren optical system, holography) should be used so that convection and mixing can be readily observed.

VI. CONCLUSIONS

Each of the Skylab fluid mechanics demonstrations had the objective of demonstrating a specific fluid mechanics phenomenon in a low-gravity environment. Surface tension was a dominant force in each demonstration, so the effect of this force could be readily observed. Most of the phenomena demonstrated could be categorized as the behavior of drops or bubbles. Among the phenomena demonstrated were the static interface shape of a liquid, oscillation and rotation of drops, coalescence, films, foams and the melting of ice.

In one sense, the Skylab fluid mechanics demonstrations were a feasibility demonstration. It was found that with simple experiments, very significant fluid phenomena can be investigated in a low-g environment. Large scale demonstrations (compared to what is possible on Earth) allowing direct observation of the phenomena, were performed. The period of time for the low-g test was much greater than has ever before been available. The handling and containment of the fluids while performing the demonstration was shown to be much less of a problem than was expected.

The demonstrations also identified some problems that might be encountered. The properties of the liquids used, especially their surface tension, must be established and controlled. Contaminants present in liquids can cause significant changes in the surface tension and, therefore, the behavior of the liquid. If pure oscillations of a single mode are desired or if damping coefficients are to be measured, refinements in the methods of perturbing a liquid drop are required.

Even though they were demonstrations, and not carefully performed experiments, some significant results were obtained from measurements and correlations derived from the film data. Poor data quality and lack of information on liquid volumes and liquid surface tension limited the precision of the correlations.

A number of different static interface shapes were demonstrated and correlations with calculated interface shapes were obtained. It was found that the oscillation frequency of drops with volumes of 50 and 100 cc correlate with available theory. Oscillating drops of this size have never been observed before. Coalescence was also demonstrated on a large scale.

The rotating drop demonstration was probably the most unique of the demonstrations. It was known that other forms for the rotating drop must exist, but the specific shape was not known. The "peanut" shape of the rotating drop was demonstrated. The data also provided some indication of how the elongation of this shape varies with angular rotation rate.

A method of processing metals, without a container, in low-g was demonstrated. The static and dynamic behavior of the liquid used in the process was investigated. The changes in the phenomena of immiscible liquids, liquid films, melting, films, transfer of liquids and diffusion due to a low-g environment were also demonstrated.

The results of certain of these demonstrations are directly applicable to processes performed in low-g (e.g., liquid floating zone). Other demonstrations are large scale simulations of phenomena that occur in one-g. Surface tension forces can dominate if a liquid drop is small, even though it is in a one-g environment. Low-g enables the same phenomena to be observed using a much larger liquid drop (e.g., coalescence). The low-g test eliminates the dominance of gravity from what is normally a one-g phenomenon. This allows the effects of surface tension forces, that are normally overwhelmed by gravity, to be studied. The liquid film and immiscible liquids demonstrations are examples of this application of low-g testing.

Future low-g experiments, employing the Space Shuttle, will add considerably to the understanding of fluid mechanics phenomena. Reference 18, which was summarized in Chapter V, provides a good source for recommended future fluid mechanics experiments.

VII. REFERENCES

1. O. H. Vaughan, R. E. Smith and R. J. Hung: "Skylab Fluid Mechanics Demonstration: A Study of Water Droplet Oscillations in Space." Presented at Conference on Cloud Physics, American Meteorological Society, Tucson, Arizona, October 1974.
2. O. H. Vaughan, R. E. Smith, R. J. Hung and S. T. Wu: "An Analysis of Oscillations of a Water Droplet." Presented at CIT/JPL Drops and Bubbles Colloquium, Pasadena, California, August 1974.
3. R. J. Hung, et al.: "A Zero-Gravity Demonstration of the Collision and Coalescence of Water Droplets." AIAA Paper No.74-1256, AIAA/AGU Conference on Scientific Experiments of Skylab, Huntsville, Alabama, November 1974.
4. O. H. Vaughan and C. K. Hill: "Drop Coalescence in Zero-Gravity Environment of Skylab IV." Bulletin American Meteorological Society, Vol. 55, No. 9, September 1974.
5. M. G. Klett and S. V. Bourgeois: "Analysis of Skylab IV Fluid Mechanics Science Demonstrations." LMSC-HREC TMD 390362. Lockheed Missiles and Space Co., Inc., Huntsville, Alabama, September 1974.
6. J. R. Carruthers: "The Application of Drops and Bubbles to the Science of Space Processing of Materials." Presented at the Drops and Bubbles Colloquium, Pasadena, California, September 1974.
7. J. R. Carruthers: "Studies of Liquid Floating Zones on SL-IV, the Third Skylab Mission." Unpublished report.
8. J. R. Carruthers: Paper to be presented at the AIAA/ASME 16th Structures, Structural Dynamics and Materials Conference, Denver, Colorado May 27-29.
9. M. Klett, "Analysis of Skylab IV Liquid Floating Zone", LMSC-HREC TMS390698, Lockheed Missiles and Space Co., Huntsville, Alabama, April 1975.

10. L. Lacy and H. Otto: "The Behavior of Immiscible Liquids in Space." AIAA Paper No. 74-668, AIAA/ASME Thermophysics and Heat Transfer Conference, Boston, Massachusetts, July 1974.
11. L. Lacy and H. Otto: "The Stability of Liquid Dispersions in Low-Gravity." AIAA Paper No. 74-1242, AIAA/AGU Conference on Scientific Experiments of Skylab, Huntsville, Alabama, November 1974.
12. W. Darbro, "Liquid Film Demonstration Experiment Skylab SL-4", NASA TM X-64911, NASA-MSFC, Huntsville, Alabama, January 1975.
13. F. C. Bannister: "Skylab III and IV Science Demonstrations Preliminary Report." NASA TM X-64835. NASA George C. Marshall Space Flight Center, Alabama, March 1974.
14. G. H. Otto and L. L. Lacy: "Observations of the Liquid/Solid Interface in Low-Gravity Melting." AIAA Paper No. 74-1243. Presented at AIAA/AGU Conference on Scientific Experiments of Skylab, Huntsville, Alabama, October 30, 1974.
15. V. K. Zworykin and G. A. Morton, "Television", John Wiley and Sons, Inc., New York, 1954.
16. Walter Drost-Hansen: "Aqueous Interfaces." Parts I and II in "Chemistry and Physics of Interfaces", American Chemical Society Publications, Washington, D. C., 1965.
17. J. J. Bikerman: "Surface Chemistry, Theory and Applications." Academic Press, Inc., New York, 1958.
18. F. T. Dodge, et al.: "Fluid Physics, Thermodynamics, and Heat Transfer Experiments in Space: Final Report of the Overstudy Committee." NASA CR-134742. Southwest Research Institute, San Antonio, Texas, January 1975.
19. J. D. Taylor and A. Acrivos: "On the Deformation and Drag of a Falling Viscous Drop at Low Reynolds Number." J. of Fluid Mechanics, Vol. 18, 1964.
20. J. F. Harper: "The Motion of Bubbles and Drops Through Liquids." Advances in Applied Mechanics, Vol. 12, 1975, pp 59-129.

21. S. Winnikow and B. T. Chao: "Droplet Motion in Purified Systems", Physics of Fluids, Vol. 9, No. 1, January 1966. pp 50-61.
22. H. M. Princen, "The Equilibrium Shape of Interfaces, Drops, and Bubbles", in "Surface and Colloid Science", Volume 2, E. Matijevic, Editor, John Wiley & Sons, New York, 1969.
23. L. J. Hastings and R. Rutherford III, "Low Gravity Liquid-Vapor Interface Shapes in Axisymmetric Containers and a Computer Solution", NASA TM X-53790, NASA Marshall Space Flight Center, October 7, 1968.
24. W. C. Reynolds and H. M. Satterlee, "Liquid Propellant Behavior at Low and Zero g", Chapter II in "The Dynamic Behavior of Liquids in Moving Containers", H. N. Abramson, Editor, NASA SP-106, NASA, Washington, D. C., 1966.
25. Kenneth J. Paumeister and Thomas D. Hamill: "Liquid Drops: Numerical and Asymptotic Solutions of Their Shapes" NASA TN D-4775. NASA Lewis Research Center, Cleveland, Ohio, September 1968.
26. H. M. Satterlee, et al., "Engineers Handbook: Low-G Propellant Behavior", LMSC-A874831, Lockheed Missiles and Space Co., Sunnyvale, California, 15 May 1967.
27. D. A. Fester, et al., "Space Storable Propellant Acquisition System", NASA CR 114493, Martin Marietta Corp., Denver, Colo., October 1972.
28. C. D. Brown, "Viking Orbiter 1974 Propellant Management Device", SE 010-47-01, Martin Marietta Corp., Denver, Colo., May 1973.
29. G. Brant Foote, "A Numerical Method for Studying Liquid Drop Behavior: Simple Oscillation." J. of Computational Physics, Vol. 11, 1973.
30. N. H. Reid, "The Oscillations of a Viscous Liquid Drop." Office of Naval Research Report NR-062-179. Brown University, Providence, R. I., February 1960.

31. Lord Rayleigh, "Theory of Sound." Dover Publications, New York, 1945.
32. C. A. Miller and L. E. Scriven, "The Oscillations of a Fluid Droplet Immersed in Another Fluid." J. Fluid Mechanics, Vol. 32, 1968.
33. L. D. Landau and E. M. Lifshitz, "Fluid Mechanics", Addison-Wesley Publishing Co., Inc., Reading, Massachusetts, 1959.
34. Sir H. Lamb, "Hydrodynamics." Dover Publications, New York, 1945.
35. Chun Huh and L. E. Scriven: "Hydrodynamic Model of Steady Movement of a Solid/Liquid/Fluid Contact Line." J. of Colloid and Interface Science, Vol. 35, No. 1, January 1971.
36. P. R. Brazier-Smith, et al.: "The Interaction of Falling Water Drops: Coalescence." Proceedings of the Royal Society of London, Vol. 326A, 1972.
37. C. V. Boys, "Soap Bubbles: Their Colors and Forces Which Mold Them" Dover Publications, New York, NY 1959.
38. Lord Rayleigh, Phil. Mag. Vol 28, page 161, 1914.
39. S. Chandrasekhar: "The Stability of a Rotating Liquid Drop." Proceedings of the Royal Society of London, Vol. 286A, 25 May 1965.
40. D. K. Ross: "The Shape and Energy of a Revolving Liquid Mass Held Together by Surface Tension." Australian J. of Physics, Vol. 21, 1968.
41. D. K. Ross: "The Stability of a Rotating Liquid Mass Held Together by Surface Tension." Australian J. of Physics, Vol. 21, 1968.
42. R. A. Lyttleton, "The Stability of Rotating Liquid Masses", Cambridge University Press, 1953.
43. M. J. Pugh: "Rotation of Lunar Dumbbell-Shaped Globules during Formation." Nature, Vol. 237, May 1972.

44. S. Tolansky: "Interferometric Examination of Small Glassy Spherules and Related Objects in a 5-Gram Lunar Dust Sample." *Science*, Vol. 167, January 1970.
45. M. Fulchignoni, et al.: "Glassy Spheroids in Lunar Fines from Apollo 12 Samples 12070,37; 12001,73; and 12057,60." *Proceedings of the Second Lunar Science Conference*, Vol. 1, the MIT Press, 1971.
46. A. W. Adamson, "Physical Chemistry of Surfaces" Intersciences Publishers. New York, NY 1960.
47. J. J. Bikerman, "Surface Chemistry: Theory and Application" Academic Press, New York, NY, 1958.
48. C.S.M. Marangoni, *Nuovo Cimento*, Volume 11, Series 2, 1872.
49. J. L. McGrew, et al., "The Effect of Temperature Induced Surface Tension Gradients on Bubble Mechanics", *Applied Science Research*, Vol. 29, June 1974, pp 195-210.
50. L. E. Scriven and C. V. Sternling, "The Marangoni Effects", *Nature*, Vol. 187, July 16, 1960, pp 186-188.
51. B. Facemire, et al.: "MSFC Science Demonstrations Performed by Pilot J. Lousma on Skylab III." *Space Sciences Laboratory*, NASA George C. Marshall Space Flight Center, Alabama, November 5, 1973.
52. M. Kornfeld and L. Suvarov: "On the Destructive Action of Cavitation." *J. of Applied Physics*, Vol. 15, No. 6, 1944, pp 495-506.
53. "Proceedings of Colloquium on Drops and Bubbles", California Institute of Technology, Pasadena, Calif., September 1974 (To be published Summer 1975).
54. Arthur R. Nelson and Narayan R. Gokhale, "Oscillation Frequencies of Freely Suspended Water Drops." *J. of Geophysical Research*, Vol. 77, No. 14, May 20, 1972.
55. E. C. McKannan and R. M. Poorman, "Skylab M551 Metals Melting Experiment", *Proceedings of the Third Space Processing Symposium*, Volume 1, NASA Marshall Space Flight Center, May 1974.

56. J. R. Williams, "Skylab Experiment M551 Exothermic Brazing", Proceedings of the Third Space Processing Symposium, Volume 1, NASA Marshall Space Flight Center, May 1974.
57. D. J. Larson, "Skylab M553 Sphere Forming Experiment", Proceedings of the Third Space Processing Symposium, Vol. 1, NASA Marshall Space Flight Center, May 1974.
58. R. V. Greco and R. E. Turner, "Cloud Physics Laboratory: A Step Toward Weather Control", Astronautics and Aeronautics, Vol. 13, No. 3, March 1975, pp 44-48.
59. H. B. Floyd: "Student Experiments on Skylab." AJAA Paper 74-1251. Presented at AIAA/AGU Conference on Scientific Experiments of Skylab, Huntsville, Alabama, October 30-November 1, 1974.
60. "MSFC Skylab Student Project Report." NASA TM X-64866. NASA George C. Marshall Space Flight Center, Alabama, August 1974.
61. K. K. Knapp: "Zero-G Liquid Studies: Critical State and Liquid Drop Dynamics." EOS Report 7170-Final. Electro-Optical Systems, Inc. Pasadena, California, 2 November 1967.
62. R. M. Schotland: "The Collision Efficiency of Cloud Drops of Equal Size." J. of Meteorology, Vol. 14, No. 5, October 1957.
63. J. R. Adam, et al., "The Collision, Coalescence, and Disruption of Water Droplets", J. of Applied Physics, Vol. 39, No. 11, October 1968.
64. N. R. Cotton and N. R. Gokhale, "Collision, Coalescence, and Breakup of Large Water Drops in a Vertical Wind Tunnel", J. of Geophysical Research, Vol. 72, No. 16, August 15, 1967.

APPENDIX A FILM DATA IDENTIFICATION

The purpose of this appendix is to give the specific identification of the film data used in performing the analysis presented in this report.

The film library at the NASA Johnson Space Center, Houston, Texas has kinescope copies of all the videotapes from the Skylab missions. This agency should be contacted if copies of any of these films are desired.

TITLE	IDENTIFICATION NUMBERS	LENGTH (FEET)	DAY OF YEAR	SOUND	REMARKS
Water Drop	SLIII-Tape 11, Part 1	466	239	Yes	Drop on Straw
Liquid Motion	SLIII-Tape 13, Part 2	111	245	Yes	ED-72 Student Experiment Failure
Liquid Motion	SLIII-Tape 14, Parts 1&2	72	247	Yes	Drop on thread (SLIII)
Immiscible Liquids	SLIV-Tape 8, Part 1	319	004	No	
Fluid Mechanics Series	SLIV-Tape 8, Part 2	310	005	Yes	Seesile Drop
Fluid Mechanics Series	SLIV-Tape 9, Part 1	728	006	Yes	
Liquid Floating Zone	SLIV-Tape 10, Parts 1	983	012	Yes	
Liquid Floating Zone	SLIV-Tape 10, Part 2	898	013	Yes	
Liquid Floating Zone	SLIV-Tape 12, Part 1	536	013	Yes	
Liquid Floating Zone	SLIV-Tape 12, Part 2	868	014	Yes	
Liquid Floating Zone	SLIV-Tape 12, Part 3	236	014	Yes	
Liquid Floating Zone	SLIV-Tape 12, Part 4	374	015	Yes	
Fluid Mechanics Series	SLIV-Tape 13, Part 2	613	018	No	Oscillating Drops - Poorer Quality
Fluid Mechanics Series	SLIV-Tape 13, Part 3	161	019	Yes	Rotating Drops
Fluid Mechanics Series	SLIV-Tape 14, Part 3	700	023	Yes	Oscillating Drop
Fluid Mechanics Series	SLIV-Tape 15, Part 1	569	024	Yes	Coealescence
Liquid Films	SLIV-Tape 15, Part 3	910	025	Yes	
Fluid Mechanics Series	SLIV-Tape 16, Part 1	415	026	Yes	Rotating Drop

APPENDIX B ANALYTICAL DERIVATIONS

Determination of the Interface Shape of a Drop on a String in Zero Gravity.

The shape of a drop on a string in zero gravity is totally determined by the capillary forces. Assuming the drop is axisymmetric, the shape is given by equation (1).

$$\sigma \left(\frac{1}{R_1} + \frac{1}{R_2} \right) = \text{constant} \quad (1)$$

Because the drop is symmetrical, the curvature can be expressed as follows:

$$\frac{1}{r} \frac{d}{dr} \left[\frac{r \frac{d\eta}{dr}}{\sqrt{1 + \left(\frac{d\eta}{dr}\right)^2}} \right] = c_1 \quad (2)$$

where r is the radial coordinate, η the longitudinal coordinate from some reference point, and c_1 is an arbitrary constant. This equation may be integrated once to give

$$\frac{d\eta}{dr} = \frac{\frac{1}{r} \left(\frac{c_1 r^2}{2} + c_2 \right)}{\sqrt{1 - \frac{1}{r^2} \left(\frac{c_1 r^2}{2} + c_2 \right)}} \quad (3)$$

where c_1 and c_2 are arbitrary constants which are determined by the boundary conditions

$$r = r_t \quad (\text{thread radius) at } \eta = 0 \quad (4)$$

and

$$\frac{d\eta}{dr} = \tan\left(\frac{\pi}{2} - \Theta\right) \quad \text{at } \eta = 0 \quad \text{and } r = r_t \quad (5)$$

Using equation (3), with the boundary conditions, the constant c_2 may be found directly. The value of c_1 determines the volume of the drop. Its value is found by a finite difference iteration technique. Using a small increment for η and guessing a value for c_1 , equation (2) is solved for Δr . Both r and η are incremented and the calculation is continued around the drop. Only one-quarter of the drop needs to be calculated due to symmetry. The volume of the calculated drop shape is computed. c_1 is adjusted accordingly until the desired drop volume is obtained.